

**S-NITROSYLATION IN BRAIN OF MICE EXPOSED TO LOW OR HIGH  
DOSES OF GAMMA RAYS: A BIOINFORMATIC INVESTIGATION OF THE  
MODULATED PATHWAYS**

**by**

**FADIA NICOLAS**

**A Dissertation Submitted to**

**Rutgers, The State University of New Jersey**

**School of Health Professions**

**in Partial Fulfillment of the Requirements for the Degree of**

**Doctor of Philosophy**

**Graduate Program in Biomedical Informatics**

**Department of Health Informatics**

**May, 2018**



**S-NITROSYLATION IN BRAIN OF MICE EXPOSED TO LOW OR HIGH  
DOSES OF GAMMA RAYS: A BIOINFORMATIC INVESTIGATION OF THE  
MODULATED PATHWAYS**

**by**

**Fadia Nicolas**

**Dissertation Committee**

Masayuki Shibata Ph.D., Professor Emeritus, Rutgers, SHP

Edouard I. Azzam Ph.D., Professor, Rutgers, NJMS

Gwendolyn M. Mahon Ph.D., Dean, Professor, Rutgers, SHP

**Approved by the Dissertation Committee**

\_\_\_\_\_ **Date** \_\_\_\_\_  
\_\_\_\_\_ **Date** \_\_\_\_\_  
\_\_\_\_\_ **Date** \_\_\_\_\_

## **ABSTRACT OF THE DISSERTATION**

### **S-NITROSYLATION IN BRAIN OF MICE EXPOSED TO LOW OR HIGH DOSES OF GAMMA RAYS: A BIOINFORMATIC INVESTIGATION OF THE MODULATED PATHWAYS**

by Fadia Nicolas

Extensive experimental studies and several human epidemiological surveys have revealed that exposure to high doses of ionizing radiation (>100 mSv) causes significant adverse health outcomes. The mechanisms underlying these effects have been well characterized. In contrast, the biological effects and health risks of exposure to low doses of radiation (<100 mSv) continue to be unclear and are a current subject of conflicting considerations. Due to insufficient statistical power in the limited number of available epidemiological studies evaluating health risks of human exposures to effective doses less than 100 mSv, mechanistic studies in cultured cells and animal models have been considered to be vital for understanding biological effects, and reducing the uncertainty in predicting health risks.

This project builds on the body of studies characterizing the biochemical and biological effects of low dose ionizing radiation, but the emphasis is on characterizing post translational modification of proteins, namely S-nitrosylation, an area that is under-studied, even though it could greatly impact radiation sensitivity. Here, changes in S-nitrosylation were studied following *in vivo* exposure to either a low (0.1 Gy) or high doses (4 Gy) of <sup>137</sup>Cs  $\gamma$  rays, which mimics doses received in diagnostic and therapeutic radiation, respectively. The goal was to investigate whether similar or distinct S-nitrosylation events

are induced in brain tissue following low and high dose  $\gamma$  ray irradiation to test the following hypothesis: “Depending on radiation dose, S-nitrosylation triggers groups of proteins into participating in specific pathways that are protective (e.g. DNA repair, antioxidation reactions) or detrimental (loss of healthy cells, oxidative stress)”.

Young adult C57BL/6J male mice were exposed to either 0, 0.1 or 4 Gy of Cesium-137  $\gamma$  rays delivered uniformly to the whole body. Thirteen days after irradiation, the animals were euthanized, and the brains were harvested. The proteins were immediately extracted and processed for mass spectrometry analyses of global changes in S-nitrosylation. Using Bioinformatic tools, the mass spectrometry results were analyzed by the R/Bioconductor statistical package. Several clustering approaches were used in order to create groups of proteins showing similar levels of S-nitrosylation for dose independent responses to radiation exposure, and dissimilar levels of S-nitrosylation for dose dependent responses. Clustering methods used a range of methods from purely mathematical to more intuitive manual approaches with somewhat arbitrary cutoff to analyze the proteomic data from irradiated and control samples. Additional clustering techniques like k-means and hierarchical clustering with several different numbers of clusters were applied to eliminate the cutoff bias. In addition, Ingenuity Pathway Analysis (IPA) software package was used to elucidate biological significance of the different groups of proteins. Depending on the clustering approaches used, several significant pathways were identified. For example, relative to control, the neuronal nitric oxide synthase (nNOS) pathway showed inactivation under low dose irradiation and activation under high dose irradiation. This pathway is under control of the N-methyl-D-aspartate receptor (NMDAR) activity, which becomes hyper-activated under high dose irradiation resulting in neurotoxicity.

In conclusion, our results suggest that mouse exposure to low doses of Cesium-137  $\gamma$  rays may result in modulation of signaling pathways that promote protective effects through S-nitrosylation of certain key proteins and de-S-nitrosylation of others. This is an area that needs further investigation to elucidate the exact mechanism by which S-nitrosylation occurs, and to confirm the role of the modulated pathways suggested by IPA in regulating cellular/tissue responses that impact sensitivity to radiation.

## **Acknowledgements**

Many people were involved in my research on nitrosylation study. I would like to thank Dr. Masayuki Shibata, my advisor in the Biomedical Informatics program and Dr. Edouard Azzam from the Department of Radiology. Dr. Shibata has been my advisor and professor from the beginning of my enrollment in the School of Health Professions. Dr. Azzam has been my mentor and my dissertation advisor. You took time away from your research and teaching to assist me in my analysis. I am very thankful for your efforts. I am especially thankful for your patience throughout my years of study.

I would also like to acknowledge the committee members, advisors and readers of my dissertation. Dr. Mahon, dean of the school of health professions, Dr. Antonina Mitrofanova, assistant professor of the school of health professions, Dr. Shankar Srinivasan, associate professor and program director of the school of health professions, Dr. Robert Donnelly, department of pathology and laboratory medicine. Your guidance and critique of my dissertation were valuable to my success as a doctorate candidate.

Many thanks to my family. Your support has allowed me to pursue my dream of doing meaningful research and completing my PhD. I could not have made it this far without all of your assistance.

## Table of Contents

<b>Final Dissertation Approval Form .....</b>	<b>ii</b>
<b>ABSTRACT OF THE DISSERTATION .....</b>	<b>iii</b>
<b>Acknowledgements .....</b>	<b>vi</b>
<b>List of Tables .....</b>	<b>xi</b>
<b>List of Figures .....</b>	<b>xii</b>
<b>List of Abbreviations .....</b>	<b>xv</b>
<b>Publication of Chapters and Role of Author.....</b>	<b>xvii</b>
<b>I Introduction .....</b>	<b>1</b>
1.1 Statement of the Problem .....	2
1.2 Background .....	2
1.3 Objectives and Goals of the Research.....	4
<b>II Literature Review .....</b>	<b>5</b>
2.1 Radiation Exposure and the Cellular Response .....	5
2.1.1 Radiation/Ionizing Radiation.....	5
2.1.2 Low Dose Ionizing Radiation.....	10
2.1.3 The Linear No-Threshold (LNT) Model .....	11
2.1.4 Limits of Epidemiology.....	14

2.2 Protein S-Nitrosylation .....	15
2.2.1 Mechanism of S-Nitrosylation/De-Nitrosylation .....	16
2.2.2 S-Nitrosylation in Controlling Brain Function.....	21
2.2.3 Ionizing Radiation and Nitrosylation .....	24
2.3 Bioinformatic Analysis of S-Nitrosylation .....	27
2.3.1 R and Bioconductor for Proteomic Studies .....	28
2.3.2 Gene Ontology.....	35
2.3.3 Network and Pathway Analysis.....	36
2.3.4 Database of Protein Post-Translational Modifications (PTMs) .....	40
2.4 Identifying Biomarkers of Ionizing Radiation .....	44
<b>III Materials and Methods.....</b>	<b>47</b>
3.1 Animal Irradiation and Mass Spectrometry .....	47
3.2 Proteomics Data Description and Pre-processing .....	48
3.2.1 Proteomics Data Description.....	48
3.2.2 Proteomics Data Pre-processing.....	48
3.2.3 Calculations of Changes in Nitrosylated Proteins after Irradiation.....	49
3.3 Grouping .....	50
3.3.1 No Grouping (Whole Data Set).....	51
3.3.2 Clustering with R.....	55
3.3.3 Manual Clustering .....	59
3.3.4 Clustering from 2 to 10: Membership Changes .....	60

3.4 Ontology and Pathway Analysis .....	61
3.4.1 Protein Functional Classification (PANTHER) .....	61
3.4.2 Ingenuity Pathway Analysis (IPA) .....	61
<b>IV Results .....</b>	<b>63</b>
4.1 Grouping .....	63
4.1.1 Whole Data Set (One Group) .....	63
4.1.2 Clustering with R.....	72
4.1.3 Cluster Analysis with R: Membership Changes.....	83
4.1.4 Manual Clustering .....	86
4.2 Molecular Function and Biological Process .....	101
4.2.1 Whole Data Set (One Group) .....	101
4.2.2 Optimum Cluster of 2 from R .....	106
4.2.3 Hierarchical Clustering.....	115
4.2.4 Manual Clustering .....	117
<b>V Discussion .....</b>	<b>128</b>
5.1 Irradiation Alters the Level of Protein S-Nitrosylation .....	128
5.1.1 Levels and Changes in S-Nitrosylation following <sup>137</sup> Cs γ Ray Irradiation ...	128
5.2 Clustering of S-Nitrosylated Proteins .....	130
5.3 Characterization of Protein Clusters through Ingenuity Pathway Analysis.....	131
5.3.1 Pathways Identified Decreases in Nitrosylation at Low Dose IR .....	132

5.3.2 Cell Death and Apoptotic Pathways Identified Increased in Nitrosylation...	139
5.4 Irradiation in the Treatment of Neurodegenerative Diseases.....	142
5.4.1 Low Dose Radiation and Moderate Increase in SNO/Adaptation Process ...	142
5.5 Biomarker Discovery .....	143
<b>VI Conclusion and Future Directions .....</b>	<b>144</b>
<b>VII Appendix.....</b>	<b>148</b>
7.1 “Radiation Treatment and Mass Spectrometry Protocol.....	148
7.2 Copyright Permission.....	152
7.2.1 Proteomes— Open Access Journal .....	152
7.2.2 IPA Copyright Permission.....	152
<b>VIII References .....</b>	<b>153</b>

## List of Tables

Table 1. Proteins with undetectable nitrosylation.....	49
Table 2. Clustering of proteins into 9 groups .....	60
Table 3. Statistical Output in R: Summary and Describe function.....	69
Table 4. Percent of proteins with increase, no change or decrease in nitrosylation. ....	70
Table 5. ClValid best cluster by hierarchical and Silhouette method.....	79
Table 6. Protein membership changes per number of clusters .....	85
Table 7. Protein groups with increase/decrease in SNO.....	86
Table 8. Heat table: No change in SNO at 0.1 Gy, increase at 4 Gy. ....	88
Table 9. Heat table: No change in SNO at 0.1 Gy, no change at 4 Gy.....	90
Table 10. Heat Table: No change in SNO at 0.1 Gy, decrease at 4 Gy. ....	91
Table 11. Heat table: decrease in SNO at 0.1 Gy, increase at 4 Gy. ....	93
Table 12. Nitrosylation decrease at 0.1 Gy and 4 Gy. ....	95
Table 13. Nitrosylation decrease at 0.1 Gy and no change at 4 Gy.....	97
Table 14. Nitrosylation increase at 0.1 Gy and decrease at 4 Gy. ....	98
Table 15. Nitrosylation increase at 0.1 Gy and no change at 4 Gy.....	99
Table 16. Nitrosylation increase at 0.1 Gy and increase at 4 Gy.....	101
Table 17. Proteins participating in the Melatonin Signaling Pathway.....	112
Table 18. Top Pathways: decrease in nitrosylation at 0.1 and 4 Gy.....	119
Table 19. Top Pathways: decrease in nitrosylation at 0.1 and no change at 4 Gy.....	120
Table 20. NMDAR subunits with their nitrosylation levels in brain of mice exposed to 0.1 or 4 Gy .....	126

## List of Figures

Figure 1. Most common types of ionizing radiation.....	6
Figure 2. Different possible extrapolations of cancer related radiation risk. ....	13
Figure 3. Limits of detectability at low dose radiation. ....	15
Figure 4. Biotin Switch Technique. ....	20
Figure 5. Fisher exact test for the overlap between user and reference dataset.....	37
Figure 6. High dose radiation and Alzheimer disease. ....	40
Figure 7. Animal irradiation and experimental groups.....	47
Figure 8. Frequency distribution of S-nitrosylated proteins .....	64
Figure 9. S-nitrosylated protein levels with spectral count above 80 .....	65
Figure 10. S-nitrosylation after exposure to low and high dose $\gamma$ radiation .....	66
Figure 11. Scatterplot in excel showing changes in nitrosylation level.....	66
Figure 12. Boxplot displaying the data through the quartile ranges. ....	70
Figure 13. Log2 Scatter plot showing the spread of the data.....	71
Figure 14. Various density plot displays in R.....	72
Figure 15. Scree plot .....	74
Figure 16. Plot showing the clustering by k-means algorithm. ....	74
Figure 17. PAM clustering of protein data .....	75
Figure 18. Average Silhouette with k cluster equals 2. ....	76
Figure 19. NbClust with frequency of indices optimal clusters K=2. ....	76
Figure 20. Best clustering solution in R using PAM. ....	77
Figure 21. Best clustering solution in R using Calinski method.....	78
Figure 22. R: Identifying optimal clustering solution.....	79

Figure 23. Plots: connectivity, Dunn Index, and Silhouette Width. ....	80
Figure 24. OptCluster: the optimal cluster solution with iterative runs.....	81
Figure 25. HeatMap data showing differential nitrosylation. ....	82
Figure 26. Shiny Interactive HeatMap application .....	83
Figure 27. Membership changes as the number of clusters is increased. ....	84
Figure 28. fviz function displaying membership changes .....	84
Figure 29. Dendrogram of the hierarchical clustering of proteins.....	85
Figure 30. Scatter plot: No change in SNO at 0.1 Gy with an increase at 4 Gy.....	87
Figure 31. Scatter plot: No change in SNO at 0.1 Gy, no change at 4 Gy .....	89
Figure 32. Scatter plot: No change in SNO at 0.1 Gy, decrease at 4 Gy. ....	91
Figure 33. Scatter plot: Decrease in SNO at 0.1 Gy, increase at 4 Gy. ....	92
Figure 34. Decrease in nitrosylation after 0.1 Gy and 4 Gy irradiation.....	94
Figure 35. Decrease in nitrosylation at 0.1 Gy and no change at 4 Gy irradiation.....	96
Figure 36. Increase in nitrosylation after 0.1 Gy and decrease after 4 Gy .....	98
Figure 37. Scatter plot: Increase in SNO after 0.1 Gy and no change after 4 Gy exposures. .....	99
Figure 38. Increase in nitrosylation following 0.1 Gy and 4 Gy exposures .....	100
Figure 39. PANTHER's Molecular Function classification .....	102
Figure 40. PANTHER's Biological Process classification.....	103
Figure 41. nNOS Pathway Heat Map .....	104
Figure 42. IPA generated nNOS signaling pathway .....	105
Figure 43. Cell to cell signaling, nervous system development network .....	105
Figure 44. R two cluster solution at low and high dose $\gamma$ -irradiation .....	106

Figure 45. Bar Chart of Cluster 1 (decrease in nitrosylation).....	107
Figure 46. Neuropathic Pain Signaling Pathway .....	109
Figure 47. Synaptic Long Term Potentiation Pathway .....	110
Figure 48. CREB Signaling in neurons.....	111
Figure 49. Melatonin Signaling Pathway.....	112
Figure 50. LogR10 Pathway from CL2 (Top) and LogR400 CL2 (bottom). ....	114
Figure 51. Consistent clusters showing differential effect of irradiation.....	115
Figure 52. Different pathways identified with different clusterings of proteins.....	116
Figure 53. Parkinson and EGF Pathways .....	116
Figure 54. ALS, Neuropathic Pain, Synaptic LTP and nNOS Signaling .....	118
Figure 55. Phagosome Maturation Pathway .....	120
Figure 56. Pathway analysis, heatmap and networks .....	121
Figure 57. Diphtamide Biosynthesis Pathway.....	122
Figure 58. TCA Cycle II Pathway .....	123
Figure 59. Top pathways: decrease in SNO at 0.1 Gy and increase at 4 Gy .....	124
Figure 60. ALS signaling Pathway as top reported pathway.....	125
Figure 61. Pharmacological drugs to control the activity of NMDAR.....	126
Figure 62. Disease and Functions and Upstream Regulators .....	126
Figure 63. Western Blot: Modulation of S-nitrosylation by ionizing radiation.....	129
Figure 64. Modulation of S-nitrosylation by ionizing radiation and/or radiocontrast agent. .....	150

## **List of Abbreviations**

AD = Alzheimer disease

ATM = Ataxia telangiectasia mutated

ATR = Ataxia telangiectasia mutated and Rad3 related

c-JNK = c-Jun NH<sub>2</sub>-terminal kinase

COX-2 = Cyclooxygenase-2

Cx = Connexin

DMSO = Dimethyl sulfoxide

DNA-PK = DNA-dependent protein kinase

DRP1 = Dynamin-1-like protein

ERK = Extracellular related kinase

GEF = guanine nucleotide exchange factor

Hsp72 = Heat shock protein 72

IL-8 = Interleukin-8

HZE = High charge (Z) and high energy (E)

LET = Linear energy transfer

MAPK = Mitogen-activated protein kinase

MS= Mass Spectrometry

NAD(P)H = Nicotinamide adenine dinucleotide phosphate

NCAM1= Neural cell adhesion molecule 1

NFκB = Nuclear factor κB

NO• = Nitric oxide

PD = Parkinson disease

RNS = Reactive nitrogen species

ROS = Reactive oxygen species

SOD = Superoxide dismutase

SOM = Self organizing map

TGF- $\beta$ 1 = Transforming growth factor  $\beta$ 1

TNF-  $\alpha$  = Tumor necrosis factor- $\alpha$

## **Publication of Chapters and Role of Author**

This dissertation contains several parts from the following previously published paper. T

**Title:** S-Nitrosylation in Organs of Mice Exposed to Low or High Doses of  $\gamma$ -Rays: The Modulating Effect of Iodine Contrast Agent at a Low Radiation Dose

**Journal:** Proteomes 2015, 3(2), 56-73; doi:10.3390/proteomes3020056

**Authors:** Fadia Nicolas,<sup>1</sup> Changgong Wu,<sup>2</sup> Salwa Bukhari,<sup>3</sup> Sonia M. de Toledo,<sup>4</sup> Hong Li,<sup>5</sup> Masayuki Shibata,<sup>6</sup> and Edouard I. Azzam.<sup>7</sup>

**Author Affiliations:** <sup>1</sup> Department of Health Informatics, Rutgers School of Health Related Professions, Newark, NJ 07107, USA; <sup>2</sup> Department of Biochemistry and Molecular Biology, Rutgers New Jersey Medical School, Newark, NJ 07103, USA; <sup>3</sup> Department of Radiology, Rutgers New Jersey Medical School, Newark, NJ 07103, USA; <sup>4</sup> Department of Radiology, Rutgers New Jersey Medical School, Newark, NJ 07103, USA; <sup>5</sup> Department of Biochemistry and Molecular Biology, Rutgers New Jersey Medical School, Newark, NJ 07103, USA; <sup>6</sup> Department of Health Informatics, Rutgers School of Health Related Professions, Newark, NJ 07107, USA; <sup>7</sup> Department of Radiology, RUTGERS New Jersey Medical School, Newark, NJ 07103, USA

**Author Contributions:** EIA and MS conceived and designed the experiments. FN, CW and SB performed the experiments. MS, EIA, FN, CW, SB, SDT, and HL analyzed the data. MS and EIA wrote the manuscript.

## I Introduction

Living matter on earth has evolved in an environment in which ionizing radiation has been a primordial constituent. Human and non-human biota are continuously exposed to ionizing radiation from natural sources such as cosmic rays, radon decay products in the air, and radionuclides in food and water. Moreover, since Wilhelm Roentgen discovered X-rays in 1895, humans have been exposed to additional radiation from man-made sources, in particular medical diagnostic procedures, which use has dramatically increased in medical practice during the last three decades. In its Report 160 released in 2009, the National Council on Radiation Protection and Measurements in the USA highlighted that medical imaging procedures constitute ~48% of the radiation exposure to the US population, whereas in 1980, they represented only 15% of the annual exposure. Due to this dramatic rise, the effective dose per individual in the US population has increased from 3.6 mSv in 1980 to 6.2 mSv in 2006.<sup>1</sup>

Experimental exposures of human and non-human cells to high doses of ionizing radiation (>100 mSv) have been extensively reported to produce immediate and delayed harmful biological outcomes, including lethal effects and enduring perturbations in metabolic activity that is accompanied by genomic instability in the surviving cells.<sup>2</sup> The adverse health effects of such exposures were described within a few years following the discovery of X rays. Our understanding of their underlying mechanism has greatly advanced during the past five decades.<sup>3,4</sup> In contrast, the question of whether exposures to low doses of radiation (<100 mSv) also induce significant human health risks is a topic of widespread deliberations and remains controversial.<sup>5,6</sup> In its BEIR VII report,<sup>7</sup> the National

Academies of Sciences in the USA concluded that “statistical limitations make it difficult to evaluate cancer risks in humans at doses below 100 mSv”. In effect, cohorts of  $10^9$  and  $5 \times 10^6$  individuals would be required to detect excess risk of health hazards following exposures to 1 or 10 mSv, respectively.<sup>7</sup> In particular, doses in this range are received during mammography ( $\sim 2.5$  mSv), positron emission tomography ( $\sim 3.7$  mSv), technetium-99 cardiac scans ( $\sim 4.4$  mSv), other radiological procedures, and may be received during occupational activities.<sup>1</sup>

### **1.1 Statement of the Problem**

The statistical power of existing human epidemiological studies is limited. As a result, we are unable to determine with confidence whether exposures to low dose ionizing radiation increase (or accelerate) the normal incidence of cancer and degenerative diseases as humans age. Therefore, scholarly bodies considered that mechanistic experimental studies are valuable for elucidating biological effects, and may help reduce the uncertainty in predicting health risks following exposures to low dose ionizing radiation.<sup>7</sup> Clearly, in animal or tissue culture studies, a tight control of many variables (*e.g.*, genetic background, age, gender, stress etc.) that can impact biological outcome is possible. As a result, these studies can contribute to clearer interpretations of existing human epidemiological surveys of health effects, and may reduce the uncertainty in predicting adverse health outcomes.<sup>8,9</sup>

### **1.2 Background**

The background for this thesis project has been described in our publication<sup>10</sup> “To gain insight into the molecular and biochemical events underling the cellular responses at low doses of ionizing radiation, changes were examined in gene expression at the levels of mRNA,<sup>11-14</sup> microRNA,<sup>15,16</sup> and protein<sup>17-19</sup> in rodent and human cells. Here, we build on

these studies but characterize post-translational modification of proteins, an area that is under-studied in the radiation sciences.<sup>20</sup> We used an *in vivo* approach and examined changes in S-nitrosylation in organs of young adult C57BL/6J male mice at 2 weeks following exposure to low (0.1 Gy) or high (4 Gy) acute doses of <sup>137</sup>Cs  $\gamma$  rays delivered to the whole body.

S-nitrosylation is the covalent addition of nitric oxide (NO<sup>\*</sup>) onto the sulfur atom of a cysteine residue to form S-nitrosothiols (SNOs). At normal homeostatic concentration of NO<sup>\*</sup>, nitrosylation is essential for normal protein function, including enzyme activation, protein-protein interactions and cellular trafficking.<sup>21,22</sup> Conversely, aberrant S-nitrosylation has been implicated in oncogene activation<sup>23</sup> and in neurodegenerative diseases.<sup>24</sup> Among the many protein targeted by nitrosylation, several mediate the response to ionizing radiation, including caspases, HIF-1 $\alpha$ , thioredoxin, manganese superoxide dismutase, NF- $\kappa$ B, p53 and Bcl-2.<sup>22,25</sup> Despite the importance of S-nitrosylation in modulating protein function and location, and the well-established knowledge that exposure to ionizing radiation triggers NO<sup>\*</sup> generation,<sup>26,27</sup> the modification by radiation of specific cysteine residues *in vivo* are still vastly unknown. In this study, we characterized S-nitrosylation following parallel exposures of mice to 0.1 Gy of <sup>137</sup>Cs  $\gamma$  rays, which mimics doses that are often received during radiographic scans (*e.g.* computed tomography), or 4 Gy, which may be received during fractionated radiotherapy regimens or unintended exposures. To enhance our understanding of the effects of contrast agents used in imaging procedures, we also analyzed SNO proteins in organs of mice exposed to 0.1 Gy in the presence or absence of iopamidol, which is commonly used in computed tomography (CT) procedures and other X ray examinations” (the results from the studies

with contrast agents have been described in our published paper<sup>10</sup>, and are not further discussed in this dissertation).

### **1.3 Objectives and Goals of the Research**

The goal of the study was to investigate whether similar or distinct nitrosylation patterns are induced following *in vivo* exposure to low (0.1 Gy) or high (4 Gy) doses of Cesium-137  $\gamma$  rays, and to increase knowledge of the changes induced by S-nitrosylation in signal transduction. Bioinformatics tools were used to analyze the results and identify potentially modulated signaling pathways. Using young adult male C57BL/6J mice, the specific aims were as follows:

- 1) To determine if there is a differential effect of low dose ionizing radiation (LDIR) and high dose ionizing radiation (HDIR) on protein nitrosylation long after (13 days) whole body exposure to Cesium-137  $\gamma$  rays.
- 2) To determine whether the differential nitrosylation of proteins affects the molecular mechanisms, pathways and networks leading to either cell survival or cell death under varying conditions of radiation.
- 3) To identify biomarkers that can be used in molecular epidemiological studies, which may provide insight into the health effect of low dose radiation exposures.

The most relevant changes in proteins associated with changes detected at two weeks after low vs high dose irradiation will be investigated. Application of bioinformatics algorithms and pathway analysis will identify proteins with a possible role in conferring resistance and or susceptibility to a high dose of radiation.

## II Literature Review

### 2.1 Radiation Exposure and the Cellular Response

#### 2.1.1 Radiation/Ionizing Radiation

Radiation is a natural physical phenomenon and can be also generated artificially. It consists in the emission or transmission of energy through space. It has existed all along and consists of electromagnetic waves or charged particles. The electromagnetic forms, include radio-waves, microwaves, infrared radiation, visible and ultraviolet light as well as X- and  $\gamma$  rays. The X and  $\gamma$  rays are distinguished from other electromagnetic radiations by their very short wavelength, high frequency and very high energy. Compared to other electromagnetic radiations, they are highly penetrating. When absorbed into biological matter, they lead to localized release of large amounts of energy that results in excitation and ionization events. An *ionizing radiation* is the type of radiation with enough energy to release one or more orbital electrons from an atom or molecule of the absorbing material producing charged atom or molecule called an ion.

While X and  $\gamma$  rays are electromagnetic radiations, energetic electrons, protons, neutrons,  $\alpha$  particles and heavy charged particles are different forms of particulate ionizing radiation.<sup>28</sup> When  $\alpha$ -particle emitters are inhaled or when biological material is traversed by other types of energetic particles, the physical state of the absorbing atoms is also modified due to excitations, ionizations and other events (*e.g.*, fragmentations of the irradiating particles and of the absorbing materials), which deregulates normal biological processes as in the case of electromagnetic radiations,. Although in this project, nitrosylation events in tissues are compared following exposure to  $^{137}\text{Cs}$   $\gamma$  rays, performing

similar studies following exposure to particulate radiations that vary in their biophysical characteristics is also of great interest and is relevant to both radiation protection and radiotherapy. Particulate radiations (*e.g.* carbon ions, protons) are increasingly being used in cancer therapy,<sup>29</sup> and exposure to such radiations may occur during mining activities (*e.g.* uranium mining) and prolonged travel in deep space.<sup>30,31</sup>

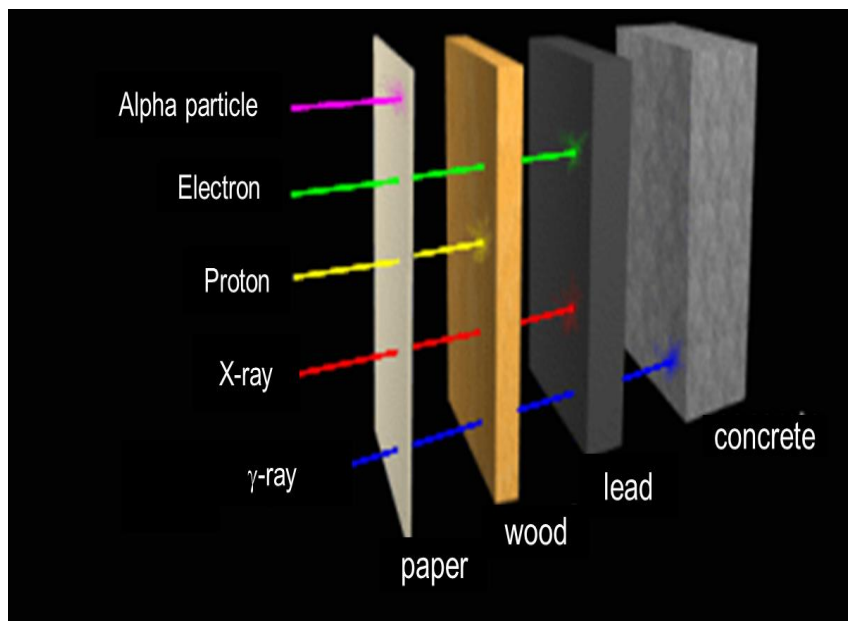


Figure 1. Most common types of ionizing radiation  
The penetration power of a specific radiation type is dependent on its energy.

#### 2.1.1.1 Interaction with Matter

The biochemical changes induced by ionizing radiation and the health effects they may cause depend on the quantity of energy absorbed by the living target mass. They also strongly depend on the spatial distribution of the absorbed energy. For a given dose, the deposition of energy in individual cells and in tissues exposed to X or  $\gamma$  rays is relatively uniform even at low mean absorbed doses ( $\sim 1$  cGy), with every cell receiving a similar

dose.<sup>28</sup> In contrast, the deposition of densely ionizing particulate radiations is non-uniform, particularly at low fluences.<sup>31</sup>

Mammalian cells consist primarily of water (~80% of the constituents). Therefore, a detailed understanding of the radiolysis of water is crucial for interpretation of radiobiological effects. As highlighted earlier in this dissertation, the absorption of ionizing radiations by water molecules results in both excitations and ionizations leading to the production of primary and secondary free radicals. These are short-lived, and in turn are capable of attacking other essential molecules such as DNA, proteins and lipids (indirect effect). A free radical has been defined as “any atom or molecule that has a single unpaired electron in an outer shell”.<sup>28</sup> In biological systems, organic radicals ( $R^\bullet$ ), including DNA radicals, are also formed by H-abstraction reactions (initiated by  $\cdot OH$  radicals for example).<sup>32,33</sup> The primary radiolytic species produced in the radiolysis of pure deaerated water quantitatively are  $e^-_{aq}$ ,  $\cdot OH$ ,  $H^\bullet$ ,  $H_2$ , and  $H_2O_2$ .<sup>34,35</sup>

It is now clear that the initial insult caused by free radicals produced through water radiolysis affects intracellular oxidation/reduction (redox) reactions.<sup>32</sup> For example, ionizing radiation can stimulate the activity of inducible oxidases and nitric oxide synthase (NOS) in the cells with which it interacts.<sup>33</sup> Activation of these enzymes leads to the generation of large amounts of reactive oxygen species (ROS) and reactive nitrogen species (RNS). The primary RNS produced through activation of nitric oxide synthases is nitric oxide ( $NO^\bullet$ ). The ROS and RNS interact with cellular molecules (lipids, proteins and DNA) and can result in major changes in their structure and activity. The ROS and RNS have numerous roles that depend on their concentrations. At normal physiologic levels, ROS/RNS play a significant role in signal transduction functions critical for healthy

survival.<sup>36</sup> However, at abnormal levels, they function as harmful agents and are associated with aberrations in several cellular processes (e.g., cell proliferation).<sup>31,37,38</sup> In summary, ionizing radiation is a strong inducer of ROS and RNS<sup>39</sup> that mediate essential normal processes in concentration, reactivity, spatial and temporal distribution dependent manner. The ROS and RNS may have a role in induction of adaptive/protective responses, or may contribute to expression of a genomic instability in cells that survive the radiation exposure and in their progeny. They may also mediate effects that lead to significant changes in bystander cells that neighbor the irradiated cells.<sup>40-43</sup>

At normal conditions of homeostatic metabolism of oxygen, about 10<sup>9</sup> ROS/cell/day are generated.<sup>44</sup> In contrast to this background level, only a few hundred ROS are produced from water radiolysis due to cellular exposure to low doses of sparsely ionizing radiation.<sup>45</sup> Remarkably, cells perceive this increase and up-regulate signaling pathways to offset the effects of the subtle increase over basal levels in reactive species. At basal homeostatic levels, ROS and RNS control normal cellular functions through a tight control of the redox environment.<sup>32,46</sup> They partake in essential signaling pathways that are critical for normal cell/tissue functions: For example, they contribute to the regulation of expression of specific genes,<sup>47-50</sup> modulation of ion channel activities,<sup>51</sup> and the mimicking/modulation of intermediates (*e.g.* second messengers) in signal transduction.<sup>52</sup> In contrast, at levels that far exceed homeostatic levels, they contribute to deleterious effects.<sup>2</sup>

Exposure to ionizing radiation may also trigger harmful chronic inflammation, which is a dynamic and progressive process associated with excess production of ROS and RNS. Macrophages and neutrophils generate diffusible reactive species, including ROS

and RNS when recruited to inflammation sites. These species can cause a large spectrum of oxidative changes in nearby macromolecules, which results in functional changes to the signal transduction processes that these macromolecules participate in. As would be expected, such changes can greatly affect healthy survival.

#### 2.1.1.2 Units of Dose

The concept of dose has been commonly used to describe radiation exposure.

##### 2.1.1.2.1 Definitions

In the textbook titled ‘Radiobiology for the Radiologist’, Hall and Giaccia report that the “Roentgen is a legacy unit of exposure to ionizing radiation named after Wilhelm Röntgen, the German scientist who discovered X rays in 1895. It is the amount of  $\gamma$  or X rays required to produce ions carrying one electrostatic unit of electrical charge (either positive or negative) in 1 cm<sup>3</sup> of dry air under standard conditions.”<sup>28</sup>

The absorbed dose provides information on the amount of energy deposited by any type of radiation. It is described by the International Commission on Radiological Units and Measurements (ICRU) as the “energy absorbed, at a specific point, per unit mass (inert or living).”<sup>53</sup> The unit used is called the Gray (Gy) in tribute to the British physicist Harold Gray. According to the ICRU “one gray is equivalent to one joule of ionizing radiation energy absorbed per kilogram of tissue.”<sup>53</sup> This is not to be confounded with the equivalent dose measured in Sievert (Sv).<sup>54</sup>

##### 2.1.1.2.2 Dose Equivalency

In radiation protection, the dose equivalent rather than the absorbed dose is used. This stems from the experimental findings demonstrating that at equal absorbed dose, the

induced deleterious effects vary with the type of radiation impinging on living matter, with densely ionizing radiations (*e.g.*  $\alpha$  particles, high atomic number ( $Z$ ) and high energy ( $E$ ) particles) being more proficient at causing damage per unit absorbed dose than sparsely ionizing radiations (*e.g.*, X and  $\gamma$  rays). According to ICRU Report 51, “the dose equivalent is defined as the amount of absorbed dose multiplied by a quality factor or weighting factor ( $W_R$ ) of the type of radiation in question (*e.g.*, the quality factor of  $\alpha$  particles or HZE particles can be as high as 20)”. The dose equivalent is calculated in Sievert (Sv) as an acknowledgment to Rolf Sievert, a Swedish medical physicist who made major contributions to research related to measurements of radiation dose.

### **2.1.2 Low Dose Ionizing Radiation**

A low dose of ionizing radiation has been in general considered as a dose below which there is no significant difference in the frequency of cancers between the irradiated and unirradiated control groups. The United Nations Scientific Committee on the Effects of Atomic Radiation (UNSCEAR)<sup>55</sup> and the National Academy of Sciences in the United States<sup>56</sup> have concluded that the topic of “low dose radiation corresponds to studies of doses below 100 mSv received in a short time”. This dose of 100 mSv represents 0.1 Gy when X or  $\gamma$  rays are considered and 0.005 Gy if the biological material is exposed to  $\alpha$  particles (2-10 MeV). For the studies in this thesis project, wild-type C57Bl/6J male mice were irradiated with either 0.1 or 4 Gy of  $^{137}\text{Cs}$   $\gamma$  rays, which results in uniform irradiation of the whole body, albeit at different levels. Exposure to these doses is expected to result in complex cellular and molecular responses. Depending on the dose, the cellular/tissue responses and modifications can have two outcomes: damage recognition and repair to ensure cell survival or cell death (apoptosis) that can affect tissue function. We hypothesize

that whole body exposure of mice to low dose  $^{137}\text{Cs}$   $\gamma$  rays (0.1 Gy) elicits a protective response in the brain involving modes of intercellular communications, modulation of signal transduction, and the DNA damage response. It results in the induction of genes involved in protective and reparative mechanisms and the down regulation of genes involved in neural signaling activity.<sup>57</sup> We also hypothesize that exposure to high dose of  $^{137}\text{Cs}$   $\gamma$  rays (4 Gy) activates, in the brain, pathways involved in apoptosis and cell death.<sup>57,58</sup>

### **2.1.3 The Linear No-Threshold (LNT) Model**

The biological changes and the health risks to humans from exposures to high doses of ionizing radiation have been inferred through a large body of experimental studies in model systems. They were also derived from epidemiological assessments of survivors of radiation accidents, nuclear workers, radiotherapy patients, and in particular the survivors of the atomic bombs dropped at the cities of Hiroshima and Nagasaki in Japan in 1945.<sup>7</sup> These studies have shown that human exposure to acute high doses causes detrimental health outcomes, including, but not exclusively, cancer induction and degenerative health conditions.<sup>59</sup> In contrast, the health effects of exposure to low doses of ionizing radiation remain ambiguous.

To estimate health risks at low doses, the International Commission on Radiation Protection (ICRP) has adopted a conservative view, and supported the consideration of a linear relationship between radiation dose and cancer risk. In this linear no-threshold (LNT) model, “it is assumed that exposure to any dose of radiation, however small, increases the risk of detrimental health effects. Furthermore, the effects of successive doses are assumed to be additive.”<sup>60</sup> In these prudent suppositions, the extrapolations from data obtained at

high dose radiation were used to estimate the risk at low doses of ionizing radiation (below 100 mSv).

However, the soundness of using this dose-response model has been questioned. In fact, a linear dose response would suggest that similar molecular events mediate the biological effects induced by both low and high doses of radiation, an aspect that this experimental research project has investigated.

According to the French Academy of Sciences, it was judged that, collectively, the various epidemiological studies did not reveal a consistent and significant enhancement in cancer frequency in humans for doses below 100 mSv<sup>61</sup>: *“In conclusion, this report doubts the validity of using the LNT in the evaluation of the carcinogenic risk of low doses (< 10,000 mrem) (= 10 cSv) and even more for very low doses (<1000 mrem) (= 1 cSv)”*.<sup>61</sup> Rather, the members of the committee involved in examining low dose effects concluded that there is a “threshold below which harmful effects are unlikely to arise” (curve **d** in Figure 2).<sup>61</sup> On the other hand, the BEIR VII report of the US Academy of Science<sup>7</sup> and analyses by other scientists (*e.g.*<sup>62</sup>) support the LNT model (curve **a** in Figure 2) as a conservative representation to estimate cancer risk at low doses and to protect vulnerable individuals that may carry genetic predisposition to the effects of radiation. The Committee Members who drafted the BEIR VII report also concurred that “at doses below 100 mSv, statistical limitations make it difficult to evaluate cancer risk in humans.”<sup>7</sup>

Indeed, epidemiological surveys assessing the health effects of low dose radiation require the follow-up of large cohorts of individuals for rather extended periods of time to reveal with confidence the risks of adverse effects. As a result, such epidemiological studies are challenging to perform and may be influenced by modulating factors (*e.g.* diet,

smoking, exposure to diagnostic radiology procedures and/or yet other harmful environmental agents, stress *etc.*) in the intervening years between exposure to radiation and the ultimate development of unfavorable health outcomes.<sup>63</sup> Due to these complications, mechanistic *in vitro* and *in vivo* studies with cultured cells and model animal systems, respectively, have been suggested by different concerned agencies as a resource that would aid in formulating adequate radiation protection standards.

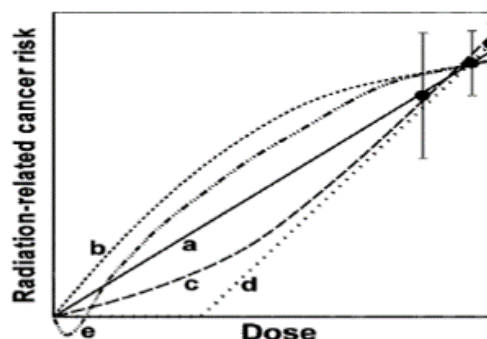


Figure 2. Different possible extrapolations of cancer related radiation risk. Curve a, linear extrapolation; curve b, downwardly curving (decreasing slope); curve c, upwardly curving (increasing slope); curve d, threshold; curve e, hormetic.

During the last three decades, growing evidence has emerged for a number of biological phenomena (*e.g.*, bystander effects, adaptive responses) that may modulate the cellular responses to low doses of ionizing radiation. These phenomena have been suggested to indicate the existence of non-linear biological responses at low doses/fluences of ionizing radiation.<sup>63-68</sup> While bystander effects refer to the spread of biochemical signals leading to biological change from the irradiated to neighboring non-irradiated (*i.e.*, bystander) cells, adaptive responses refer to the induction of mechanisms that prompt the cells to become resistant to subsequent exposures to ionizing radiation or to become protected from the harmful effects of normal metabolism.

Based on experimental evidence for the above mentioned observations and the uncertainty of estimating health risks at low doses of ionizing radiation, diverse models have been developed to describe health risks at various doses.<sup>59</sup> Whereas curve **b** in Figure 2 indicates that the LNT model underestimates risk, curve **c** shows that the LNT model overemphasizes risk. According to the J-shaped curved (curve **e** in Figure 2), exposures to very low doses of ionizing radiation may be beneficial (i.e., hormetic). Therefore, the extrapolation curves **c**, **d** and **e** question the health risk at low dose estimated by the LNT model. Whereas curve **b** likely accounts for the spread of adverse effects at low dose/low fluence from targeted cells/tissues to non-irradiated bystander cells/tissues, endogenous defense mechanisms and stimulatory pro-survival responses may underlie the risk models represented by curves **b** and **e**, respectively.

#### **2.1.4 Limits of Epidemiology**

An extensive number of experimental and epidemiological surveys of humans exposed to high doses of ionizing radiation have shown that such exposures causes significant biological changes and adverse health outcomes. The mechanisms underlying these deleterious effects are relatively well elucidated.<sup>69,70</sup> In contrast, the biological effects and health risks of exposure to low doses of ionizing radiation remain uncertain<sup>71,72</sup> and are a topic that is under intense discussion.<sup>59,62,73,74</sup> As illustrated in Figure 3, cohorts of  $10^9$  and  $5 \times 10^6$  individuals would be required to detect excess risk of health hazards following exposures to 1 or 10 mSv, respectively.

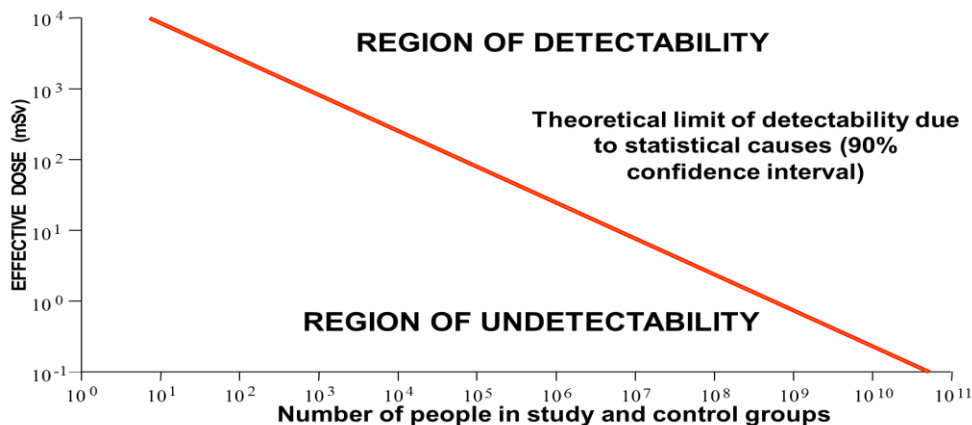


Figure 3. Limits of detectability at low dose radiation. Large cohort of individuals ( $10^7$ - $10^9$ ) are required to detect health hazards at low dose of radiation.

Whether ionizing radiation is harmful at any exposure is a discussion that continues to resonate.<sup>75</sup> While several *in vitro* and *in vivo* studies have succeeded in showing that adaptive protection is often observed at low doses, others failed to confirm such effects. This contrasts with the large body of evidence showing that at high doses, ionizing radiation causes cell death, and substantial DNA damage in surviving cells, which may persist in their progeny. In the long-term, the latter effects often lead to cancer and degenerative diseases. As a result, mechanistic studies have been considered indispensable for the elucidation of biological effects, and to help assess the extent of the health effects of exposure to low doses of radiation. To this end, this thesis project utilizes a proteomic approach to further elucidate the biological changes induced by low and high doses of Cesium-137  $\gamma$  rays.

## 2.2 Protein S-Nitrosylation

Protein S-nitrosylation is a post translational modification (PTM) process involving the addition of a nitric oxide ( $\text{NO}^*$ ) moiety onto cysteine thiols. PTM events usually involve

the modification of proteins during or after synthesis by changing the charge (covalent bond), by enzymatic cleavage/degradation or by adding of other moieties. PTMs is needed to regulate many activities including the interaction between proteins, the response to stress and other stimuli, in signaling and regulating cell processes. Many PTMs are reversible in nature and dictate when and where a cellular process need to be activated or inhibited. In their review of S-nitrosylation, Stamler *et al.*<sup>76</sup> showed that protein S-nitrosylation can affect other PTMs including phosphorylation, acetylation, S-acylation (S-palmitoylation), ubiquitinylation, sumoylation, ISGylation and redox modifications (glutathionylation, sulfhydrylation and Cys oxidations).

The study and analysis of PTMs has emerged as an important field that can lead to understanding the cause of diseases such as cancer, cardiovascular and neurodegenerative disorders.

### **2.2.1 Mechanism of S-Nitrosylation/De-Nitrosylation**

S-nitrosylation (SNO) is indeed an important PTM required to control many cellular mechanisms involved in gene expression and the activation/inhibition of many cellular processes. Central to this type of PTM is nitric oxide (NO<sup>\*</sup>), the chemical messenger capable of reacting with the cysteine residue to form S-NO. Nitric oxide is produced from L-arginine and its generation is catalyzed by nitric oxide synthases (NOS).

S-nitrosylation involves the covalent addition of a nitric oxide moiety to the thiol group of cysteine to form S-nitrosothiol (S-N=O). Thus, a protein becomes nitrosylated when a nitric oxide (NO<sup>\*</sup>) is added to the thiol group (SH). Cysteine plays an important role in maintaining the physiological status of many enzymes, receptors and transcription factors. Keeping the appropriate balance in cysteine's redox state is crucial for the normal

functioning of these proteins. The free sulfhydryl group (-SH) of a cysteine residue reacts easily with reactive oxygen/nitrogen species, and is indicative of the level of cellular oxidative stress. Post-translational modifications of reactive cysteines, such as S-nitrosylation and thiolation (addition of an SH group) control cell signaling. In particular S-nitrosylation can regulate many physiological processes.

S-nitrosylation and S-nitrosation have been interchangeably used in the literature as both refer to the addition of a nitric oxide to the thiol group. Nitrosylation involves the addition of a nitrosyl ion  $\text{NO}^-$  to a thiol, leading to the formation of the S-nitrosothiols (SNOs). Nitrosation on the other hand is the addition of a nitrosonium ion  $\text{NO}^+$  to an amine  $-\text{NH}_2$  leading to a nitrosamine.

Nitric oxide participates in various cellular signaling pathways to regulate a spectrum of neuronal functions such as development, synaptic plasticity and apoptosis. If high level of NO is produced (exogenous), this will lead to the nitrosylation at the site of the free thiol group. Close proximity usually dictates the thiol group's nitrosylation. The closer a thiol group is to the site of NOS, the more likely it will become nitrosylated. Not all cysteines in a protein are equally susceptible to S-nitrosylation. Various factors affecting susceptibility include acidic pKa, protein localization, and protein-protein interaction. At nanomolar concentration, NO contributes to the regulation of various processes in the brain, by producing the level of ROS/RNS in small amount but sufficient to affect diverse intracellular signaling pathways.<sup>77</sup> The balance of ROS/RNS production, antioxidant enzymes and other molecules influence the NO level in the brain. NO in the brain can act as neuroprotective or neurodestructive depending on the timing, duration and level of its concentration.

Nitric oxide synthases are crucial in controlling the process of nitrosylation. Three different types of nitric oxide synthases are known to be abundant in specific tissues:

- eNOS type 3: This enzyme is enriched in the smooth muscle and is involved in controlling vasodilation.
- nNOS type 1: This enzyme is found in the skeletal muscle and in neurons. It plays a role in neurotransmission, and synaptic signaling.
- iNOS type 2: This enzyme is produced in response to endotoxins and cytokines. It is an inducible nitric oxide synthase with usually a transient presence.

These NOS enzymes require oxygen, NADPH, and tetrahydrobiopterin as cofactors. The enzymatic activity of iNOS is transcriptionally regulated while the activities of nNOS and eNOS is dependent on calcium.<sup>78</sup> Nitric oxide can also be produced in a NOS independent mechanism by the action of nitrite reductases.<sup>79</sup>

Denitrosylation (removal of the NO group) can occur spontaneously in addition to being enzymatically controlled.<sup>76</sup> Some SNO proteins can spontaneously lose the NO group from their Cys thiol in a non-enzymatic manner. S-nitrosylation is a reversible reaction, and SNOs have a short half-life in the cytoplasm because of the host of reducing enzymes, including glutathione (GSH), S-nitrosogluthathione reductase (GSNOR) and thioredoxin that denitrosylate proteins. GSNOR enzyme, acts only on S-nitrosogluthathione (GSNO) (protein-SNOs are not substrates), and it indirectly affects protein S-nitrosylation by modulating the equilibrium between protein-SNO and GSNO. To preserve their activity, SNOs are usually sequestered in membranes, protein folds or in vesicles.<sup>80</sup> For example, an important family of proteins in apoptosis, caspases, are stored in the mitochondrial intermembrane space as SNOs. Caspase activation and induction of apoptosis are achieved

by rapid denitrosylation that occurs when the caspases are released to the cytoplasm in response to extra- or intracellular stimuli.

#### 2.2.1.1 Detection of S-Nitrosylation

The S-NO bond is very labile making it hard to identify the sites of nitrosylation.<sup>81</sup> Several methods have been developed to detect S-nitrosylation. All the methods listed below can detect nitrosylation. However, mass spectrometry (MS) is the only method, used downstream, that is capable of detecting the specific sites of nitrosylation<sup>82</sup>:

- Direct method: SNO specific antibody<sup>82,83</sup>
- Indirect methods: Biotin Switch Technique.
- Gel based methods (fluorescence): examples are S-FLOS, SNOflo, SNO-DIGE, Nitro DIGE
- MS based isotopic labeling methods: ICAT, SILAC
- MS based isobaric labeling: SNO-RAC, CysTMT, indoTMT

The current analysis was done by the CAPR (Center for Advanced Proteomic Research-Rutgers), for the identification, relative to control, of S-nitrosylation in brains of mice exposed to  $\gamma$  irradiation using the Biotin Switch assay and Mass Spectrometry.<sup>84</sup>

#### 2.2.1.2 Biotin Switch Technique (BST)

The BST analysis is done to identify nitrosylated proteins and their nitrosylation sites.<sup>85</sup>

The biotin switch technique encompasses 3 main steps:

1. Blocking and alkylating the free thiols using sulfhydryl reactive compounds (MMTS).
2. Selectively reducing the nitrosylated residues with ascorbate.
3. Labeling and detecting the free thiols with the thiol reactive biotinylated reagents.

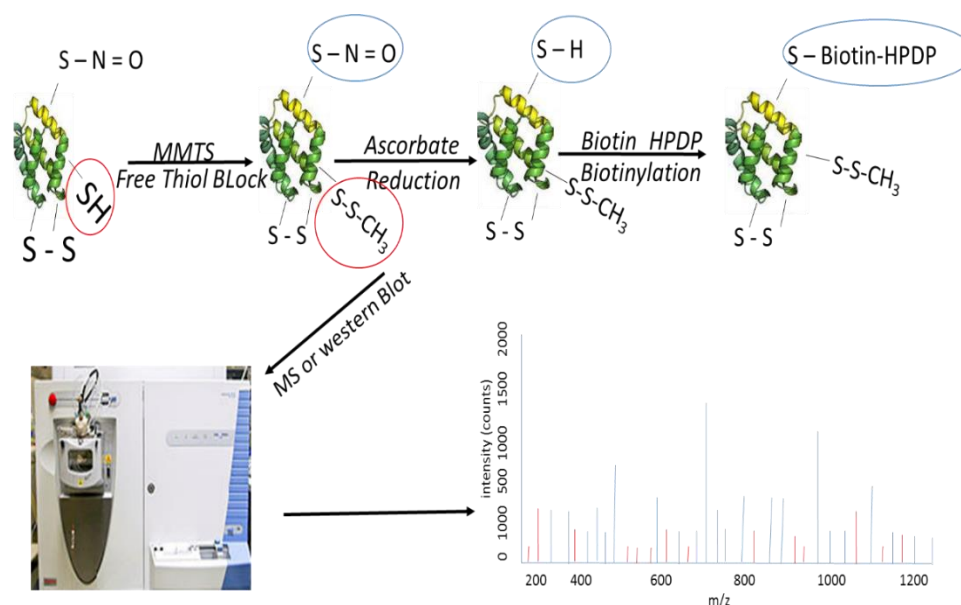


Figure 4. Biotin Switch Technique.

The Biotin Switch Technique for detection of S-nitrosylation: (1) Blocking, (2) Reducing and (3) Labeling with Biotin. Mass Spectrometry is done to identify SNO sites and peak matched against databases like Mascot.

In the biotinylation step, HPDP-Biotin, which is a pyridyldithiol-biotin compound, is added for labeling reduced thiols (-SH) by forming reversible disulfide bonds. For example, a biotinylated protein can be captured to a streptavidin column. The dithiothreitol reduction of disulfide bond allows us to recover the original target protein that was S-nitrosylated. During this step, the protein mixture is reconstituted with biotin-HPDP with or without ascorbate as control.

Zareba-Kozioł *et al.* (2014)<sup>86</sup> summarized the finding of Nakamura *et al.* (2013)<sup>24</sup> and Kohl *et al.* (2011)<sup>87</sup> on the factor of S-nitrosylation site as follow. “The key factors determining S-nitrosylation sites in proteins are: (i) spatial proximity (i.e. complexing with nNOS regulates the S-nitrosylation of *N*-methyl-D-aspartate-type glutamate receptors or NMDARs) and postsynaptic density protein 95 (PSD 95)), (ii) presence of signature SNO

motifs adjacent to target Cys residue, and (iii) local hydrophobicity (i.e. closeness to the membrane)".<sup>24</sup>

### 2.2.2 S-Nitrosylation in Controlling Brain Function

Under normal neuronal physiology, S-nitrosylation functions to maintain cell differentiation, development, and survival. Nitrosylation of caspases and HDAC2 (histone deacetylase 2) for example is needed for normal neuronal function. Caspase-3, which has a role in apoptosis, is constitutively S-nitrosylated under basal conditions, thereby inhibiting its protease activity and preventing cell death. However, in apoptotically stimulated neurons, the thioredoxin (Trx) system de-nitrosylates caspase-3 to amplify cell death signaling.<sup>24</sup> The Trx system is a class of enzymes exhibiting denitrosylase activities. It comprised of Trx1 or Trx2, cytosolic Trx reductase (TrxR), mitochondrial TrxR, and NADPH.

Nakamura and Lipton (2016)<sup>88</sup> stated the following in describing the biological consequences of S-nitrosylation:

“In addition, when NO production is moderately increased after exposure to mild neurotoxic stimuli, NO can still mediate neuroprotective effects. In part, this effect is mediated by S-nitrosylation of overly excited NMDARs or the redox-sensitive chaperone and peptidase protein DJ-1 (Parkinson protein 7/PARK7).<sup>89-91</sup> These nitrosylation reactions serve as a form of negative feedback on degenerative processes. For instance, S-nitrosylation of NMDARs downregulates their excessive activity and can thereby provide neuroprotection in experimental models of neurodegenerative conditions.<sup>89,91-94</sup> Consistent with this idea, hypo-S-nitrosylation of NMDARs under mild stress can aggravate pathological processes as a result of the lack of NO neuroprotective effects.<sup>95</sup>

By contrast, excessive production of NO can result in aberrant protein S-nitrosylation, even reacting with cysteines lacking the full nitrosylation motif, and thus contributing to the progression of neurodegeneration. Persistent hyperactivation of extrasynaptic NMDARs or increased iNOS activity in glial cells can typically result in overproduction of NO. Aberrantly formed SNO-proteins occurring under pathological nitrosative stress include, to name but a few, SNO-MEF2

(monocyte enhancer factor 2), -parkin, -PDI, -GAPDH, -XIAP, -CDK5 (cyclin-dependent kinase 5), and -DRP1 (dynamin-related protein 1/DNM1L). Our group and others have demonstrated that these SNO-proteins indeed accumulate in the brain of patients with neurodegenerative diseases (but not of controls), contributing to an array of degenerative processes such as protein misfolding (e.g., mediated by SNO-parkin and SNO-PDI), mitochondrial dysfunction (SNO-MEF2, SNO-DRP1, and SNO-parkin), synaptic damage (SNO-DRP1, SNO-CDK5, and SNO-MEF2), and neuronal cell death (SNO-MEF2, SNO-PDI, SNO-GAPDH, SNO-XIAP, and SNO-DRP1).<sup>96-102</sup> In addition, NO inhibits cGMP production via S-nitrosylation of sGC, possibly representing a negative-feedback loop to suppress the sGC/cGMP pathway.<sup>103</sup>

Other types of stressful conditions seen in studies of mouse brain (like TBI, traumatic brain injury), showed that iNOS played a major role as an antioxidant and contributes to the increase in the amount of nitrosylated proteins.<sup>104</sup>

Switzer *et al.*,<sup>23</sup> have shown that oncogene activation included the S-nitrosylation of Ras in breast cancer that is negative for the estrogen receptor (ER). Nitric oxide also activated the Ras/MEK/ERK pathway and protein Ets-1 was one of the key transcriptional mediator of oncogenic NO signaling. Other S-NO modified proteins include bd-2 (beta-defensin-2) in lung cancer, the death receptor FAS in colon and breast cancer and the associated FLICE inhibitor protein (FLIP) and caspase 9 in cholangiocarcinoma cells. In contrast, the p53 protein was found to be inactivated by NO in cancerous cases like melanoma.

In their review of protein S-nitrosylation, Li *et al.*<sup>105</sup> investigated the role of thioredoxin 1 (Trx1) in transnitrosylation and denitrosylation of target proteins, in particular those involved in the apoptotic process. For example, proteins identified as stimulating apoptosis after being nitrosylated included glyceraldehyde-3-phosphate dehydrogenase and Fas. Conversely, S-nitrosylation of proteins like capsase-3 and Bcl-2 inhibited apoptosis. In another study, Feng *et al.*<sup>106</sup> showed that S-nitrosylation regulates

Extracellular Signal Regulated Kinase (ERK) activity, a member of the mitogen activated protein kinase (MAPK) family. S-nitrosylation by nitric oxide inhibits ERK phosphorylation and triggers the apoptotic process. Thus S-nitrosylation of ERK is important in its regulation and its involvement in apoptosis and tumor development.

Wang *et al.*,<sup>107</sup> studied the role of S nitrosylation in the aberrant modulation of mitochondrial function, protein misfolding, synaptic loss and amyloid  $\beta$  production. They showed that excessive protein S-nitrosylation inhibited protein activity, thus compromising mitochondrial function as the source for energy production. One protein Drp1 (dynamin related guanosine triphosphatase) was shown to increase in nitrosylation in Alzheimer Disease (AD). This protein mediates membrane fission in the mitochondria (breaking down the mitochondria and its organelle leading to apoptosis), and an increase in its nitrosylation at Cys644 results in inhibition of its function. In addition, the enzyme superoxide dismutase (SOD), which scavenges superoxide anion radicals that are toxic to biological systems when in excess, can also be nitrosylated resulting in its inability to play a role as antioxidant (especially in mitochondria).<sup>108</sup> Interestingly, SOD levels were shown to be increased in AD, and it would be of interest to investigate whether this is in compensation to reduced activity as a result of nitrosylation of the protein. In addition, the brain of AD patient harbors many targets for nitrosylation, and SNO was increased in proteins related to the amyloid precursor protein, resulting in neurodegeneration and plaque formation (Tau nitrosylation).<sup>109</sup>

#### 2.2.2.1 Targeting SNO for Pharmacological Purposes

The two examples below show how the nitrosylated pathways can be manipulated in order to provide pharmacologically useful drugs to treat diseases:

- Inhibition of NMDAR with NitroMemantine: The drug NitroMemantine is a pharmacologically synthesized molecule that results in the addition of NO<sub>2</sub> to NMDA receptors and is used to diminish their hyperactivation, especially when they are extrasynaptic. The drug can either sit between the 2 subunits of NMDAR (GluN1 and 2) blocking the associated ion channel, or by having the nitro group of the drug react with the redox sensitive thiol group on the surface of the NMDAR. Note that excessive concentration of glycine and glutamate (agonist) triggers the physiological activation of NMDAR (Figure 60).
- Deprenyl is a drug that may exert a protective action through its antioxidant effects or prevention of GAPDH nuclear translocation brought by increased formation of GAPDH/Siah complex through nitrosylation of GAPDH. Thus, deprenyl exhibited potent neuroprotective activity in PD models (effect not duplicated in human models/clinical trials). Pharmacologic blockade of the GAPDH mediated apoptotic cell death cascade by preventing GAPDH/Siah complex formation may be useful in neuroprotection.<sup>110</sup>

### 2.2.3 Ionizing Radiation and Nitrosylation

Ionizing radiation causes the generation of large amounts of ROS and RNS<sup>33</sup>. These species may mediate adaptive/protective responses or alternatively genomic instability in progeny of irradiated cells and their neighboring bystander cells.<sup>40-43</sup> Recent studies by Masaki *et al.*,<sup>111</sup> showed that ionizing radiation increased the level of nitrosylation in endothelial cells (hind legs of mice) resulting in increased partial oxygen tension (pO<sub>2</sub>) in tumor cells and increasing tumor sensitivity to radiotherapy. Inhibition of nitrosylation by the addition of the inhibitor L-Name decreased the anti-tumor effect of ionizing radiation. This study

showed that ionizing radiation affects the nitrosylation levels of proteins and plays a role in tumor sensitivity and progression.

Homeostatic ROS/RNS levels are essential for maintaining normal cellular functions. They have a role in regulating the expression of specific genes,<sup>47-50</sup> modulating ion channel activities,<sup>51</sup> and mimicking or affecting intermediates (*e.g.* second messengers) in signal transduction.<sup>52</sup>

Under low dose ionizing radiation ( $\gamma$  rays  $\leq 0.1$  Gy) exposures, mechanisms are activated to counteract the damage and ensure cell survival by triggering specific apoptotic pathway when needed to clear damaged cells.<sup>58</sup> Herman *et al.*, found that low dose ionizing radiation (LDIR) resulted in dose dependent activation of NF $\kappa$ B and manganese SOD2 in mouse brain.<sup>112</sup> Another study by Guan *et al.*, showed that S-nitrosylation can play a role in suppressing radiation induced apoptosis.<sup>113</sup> LDIR was also found to play a protective effect against neurodegeneration by up-regulating the antioxidative gene peroxiredoxin-2 (Prdx2).<sup>114</sup> However when Prdx2 becomes S-nitrosylated (cysteines C51 and C172) by reacting with NO, its reaction with peroxides is inhibited. S-nitrosylation of Prx2 inhibited its protective function and led to increased oxidative stress by preventing its reaction with peroxides, which may have contributed to neuronal cell death and the neurodegeneration observed in PD.<sup>115</sup>

ERK (extracellular signal-regulated kinase) belongs to the MAPK (mitogen activated protein kinase superfamily) is S-nitrosylated by NO resulting in an inhibition of its phosphorylation and results in apoptotic activation and has a role in tumor development. Feng *et al.*,<sup>106</sup> identified Cys183 as a potential S-nitrosylated site in ERK. In addition, Guan *et al.*,<sup>113</sup> showed that cellular exposure to radiation resulted in increased anti-apoptotic

activity of MKP (mitogen Kinase phosphatase) by S-nitrosylation on cysteine 258. MKP-1 inactivated MAPK signaling by dephosphorylating ERK, JNK, and p38 (JNK and p38 are members of the MAPK pathways). In addition, MKP-1 selectively dephosphorylates  $\gamma$  radiation mediated activation of JNK but not ERK.

Under hypoxic conditions tumor cells undergo mutations which render them resistant to ionizing radiation. Hypoxia inducible factor (HIF-1), is one of the proteins involved in the adaptation of neoplasm to hypoxia. The vascular endothelial growth factor (VEGF) is also an angiogenic factor in endothelial cells protecting them from apoptosis by activating Raf signaling pathway. Radiation causes an increase in the expression of VEGF through MAPK pathway.

CD-31 is a platelet endothelial cell adhesion molecule, and HPSE-1 is a heparanase with a critical role in tumor angiogenesis and metastasis. Zhang *et al.*,<sup>19</sup> studied the effect of ionizing radiation on the expression of these proteins. At low dose of radiation HIF-1 and HPSE-1 were inhibited improving tumor hypoxia. In contrast, the higher dose upregulated HIF-1, HPSE-1, VEGF and CD31 worsening tumor hypoxia. It was also noted that HIF-1 had an enhanced stability due to its nitrosylation by NO. The authors hypothesized that a development of a protocol of low dose radiation followed by high dose might improve tumor hypoxia and enhance radiosensitivity.

Katsura *et al.*,<sup>116</sup> investigated the effect of chronic low dose irradiation on neural progenitor cells (31, 124, 496 mGy from cesium-137  $\gamma$  rays delivered over 72 hours). The study showed that gene expression was dose dependently changed. Inflammation pathways were reported to be activated at 31 mGy. DNA repair and cell adhesion molecules were

altered at 124 mGy while DNA synthesis, apoptosis, metabolism and neural differentiation were affected by 496 mGy.

The enzymes GADPH (glyceraldehyde-3-phosphate dehydrogenase), lactate dehydrogenase A and MCT1 (monocarboxylate transporter) become highly expressed in breast cancer cells maintained in culture and their activation is increased by high dose radiation (6 Gy of X rays). These enzymes play a critical role in glycolysis (conversion of pyruvate to lactate) and their activation results in senescence of the cancer cells.<sup>117</sup> Pathways found to be induced by radiation included: AMPK (monophosphate-activated protein kinase), nuclear factor B (NF- $\kappa$ B) to promote senescence. GADPH undergoes also nitrosylation under stress induced apoptosis. This will trigger GADPH to bind to Siah1 (an E3 ubiquitin ligase) and translocate to the nucleus.<sup>99</sup> S-nitrosylation plays a role in tyrosine phosphorylation of CBL by linking CBL to the insulin receptor. It is required for insulin-stimulated glucose transport and is involved in formation of actin stress fibers and focal adhesions. It is clear from these studies that high dose (4 Gy) X ray exposure activates pathways involved in apoptosis and cell death.<sup>58</sup>

### **2.3 Bioinformatic Analysis of S-Nitrosylation**

Using bioinformatics tools and accumulated knowledge base can facilitate, automate, and standardize the analysis of proteomic data. In this thesis, the aim is to obtain functional interpretation of proteomics data and to examine what “omics” tools are best suited for this task. Bioinformatic analysis of proteomic data can consist of the following 3 steps<sup>118,119</sup>: 1) To distinguish the abundance level of proteins (proteins exhibiting similar increase or decrease in expression compared to a reference set). Statistical analysis is applied in this case to distinguish differential expression, and an optimal threshold is

usually set to remove noisy data while keeping a balance of sensitivity and specificity. 2) Meaningful grouping (Clustering) of the high dimensional data is done next to select the optimal number of clusters and translate each group of differentially expressed proteins into a functional biological insight. 3) To predict or identify protein sets that have different biological function (normal pathological vs. disease state) and the biomarkers characterizing them. Steps 2 and 3 are accomplished by applying ontology and pathway analysis to each group of the proteins. In a study by Rabilloud *et al.*,<sup>118</sup> pathway analysis was highlighted as an important tool to deal with massive proteomic data. Wu *et al.*,<sup>119</sup> also identified two main approaches in pathway analysis: Integration of functional information (aggregating genes and proteins according to their function) and integration of topological information (regulatory relationship). Rich features in the 2 areas will greatly enhance and streamline the analysis of the complex molecular mechanisms in proteomic data. The following section describes the bioinformatics software used to analyze the data, perform the clustering and identify biologically significant groups for functional and pathway analysis.

### **2.3.1 R and Bioconductor for Proteomic Studies**

R is an open source statistical programming with broad use in computational biology and bioinformatics (<http://www.bioconductor.org/>). R has an exponentially growing number of data analysis packages. Data can be quantified using the extensive statistical software built into R (relative label free and labelled quantitation), and can be visualized via plots to assess the intrinsic features at many levels. Because this software is open sourced, new packages extending the statistical capabilities of R are developed and become readily accessible to all users through repositories such as the Comprehensive R

Archive Network (CRAN) and Bioconductor. A variety of R packages providing tools for cluster analysis are found at these repositories as well as cluster validation measures.<sup>120</sup>

### 2.3.1.1 Statistical Analysis

The extensive statistical packages in R are used to test whether the proteins are differentially expressed with sufficient confidence. Examples of R statistical functions include Summary () function, Describe () function, Scale () function, and Parametric vs. Non-Parametric analysis. Several clustering algorithms are tested and the results obtained leads to which cluster produces efficient functional and network associations. The R statistical packages have been shown to be essential in genomic studies and study of post-translational modification including S-nitrosylation. In 2012, Guo *et al.*<sup>121</sup> used R to analyze the vasculome of the mouse brain. They used RMA algorithm (Robust Multi-Array Average), a technique used for Affy data normalization (DNA microarray chips developed by Affymetrix) where the amount of probe binding to an RNA target on a microarray chip is measured and only data with expression above a certain threshold were kept for further analysis. The enriched pathways from the selected genes were identified using the Fisher's exact test. The analysis showed that under nitrosative stress the glutamate receptors (Gria2, Gria3, Grin2b and Grm5 for AMPA2, AMPA3, NMDA2B and mGluR5 respectively) become over activated and can lead to excitotoxicity in neuronal compartments.<sup>121</sup> In a study by Foggia,<sup>122</sup> the Bioconductor QualiMetric package was used to detect outlier and the famous Limma package to identify differentially expressed genes. In the study, overexpression of the Polycomb group (PcG) protein Bmi1 was found to be mediated by metallothionein 1 (MT1)–driven modulation of resistance to oxidative stress in the satellite cell population (stem cell). These changes led to a remarkable improvement

of muscle function in a mouse model of Duchenne muscular dystrophy. Overexpression of Bmi1 results in reduced nitrosylation of the Mef2c protein, which is important in muscle regeneration but whose action is inhibited by nitrosylation.<sup>122</sup>

#### 2.3.1.2 Cluster Analysis

Clustering the proteomics data divides the data into subsets where each subset has maximum similarity of data within the subset and maximum dissimilarity with other subsets. Different methods are employed to accomplish the clustering of data and the choice depends on the type of data and study under analysis.

The common clustering models used are the centroid model (k-means, fuzzy c-mean) and the connectivity model (Self-organizing map, hierarchical clustering) based on distance connectivity.

##### 2.3.1.2.1 K-means Clustering

This algorithm classifies a dataset via a specific number of clusters (k clusters). A centroid for each cluster is defined as to separate the groups. Each point under each dataset is then associated with the nearest centroid. A loop is generated where the k centroids alter their location gradually until no more changes are created. The final result is the clusters belonging to their corresponding centroid.<sup>123</sup>

##### 2.3.1.2.2 Fuzzy c-Means Clustering

Fuzzy clustering means that the data grouped into one group is not hard but fuzzy, meaning that the data can belong to more than one group (as opposed to hard clustering where the data belongs to only one group). This is one of the most used clustering algorithms where a membership value is associated with each element. In fuzzy means we have a dataset of

N elements divided into a group of c-fuzzy clusters. The outcome is a set of clusters with a partition matrix W and a degree to which each member belongs to a cluster.<sup>124</sup>

#### 2.3.1.2.3 Self Organizing Maps

Self-Organizing Maps (SOMs) are a type of artificial neural networks that is trained using unsupervised learning. They have two modes, one for training and one for mapping the data. The training mode constructs a map using input examples while the mapping classifies a new input vector.<sup>125</sup> SOM has been used to identify protein profiles in response to various stimuli, which aid in understanding molecular pathways and assist in the development of more effective drugs.<sup>126</sup> Katsura *et al.*,<sup>116</sup> used bioinformatics tools including clustering, heatmap and SOM to identify differentially expressed genes affected by different doses of radiation in neural progenitor cells.<sup>116</sup>

#### 2.3.1.2.4 Hierarchical Clustering

In this method, a hierarchy of clusters is built. The strategy falls into two categories: Agglomerative and divisive. Agglomerative approach (agnes) is a bottom-up technique where pair of clusters are merged together as they move up the hierarchy, while divisive (diana) clustering is a top-down approach where the clusters are split recursively as they move down the hierarchy. The two categories are determined based on the greedy algorithm and are represented by a dendrogram. The greedy algorithm attempts at finding an optimal solution using the minimum number of steps. Hierarchical clustering (HC) is widely used in analyzing the differential expression of genes/proteins. Many studies have relied on this technique. In their radiation research, Oh *et al.*,<sup>119,127</sup> used HC to cluster gene sets that are differentially expressed due to radiation and compare the cluster to the gene

sets differentially expressed due to chemotherapy. They were able to identify a set of 30 genes with predictive information for disease prognosis.<sup>127</sup>

### 2.3.1.3 Distance Measures

In measuring the closeness of two clusters, three methods are widely used: the average linkage (distance between the means of two clusters), the complete linkage (maximum distance between the elements of each cluster) and the single linkage (minimum distance between the elements of each cluster). The following distance measures are implemented in R.

#### 2.3.1.3.1 Euclidean Distance

It measures the length (shortest path) of the line connecting two vectors (x, y) using the Pythagorean formula. The x and y are subtracted directly from each other and converting the values to log ratios is needed to handle negative values.

#### 2.3.1.3.2 Manhattan Distance

It computes the distance between 2 points based on the sum of a strict horizontal or vertical line.

#### 2.3.1.3.3 Pearson Distance Correlation

This is the most commonly used and it is a parametric distance measure that depends on the data distribution (whether data is normal or not). Gene Pattern software web site<sup>128</sup> at Broad Institute describe it as “Pearson's correlation coefficient between two variables is defined as the covariance of the two variables divided by the product of their standard deviations. It is a measure for how well a straight line can be fitted to a scatter plot of x and y. If all the points in the scatter plot lie on a straight line, the Pearson correlation coefficient

is either +1 or -1, depending on whether the slope of line is positive or negative. If it is equal to zero, there is no correlation between x and y.”

#### 2.3.1.3.4 Spearman Rank Correlation

This distance is an example of non-parametric distance measure. It is more robust against outliers than the Pearson measure. Each data value is replaced by their rank when the data in each vector is ordered by values. The correlation between the 2 rank vectors is then calculated.

#### 2.3.1.3.5 Eisen Cosine Correlation

It measures the cosine angle between 2 vectors. It is thus a judgment of orientation and not magnitude.

#### 2.3.1.3.6 Kendall Correlation

It measures the correspondence between the ranking of x and y. This is another non-parametric distance measure.

#### 2.3.1.4 Selecting a Clustering Algorithm

Different clustering algorithms can result in different groupings of the data. It is therefore important to determine the best methodology to group the proteomic data. R provides many tools pertaining to this task, from analyzing the clustering feasibility to selecting the best number of clusters. Many packages are available with indices used to determine the optimal number of clusters. The indices include the Gap statistic, the silhouette method, Hartigan, Hubert and up to 26 other indices.<sup>129</sup> In addition, the OptCluster package was recently added to R with the purpose of finding the best clustering solution.<sup>130</sup> The last step in cluster selection is the validation and this is done with the R package clValid.<sup>131</sup>

#### 2.3.1.4.1 clValid

The clValid package offers nine different cluster validation measures and can create ranked lists of clustering algorithms based on the calculated validation scores for each validation measure chosen.

#### 2.3.1.4.2 NbClust

The package NbClust<sup>129</sup> provides two clustering algorithms and thirty cluster validation measures to determine the relevant number of clusters in a dataset. The “best” choice for number of clusters is determined by a majority rule. The Calinski criterion for cluster validation will also be selected as an example for the validation.<sup>132</sup> The Calinski-Harabasz index (*CH*) measures separation based on the maximum distance between cluster centers, and measures compactness based on the sum of distances between objects and their cluster center. The result is a choice of the best clustering solution in the data.

#### 2.3.1.5 R for the Analysis of S-Nitrosylation

Although R has been extensively used in analyzing proteomic data in general, its use in nitrosylation related studies has only emerged as recent as 2013. Niranjani *et al.*,<sup>133</sup> analyzed the redox changes in plants due to ozone and drought stresses. Statistical package in RStudio was used to identify differentially affected genes by Reactive Oxygen Species (ROS) and Reactive Nitrogen Species (RNS), which helps in elucidating induced defense mechanism(s). Delobel *et al.*,<sup>134</sup> studied red blood cell exposure to oxidative stress and cysteine modification after prolonged storage at 4°C (6-41 days). Their study showed that all cysteines in proteins are not equally affected by oxidation. Some proteins' extreme oxidation leads to an irreversible state while other proteins are not affected by oxidation. For irreversible oxidation, the antioxidant enzyme catalase was found to be the target of

the oxidative cysteine alteration while the enzymes peroxiredoxin-1 and DJ-1 were the target of reversible cysteine oxidation. They used R statistical package and one way ANOVA to analyze oxidation and nitrosylation of cysteine residues. Tran *et al.*,<sup>135</sup> studied the effect of sphingosine-1-phosphate action in Duchenne muscular dystrophy (DMD) model in *Drosophila*. Their result showed that an increase in the level of bioactive SP1 and the decrease in the HDAC protein suppress dystrophic muscle degeneration. This process is due to the fact that HDAC's activity is reduced through its nitrosylation by NO, a product of nNOS in DMD. Nguyen-Tran et al. (2014)<sup>136</sup> reported that “The nNOS localizes to the normal DGC (dystrophin glycoprotein), but is mislocalized in individuals with DMD because of the defects in the DGC,<sup>137</sup> which results in lower NO levels in the nucleus. Lack of NO in the nucleus of mdx mice has been shown to increase HDAC2 activity and consequently silences key muscle genes, whereas increased levels of NO can rescue dystrophic phenotypes in mdx mice.” In the study, RStudio was used to generate density blots for gene expression in control and SP1 injected muscles.

### 2.3.2 Gene Ontology

This step of the analysis is done to elucidate the functional interpretation and functional enrichment in the data.<sup>138</sup> A summary of the overrepresented protein functions is produced displaying the global findings instead of individual protein entries. Network analysis will complement the functional study and map the individual proteins to a network or pathway.<sup>139</sup> Proteins found to participate in the same network with similar ontologies and similar expression can lead to new discoveries and hypothesis in a proteomic experiment.

Chen *et al.* (2016),<sup>140</sup> used gene ontology to analyze Global S-nitrosylation of proteins in brain tissues of different human prion diseases. The study revealed the changes

in function of the differentially nitrosylated proteins in the disease state vs physiological state. Pathway analysis also identified the most commonly affected pathways.

#### 2.3.2.1 The PANTHER (Protein Analysis Through Evolutionary Relationships)

The PANTHER database<sup>141</sup> is a database that can be used to classify genes and proteins using 4 different categories: evolutionary group based on protein family and subfamily, molecular function, biological process or participating in similar pathways. It is part of the GO (Gene Ontology) reference genome project, and is curated following a rigorous classification algorithm.<sup>141</sup> In addition to classification, PANTHER has a tool for enrichment analysis of genes/proteins where the dataset can be uploaded along with the expression values, and the user can analyze which pathways are enriched in the data.

PANTHER is a widely used database in proteomic research. It is a valuable tool in categorizing proteins and analyzing their relationships. Many studies have relied on PANTHER for pathway and functional correlation analysis. For example, Sievert *et al.*<sup>142</sup> used quantitative proteomics and PANTHER analysis to identify novel radiation target in the *Mus musculus* heart. The largest group in their data had a catalytic molecular function and the proteins involved in receptor activity and antioxidant defense were more prominent following exposure to high dose radiation.

#### 2.3.3 Network and Pathway Analysis

Sun *et al.* (2013)<sup>143</sup> explained the Ingenuity Pathway Analysis in the following manner.

“Ingenuity Pathways Analysis (IPA; <http://www.ingenuity.com>) is a web-based software application that identifies biological pathways and functions relevant to bio-molecules of interest. To scrutinize the systematic influence of the treatment related metabolites, we uploaded the metabolite lists (with KEGG IDs) and the change directions of these metabolites onto an IPA server. Canonical pathways and molecular interaction networks were generated based on the knowledge sorted in the Ingenuity Pathway Knowledge Base. A ratio of the number

of metabolites that map to the canonical pathway divided by the total number of molecules that map to the pathway was displayed. Fisher's exact test was used to calculate a p-value determining the probability that the association between the metabolites and the canonical pathway was explained by chance alone."

### 2.3.3.1 Fisher's Exact Test

Two datasets are used in Fisher's exact test, the uploaded user dataset and a particular pathway or function reference in the knowledge base. The following description of Fisher's Exact Test was taken from the Qiagen IPA training slides.

"The null hypothesis: The overlap (association) between the dataset and the function/pathway is due to chance. In other words, they are independent of each other. If the proportions mapping to a function or pathway are similar between the sample and the reference, there is not likely to be a biological effect. The calculation returns a p-value: From 0-1, where values  $<0.05$  are generally considered significant."

The test looks at the number of genes:

- That match between pathway and dataset
- That are in pathway but did not match dataset
- That are in dataset but did not match pathway
- That were possible to assay in the experiment but are not in the pathway or dataset (this is usually called the "reference set" and is ~the set of all genes on the array platform)

The calculation returns a p-value: From 0-1, where values  $<0.05$  are generally considered significant)

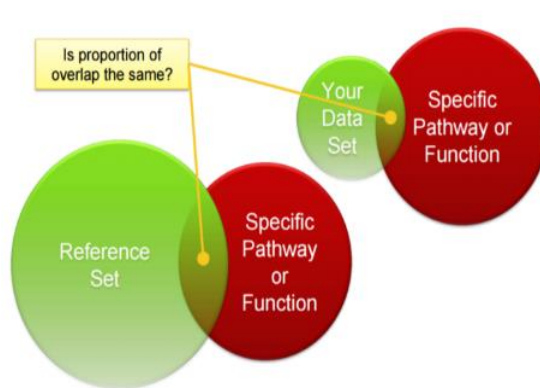


Figure 5. Fisher exact test for the overlap between user and reference dataset

For example:

- Dataset (significantly differentially expressed) of 286 genes
- Pathway of 81 genes
- Where 5 of the dataset genes overlap those in the pathway
- And the platform measured about 12,000 genes

a	5	b	76
Observed Overlap		Genes in pathway but not in dataset	
c	281	d	11,715
Genes in dataset but not in pathway		Genes in reference set	

What is the significance of that overlap?  $P = 0.043$  is less than 0.05 and therefore significant.

$$x = \frac{(a+b)!(c+d)!(a+c)!(b+d)!}{(a+b+c+d)!a!b!c!d!}$$

”

The network score is also calculated with the right-tailed Fisher’s Exact Test. The higher the score is, the more biologically relevant the submitted molecules are to the network.

IPA can transform a list of proteins into a set of relevant networks through the extensive records manually curated in the Ingenuity Pathways Knowledge Base (IPKB).

Networks are useful for the following purposes.

1. Understand how genes/proteins of interest are biologically related and how they work together at the molecular level.
2. Highly-interconnected networks are likely to represent significant biological function

In addition to p-value, the z-score is also used to calculate the statistical measure of the match between expected activation/inhibition and observed gene expression. A z-score  $>2$  or  $<-2$  is considered significant.

IPA software is extensively used in proteomic studies to understand the biological significance of differentially regulated proteins. Sinnamon *et al.* (2012)<sup>144</sup>, studied the role of Hnripab (an RNA binding protein) in mouse brain development. They used a threshold of a 1.5 ratio to study the proteins whose expression increase changed between Hnripab<sup>-/-</sup> and Hnripab<sup>+/+</sup> mice, and 0.5 for proteins whose expression decreased. IPA analysis identified cell death as the most significantly represented cellular function in the up-regulated protein list and no cellular pathway was predominantly represented from the down-regulated protein list (the top 44 entries all had equivalent significance). Another study by Nakamura *et al.*,<sup>145</sup> identified HIV/gp120 (envelope protein) as causing several neuropathological features associated dendritic and synaptic damage in the synaptosomes of mouse brain. They used a threshold of 1.5 fold change in expression between transgenic HIV/gp120 and wt and subjected the proteomics data to IPA analysis to identify pathways and network affected by HIV/gp120 infection. Proteins with values above 1.5 were considered upregulated while proteins less than 1.5 were considered downregulated. The phosphatidylinositol 3-kinase (PI3K)/protein kinase B (Akt) pathway, a neuronal survival pathway was identified as the most affected pathway. Decreased activity of Akt was seen in infected mice corresponding to an inactivation of the neuroprotective pathway. This inactivation occurred via S-nitrosylation of Akt inhibiting its activity and contributing to neuronal cell death.

IPA is instrumental when analyzing the different pathways and networks activated under varying doses of ionizing radiation. The radiation hormesis (adaptive/protective), is leading researchers into finding mechanisms involved in degenerative diseases that can be modulated by low dose ionizing radiation. As an example, ionizing radiation at high dose

(0.5 and 2 Gy) was found to increase phosphorylation of the TAU protein involved in neurodegenerative disease.<sup>146</sup> The effect of low dose on such a pathway has not been evaluated and it would be interesting to see if similar or different disease pathways are implicated. Using IPA, the pathways can be identified and the effect of low dose and high dose on the corresponding pathways can be differentiated.<sup>146</sup>

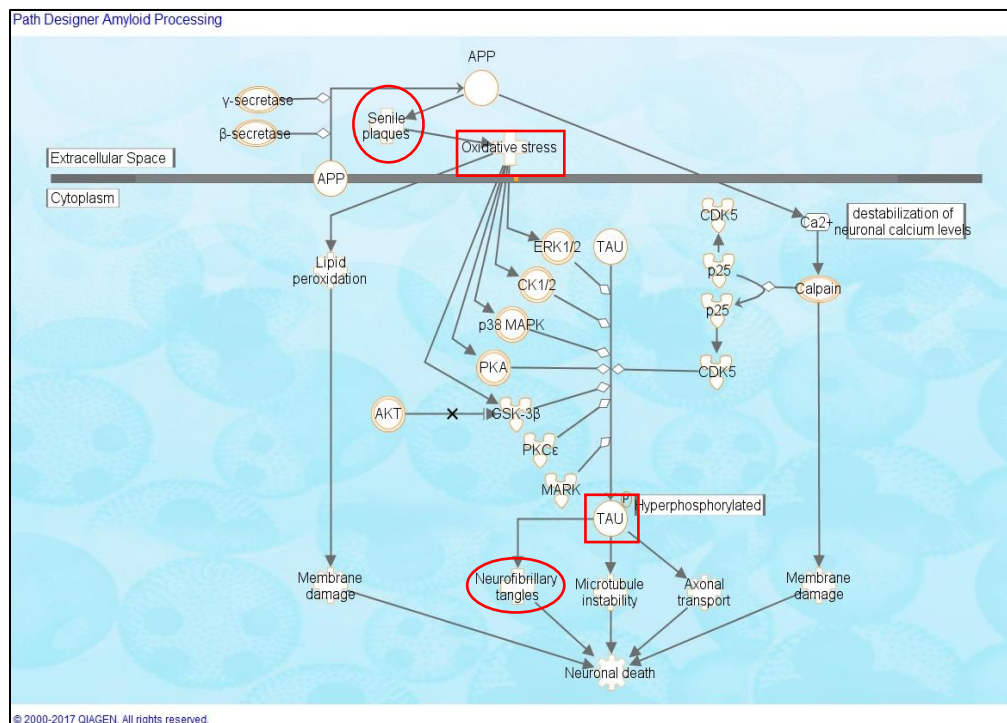


Figure 6. High dose radiation and Alzheimer disease.  
High dose Radiation results in an increase of TAU phosphorylation.<sup>147</sup>

The example above was generated using our protein data (more details in results and discussion section).

### 2.3.4 Database of Protein Post-Translational Modifications (PTMs)

The advances in proteomic and the increase in generating proteomic data necessitated the need for specific databases dedicated for the analysis of the PTM of proteins. Phosphorylation is one of the main studied area of PTM and there are well developed

databases to study this modification. Information is given about the number of phospho sites generated from mass spectrometry data (MS), downstream regulation, molecular functions and protein/protein interaction as well as pathways modulated by phosphorylation. Other PTM databases also exist but they are not as well curated as the phosphorylation databases. There is a need to develop a database dedicated to analyzing nitrosylation and the pathways affected, specifically when the pathway modulation is caused by irradiation. While IPA is a tool dedicated to gene/protein analysis, giving a wealth of information on function, disease association, pathway activation/inhibition and network formation, IPA lacks the PTMs analysis capabilities (except phosphorylation since 2017). The changes in the amount of post-translationally modified proteins including S-nitrosylation and the pathways, and interactions associated with it are lacking.

The list below although not exhaustive represents the main databases for PTMs. One database, dbSNO, is dedicated to the study of nitrosylation however it lacks the functional interactions with other proteins, there are no pathway, disease, or network associations.

#### 2.3.4.1 The dbTM

The dbTM (<http://dbPTM.mbc.nctu.edu.tw/>) is a protein post-translational modifications (PTMs) data warehouse. In 2005, it became freely available and did not have nitrosylation as part of its warehouse until the dbSNO database was developed in 2012. The dbTM is currently a warehouse for the following PTMs: Glycosylation, phosphorylation, acetylation, methylation, S-nitrosylation (db-SNO), ubiquitination, myristoylation, prenylation, S-glutathionylation and others.

#### 2.3.4.2 The dbSNO

The dbSNO (<http://dbSNO.mbc.nctu.edu.tw>) is a resource for exploring SNO sites and regulatory networks of S-nitrosylated proteins. The dbSNO web site<sup>148</sup> describes that “all manually curated SNO peptides (4165 SNO sites within 2277 proteins) to PDB protein entries by sequence identity, which provides the information of spatial amino acid composition, solvent-accessible surface area, spatially neighboring amino acids, and side chain orientation for 298 substrate cysteine residues.” The dbSNO provides structural and functional analyses, solvent accessibility, protein secondary and tertiary structures, protein domains and gene ontology. In addition, metabolic network, protein/protein interaction can be analyzed from an uploaded list. However, dbSNO does not handle expression level analysis at this time.

#### 2.3.4.3 ExPASy

The ExPASy can produce a list of PTMs via a database query ([http://www.expasy.org/proteomics/post-translational\\_modification](http://www.expasy.org/proteomics/post-translational_modification)). A nitrosylation lookup returns the following hits: 5710 for UniProtKB, 82 hits for Swiss-Model, 25 hits for STRING and 1 hit for HAMAP. String is a database of known and predicted protein interactions. The link to STRING (25 hits) reveals that only 3 of the hits are from mouse brain tissue: 1) the role of oxidative stress and antioxidant in Werner syndrome.<sup>149</sup> 2) NOS2 has nitrosylase activity and mediates cysteine S-nitrosylation of cytoplasmic target proteins such COX2.<sup>150</sup> 3) Nitric oxide S-nitrosylates serine racemase, mediating feedback inhibition of D-serine formation.<sup>151</sup> ExPASy can prove to be useful in data mining and getting information on protein nitrosylation from one database.

#### 2.3.4.4 UniProt

UniProt (<http://www.uniprot.org/uniprot>) is a database with the purpose of providing a comprehensive, high-quality accessible resource of protein sequence and functional information. The information about protein PTMs and nitrosylation is included as part of protein description when appropriate (subsection). A keyword search for nitrosylation reveals 79 proteins (mus musculus) with nitrosylation properties.

#### 2.3.4.5 PHOSIDA

PHOSIDA is a PTM database dedicated mainly to the modification of phosphorylation sites on proteins (<http://141.61.102.18/phosida/index.aspx>).

#### 2.3.4.6 Omictools

Omictools are software tools and databases for PTM analysis. Its aim is to predict the site of nitrosylation in proteins (<http://omictools.com/s-nitrosylation-sites-category>).

#### 2.3.4.7 PTMcode

PTMcode (<http://ptmcode.embl.de>) is a web resource for known and predicted functional associations between protein PTMs within and between proteins. For example, a search for mouse HDAC2 shows its nitrosylation site and that it associates with 27 other proteins subject to PTMs.

#### 2.3.4.8 GPS-SNO

The GPS-SNO provides computational prediction of protein *S*-nitrosylation sites with a modified GPS algorithm. <http://sno.biocuckoo.org/>. A collection of 467 experimentally verified *S*-nitrosylation sites in 302 unique proteins from the scientific literature are

provided. The application allows the upload of a protein sequence and the prediction of nitrosylation sites.

#### 2.3.4.9 virPTM

The virPTM (<http://virptm.hms.harvard.edu/>) is the viral post-translational modification (virPTM) database and is a repository of literature-based viral modification sites and predicted modification sites using the *scan-x* algorithm. At present the database contains only phosphorylation data to be expanded to include additional modifications.

From the above review, we can see that there is a lack of specific databases useful in understanding the alterations in protein interactions after nitrosylation. A tool is needed to create networks defining the collective interactions resulting in phenotype changes and disease development. This tool could represent a complete database housing all the information about protein-protein interactions in regard to nitrosylation changes or it could be an app/plugin designated for the analysis of nitrosylation events. The PhosphoPath app<sup>152</sup> is an example of an app developed in Cytoscape for the analysis of the phosphorylated proteins and the pathways affected. Development of a similar app for the analysis of nitrosylation would be instrumental in the analysis of nitrosylation in proteomic data.

## 2.4 Identifying Biomarkers of Ionizing Radiation

A biomarker is a measurement of the interaction between an environmental agent (*e.g.*, radiation) and a biological system (*e.g.*, redox changes/nitrosylation).<sup>153,154</sup> A good biomarker depends on the validity of the assay (minimal error), validity of the marker (what factor modulates it), suitability of the marker and its correlation with the exposure and sampling method (quantity). Biomarkers of exposure are ones that become present after

exposure to the radiation (*e.g.*, chromosomal aberration). Pernot et al. (2012)<sup>153</sup> summarized as follows:

- “Biomarkers of susceptibility can be available before, during or after exposure and can predict an increased risk of radiation induced health effects. Biomarkers of susceptibility would be expected to remain constant throughout the lifetime of an individual. However, certain gene and protein expression profiles could vary with age.
- Biomarkers of late effects can be used to assess health effects that are present a long time after exposure, before clinical detection of the radiation induced disease or death (the usual endpoints in classical epidemiological studies).
- Biomarkers of persistent effects allow the assessment of radiation effects present a long period of time after exposure.”

Use of Gene Ontology is a novel and emerging technique for biomarker discovery.

A study published in 2017<sup>154</sup> by Hall included a road map for developing radiation exposure biomarkers.

Ionizing radiation has been studied in connection with neurodegenerative diseases. Exposure to high doses of  $\gamma$  rays for example (0.5 or 2 Gy) have been implicated in increased tau phosphorylation and the development of Alzheimer disease. While the study elucidated the role of high dose radiation, it made no conclusion about the role of low dose radiation exposures and whether low dose of low LET ionizing radiation can have similar or a counteractive effect.<sup>146</sup>

The database BIDE (Brain Radiation Data Exchange) housing data on the effect of low dose radiation on the brain was developed to accelerate discoveries using omic technologies.<sup>155</sup> The aim is to discover ionizing radiation biomarkers for the potential use in epidemiological studies, a focus effort of the European project DoReMi (Low Dose Research towards Multidisciplinary Integration). The discovery of biomarkers related to transcription and translation as in our study is one of the classification given by Pernot in

2012 for biomarker discovery where proteomic is listed as one of the favorable techniques for possible biomarker discovery. It is noted in their review that at the time of publication, there were no known proteomic discoveries accomplished for the identification of post-translational modifications related to low dose ionizing radiation. As a consequence of such review, we aim to show if our study resulted in identification of biomarkers of pathways specific for low dose ionizing radiation.

### III Materials and Methods.

#### 3.1 Animal Irradiation and Mass Spectrometry

Irradiation of the mice (17 week-old male C57BL/6J mice, whole body exposed to acute  $^{137}\text{Cs}$   $\gamma$  rays) was performed by the research groups in the Department of Radiology at Rutgers NJMS. The mice were exposed to 0.1 Gy and 4 Gy at 0.1 Gy/min and 1 Gy/min dose rate, respectively. They were euthanized by  $\text{CO}_2$  asphyxiation at 13 days after irradiation. Protein extraction from the harvested organs and analysis by mass spectrometry were performed by the research groups in the Center for Advanced Proteomics Research (CAPR) at Rutgers NJMS. Animal and irradiation treatment protocol was approved by the Institutional Animal Care and Use Committee of Rutgers NJMS (Protocol # 16057). Identification of nitrosylated proteins in mice brains by mass spectroscopy analysis was performed by CAPR as well as the verification of proteomics results by immunoprecipitation and Western blotting.

The following flowchart summarizes the steps in the irradiation and isolation of nitrosylated proteins:

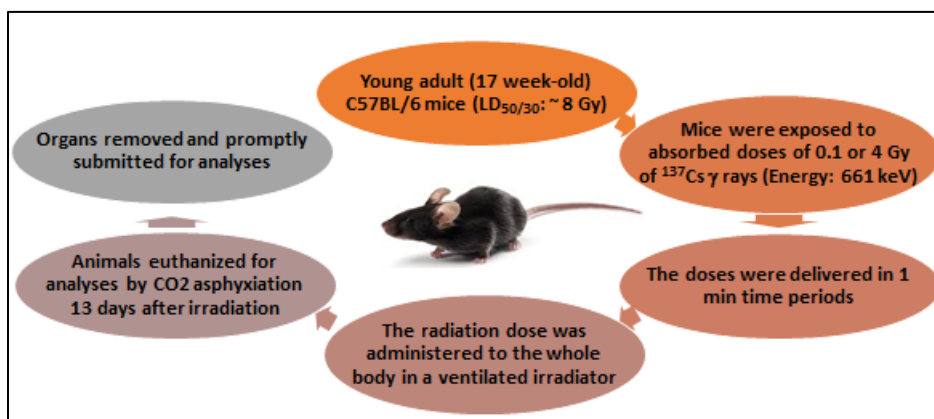


Figure 7. Animal irradiation and experimental groups  
5 mice/group: (1) sham-irradiated without contrast agent; (2) sham-irradiated with contrast agent; (3) 0.1 Gy-irradiated without contrast agent; (4) 0.1 Gy-irradiated with contrast agent; and (5) 4 Gy-irradiated without contrast agent.

### **3.2 Proteomics Data Description and Pre-processing**

This research dealt only with computational analyses of proteomics data provided by the Center for Advanced Proteomics Research (CAPR). The details of how the proteomics data were derived is described in our paper.<sup>10</sup> Thus, only a brief description is provided below.

#### **3.2.1 Proteomics Data Description**

Briefly, S-nitrosylated proteins were extracted by the modified biotin switch technique and enriched by streptavidin beads. Biotinylated proteins were digested with trypsin and released peptides were analyzed by mass spectroscopy. Identification and quantification of biotin-HPDP linked proteins were performed by CAPR using Mascot as a search engine against all the mouse protein sequences in UniRef100 protein database.

Proteomics data provided by CAPR contained the following items for each protein in a table form: the description of protein, UniProt ID, molecular weight, spectral count obtained after 0, 0.1, and 4 Gy irradiations, ratio of spectral count at 0.1 Gy over control (0 Gy) and at 4 Gy over control. A part of these data is shown in the following table.

#### **3.2.2 Proteomics Data Pre-processing**

Data pre-processing was done to remove outliers, eliminate low quality or questionable results and select proteins that are significantly differentially expressed in the data set. The first step of pre-processing entailed changing all zero values (no detection of nitrosylation), with the lowest detectable value in our dataset (1.17) and then dividing this value by 2 (0.59). This step was necessary in order to avoid division by zero (appeared in the original table provided by CAPR) - a troublesome effect in doing statistical analysis and especially when calculating fold change (FC). A total of 82 proteins (Supp. File/0.59 Values) showed

a zero value (no detection of nitrosylation in at least one of the conditions: Ctrl, 0.1 Gy or 4 Gy). The table below shows an example of some of the proteins:

Protein ID	Ctrl	0.1 Gy	4 Gy	FC 0.1/Ctrl	FC 4/Ctrl
ATP5H_MOUSE	10.31	0.59	12.07	-17.47	1.17
UCHL1_MOUSE	7.50	0.59	6.50	-12.71	-1.15
IGSF8_MOUSE	6.56	0.59	4.64	-11.12	-1.41
HNRPU_MOUSE	5.62	0.59	1.86	-9.53	-3.02
AP1M1_MOUSE	5.62	0.59	2.79	-9.53	-2.01
CAPZB_MOUSE	5.62	0.59	5.57	-9.53	-1.01
MAON_MOUSE	5.62	0.59	5.57	-9.53	-1.01
PROF1_MOUSE	5.62	0.59	5.57	-9.53	-1.01
CALR_MOUSE	10.31	1.17	6.50	-8.81	-1.59
PDXK_MOUSE	10.31	1.17	10.21	-8.81	-1.01

Table 1. Proteins with undetectable nitrosylation.

### 3.2.3 Calculations of Changes in Nitrosylated Proteins after Irradiation

Another decision in investigating the differential expression of nitrosylated proteins is the selection of how to represent the changes in the levels of nitrosylated proteins after irradiation compared to the control for the statistical analyses. Three possible ways to represent the changes are 1) a ratio (the spectral count of a protein after irradiation divided by the corresponding spectral count of control (i.e., sham-treated, 0 Gy), 2) a fold change (if the ratio value is less than 1 –i.e., decreased level of nitrosylated protein, then it's inverse value preceded by a negative sign is assigned instead), or 3) log 2 Ratio (a log transformation of ratio using base 2)

Many researchers studying gene expression use customized methods suited for their field of study. Overall, the research on the approach to be used points out to the disadvantage of using ratios because the expression of genes and proteins is not distributed symmetrically.<sup>129</sup> The example below of expression data further clarifies this point.

Ctrl	0.1 Gy	4 Gy	Ratio 0.1 Gy/Ctrl	Ratio 4 Gy/Ctrl	Fold Change 0.1 Gy/Ctrl	Fold Change 4 Gy/Ctrl	Log2Ratio 0.1 Gy/Ctrl	Log2Ratio 4 Gy/Ctrl
4	2	8	0.5	2	-2	2	-1	1

Here we see that a decrease by 2 fold at 0.1 Gy is equal to 0.5 in ratio while the same fold increase at 4 Gy is equal to 2 in ratio. This asymmetry in up/down expression is rectified in the fold change (-2 vs 2) and the Log2 ratio (-1 vs 1). However, it should be noted that if one uses fold change to represent the alterations in levels of nitrosylated proteins, a no change after irradiation compared to control is represented by either +1 or -1 fold change and there are no data points between fold change between -1 and +1. This discontinuity is rectified by the use of Log 2 Ratio.

Log2 ratio is a most widely used transformation to represent the changes in expression levels compared to control. The use of Log2 ratio makes data distributed continuously and more or less symmetrically for up and down regulated genes. Proteins expressed at a constant level (no change in nitrosylated protein level between control and after irradiation) will have a Log2 ratio of value zero. It is clear from the above description that the log 2 ratios are the best suitable methods for data analysis.

### 3.3 Grouping

One of the important aspects of data analysis is to group a set of proteins that shared very similar characteristics. Three different approaches were used to classify the groups of proteins (clustering) as shown below.

### **3.3.1 No Grouping (Whole Data Set)**

The original data set of this study contained 377 proteins, and all the 377 proteins were used as one group. Data distribution of spectral counts and changes in nitrosylation levels were examined by frequency counts, histogram and scattered plots. R packages contain various descriptive statistics functions that were used to characterize the data.

#### **3.3.1.1 Spectral Count Data Distribution**

Distribution of spectral counts at three different conditions were analyzed and displayed as histograms. In addition, a specific group was separately analyzed representing proteins showing high nitrosylation level (spectral count above 80, Supplementary file SNO > 80) under any observation (0, 0.1 or 4 Gy).

#### **3.3.1.2 Data Distribution of Changes in S-Nitrosylation Levels after Irradiation**

Similarly, data distribution of changes in nitrosylation levels after two different doses of irradiation were examined and displayed using histograms.

##### **3.3.1.2.1 Inferential Statistics: Parametric vs. Non-Parametric Analysis**

The Null hypothesis in inferential statistics refers to the lack of difference among the group of proteins tested. Although the Student's t test is one of the common statistical tests used for comparing the means of two independent or paired samples, it is not always feasible or correct to use the t test. The t tests assume that the data to be analyzed is normal, i.e. the data is not skewed. In addition, when comparing the groups of data, whether the difference between the groups is normally distributed must be examined. On the other hand, the central limit theorem states that no matter what the population distribution is, the sampling distribution tends to be normal if the sample is large enough ( $n > 30$ ). The result will allow

us to use parametric (if normal distribution) or non-parametric (not normally distributed) method like Wilcox test to do the analysis. The `rquery` function will be used to test normality.

R function `rquery.t.test()` was used to check the data and the results provide the information on which method to use (parametric or non-parametric).

The Wilcoxon Rank Sum Test uses a set of observations (N) and ranks the data from smallest value. It then adds the value of all the ranks (W) and gives a probability p whether there is a difference between two sets of data.

### 3.3.1.3 Analysis of Change in S-Nitrosylation Levels after Irradiation

Descriptive statistics for data with non-normal distribution including graphic representation by Box Plot and other graphical representations to indicate the changes in S-nitrosylation levels after mouse exposure to different doses of radiation were examined.

#### 3.3.1.3.1 Descriptive Statistics

Numerical characteristics of data sets were examined with the descriptive statistics functions described below. Descriptive statistics gives information regarding the central tendency, variability, and distribution of the variables. The focus is on changes in nitrosylation (increase or decrease) under low and high dose irradiation. Information regarding the minimum/maximum value, the Mean and Median, quartiles, kurtosis and skewedness were examined and some results were displayed with box plots. Descriptive statistics was also run on the log2 ratio data using R packages.

##### 3.3.1.3.1.1 Summary () function

This function provides the key descriptive statistical characteristics of the data.

R Code:

```
setwd("C:/Users/Nicolaf/Desktop/MYFOLD/R1/R/LogR")
LogR<-read.csv("C:/Users/Nicolaf/Desktop/MYFOLD/R1/R/LogR/Log2R.csv")
rownames(LogR)<-Fold$Protein##MAKE A COLUMN W. Row names
Fold$Protein<-NULL
vars <- c("LogR10","LogR400")
summary(LogR[vars])
```

Please refer to Supp. File/Log2R for input data.

## 3.3.1.3.1.2 Describe() function

This function in the Hmisc package provides similar descriptive statistical characteristics of the data also.

R Code:

```
setwd("C:/Users/Nicolaf/Desktop/MYFOLD/R1/R/LogR")
LogR<-read.csv("C:/Users/Nicolaf/Desktop/MYFOLD/R1/R/LogR/Log2R.csv")
rownames(LogR)<-LogR$Protein
LogR$Protein<-NULL
df<-LogR
library(Hmisc)
vars <- c("LogR10", "LogR400")
describe(df[vars])
```

## 3.3.1.3.1.3 Scale () function

This data pre-processing involves the standardization or scaling of the data. This is done in order to reduce the variability in the data especially when different measures are used (kg, km or cm). Also, if the mean and or standard deviation of the data is large, then the data should be standardized. R has a function “scale” which is used for this purpose, it performs the scaling by taking the mean of the values (or median) and the standard deviation can be used to scale the data. However, in our data the mean and STD were not large and thus did not warrant any scaling.

### 3.3.1.3.2 BoxPlot

This statistical tool groups the data through the quartiles values and provides a graphical presentation of the outliers and the quartile ranges. The Log2R data file was reformatted with 3 columns for protein ID, log 2 ratios at two different doses (Log2R10 and Log2R400). The file was renamed as (Box.csv, Suppl. file) and was used as input for the analysis.

#### R Code:

```
setwd("C:/Users/Nicolaf/Desktop/MYFOLD/R1/R/LogR")
LogR<-read.csv("C:/Users/Nicolaf/Desktop/MYFOLD/R1/R/LogR/BOXPLOT/Box.csv")
rownames(LogR)<-LogR$Protein
LogR$Protein<-NULL
dat<-LogR
df<-dat
library(easyGgplot2)
install.packages("cowplot")
library(cowplot)
df$IRR_Dose <- as.factor(df$IRR_Dose)
bp <- ggplot(df, aes(x=IRR_Dose, y=Nitro_Level, color=IRR_Dose)) +
  geom_boxplot() + theme(legend.position = "none")
# Add gridlines
ggplot2.boxplot(data=df,xName='IRR_Dose',yName='Nitro_Level',groupName='IRR_Dose')
p1<-ggplot2.boxplot(data=df,xName='IRR_Dose',yName='Nitro_Level', groupName='IRR_Dose')
ggplot2.customize(p1, ylim = c(-4,4),axisLine = c(1, "solid", "darkblue"),
mainTitle = "Boxplot of Nitrosylation Level after \n Irradiation at 10 and 4 Gy")

(Supp file/Box)
```

### 3.3.1.3.3 Scattered and Density Plots

#### 3.3.1.3.3.1 Scatter Plots

In order to remove the noise and data points with low values at every observation (Log2 0.1/0 and Log2 4/0), we filtered the proteins and removed data points  $\geq |0.5|$  (Log2 =0.5 ~ 1.4 fold change).

#### R Code:

```
plot.new()
with(Log2R,{
  plot(Log2R,
```

```

main="Nitrosylation level after irradiation:
at 0.1 Gy and 4 Gy",
xlab="Log2R 10/0 ", ylab="Log2R 400/0 cGy",
xlim=c(-4, 4), ylim=c(-4, 4),
pch=c(18,20), ###the dots are circle and triangles
col=c("red",133)##color is red and cyan blue
,cex.lab= 0.8,##reduce the axis labels by 20%
cex.main= 0.8)###reduce the main title by 20%
text(LogR10, LogR400,
      row.names(FALSE),
      cex=0.4, pos=4, col=201) } )##reduce by 60%, to the right and color black.
legend("topleft",##add legend to the graph
inset=.05, #inserted at .05
title="Log2 Ratios:", c("10/0","400/0"),
cex=0.7, pch=c(18, 20)###same pch as in plot
, col=c("red", 133))##same color as in plot above

```

### 3.3.2 Clustering with R

#### 3.3.2.1 Cluster or Not to Cluster

First, the data was analyzed with R to decide whether it should be clustered or not. Then the optimum number of clusters was analyzed by using R libraries. Using the optimum number of clusters obtained, the data was divided into the separate groups.

The first step is to decide whether the data could be clustered. All the clustering methods will return groups of clusters even if there are no meaningful clusters in the data. Thus, it is important first to assess whether the data contain meaningful clusters. There are two methods used to determine clustering tendency in R: Hopkins statistics and the Visual Assessment of Cluster Tendency (VAT). Hopkins statistic is more robust and was used in the assessment.

##### 3.3.2.1.1 Hopkins statistics

This test measures the probability of the spatial randomness of a sample. It finds the nearest neighbor of a given point, generates random simulated data and computes the distance. It calculates the mean of the nearest neighbor distance in the data divided by the sum mean of the real and simulated data. If the value of H is close to zero then the null hypothesis can

be rejected and the data can be clustered. Hopkins algorithm analyzes the data and generates random data set (with same variation and same distribution as the original dataset). It computes the distance between the points in both datasets (original and random separately). It then calculates the mean nearest neighbor in the random dataset divided by the sum of the means nearest neighbor in the real dataset and across simulated dataset: the output is the Hopkins value (H).

$$H = \frac{\sum_{i=1}^n}{\sum_{i=1}^n xi + \sum_{i=1}^n yi}$$

A value of 0.5 between the real and random data indicates that the data are uniformly distributed and can be clustered, while a value less than 0.5 is an indication of non-clustering possibility.

R Code:

```
set.seed(377)
> hopkins(random_df, n = nrow(random_df)-1)
```

### 3.3.2.2 Clustering

Clustering can be done by two different approaches, hierarchical and partitioning and hierarchical clustering.

#### 3.3.2.2.1 Partitioning Algorithm

The k means clustering is a partitioning algorithm in which the cluster is centered around the mean of the data in each cluster. The PAM clustering algorithm (partitioning around the mean) has each cluster represented by an element of the cluster. Clara (clustering large applications) is a PAM algorithm. The k means clustering algorithm requires the specification of the number of clusters in advance. Clustering is done using different values of k clusters and obtaining the wss (within sum of squares) from the number of clusters.

The bend in the plot (like the scree plot) indicates the ideal number of clusters. The wss would be used to determine the best clustering solution. A wss that minimizes the total within cluster variation (average distance of a point to the center of a cluster) is ideal. In addition, selecting an `nstart` > 25 will minimize the variation in results as does selecting the number of seeds to use (for correct replication).

Hierarchical clustering is an alternative approach to obtain the groups in the data set. An advantage in hierarchical clustering is that there is no requirement to know the number of groups in advance. The results can be viewed as a dendrogram, a tree-based representation of relationship of data points. As the user alters the desired similarity level, the number of groups will change accordingly.

The result of hierarchical clustering is a tree-based representation of the objects, which is also known as dendrogram. Observations can be subdivided into groups by cutting the dendrogram at a desired similarity level.

### 3.3.2.3 Choosing the Right Number of Clusters

There are 2 methods for determining the number of clusters. One is to optimize the wss explained above and the other one is the gap statistic. In addition, R has codes for computing 30 indices used to select the best number of clusters. This approach was used to determine the best number of clusters in our proteomics data.

#### 3.3.2.3.1 NBclust: Determining of the Best Number of Clusters

NbClust package, published by Charrad *et al.* 2014,<sup>129</sup> provides 30 indices for determining the relevant number of clusters (*e.g.*: gamma, Gap, Silhouette, Hartigan).

The indices include the Gap statistic, the silhouette method, Hartigan, Hubert and up to 26 other indices.<sup>129</sup> Where the user specifies the dissimilarity matrix to be used, the

minimum and maximum number of clusters and the indices can be specified or alternatively they can all be run. Best.nc is also included to give the best number of clusters. NbClust for all the indices will be run. In addition, the individual results from 2 selected indices will be checked (the pam NbClust and the Calinski criteria index). Some of the separate indices included in BbClust and the individual indices clustering results (like the Calinski criterion) were examined.

#### R Code NbClust Determining optimal number of clusters

```
nb <- NbClust(Log2R, distance = "euclidean", min.nc = 2,
              + max.nc = 10, method = "complete", index = "all")
#We can also use the fviz function:
fviz_nbclust(nb) + theme_minimal()
```

#### 3.3.2.3.2 clValid

This package allows us to validate the clustering analysis. Several clustering algorithms can be evaluated simultaneously to determine the most appropriate method and number of clusters for our dataset. The optimal validation scores can be displayed as well as the clustering results.<sup>131</sup> The internal validation (clValid) measures are the connectivity, Silhouette Width, and Dunn Index. The neighborhood size for the connectivity is set to 10 by default in clValid and can be changed by using the argument “neighbSize”. Agnes clustering method performs hierarchical clustering with similar result to the hierarchical clustering used in the algorithm (hence it is omitted to avoid redundancy).

#### R Code:

```
setwd("C:/Users/Nicolaf/Desktop/MYFOLD/R1/R/LogR")
LogR<-read.csv("C:/Users/Nicolaf/Desktop/MYFOLD/R1/R/LogR/Log2R.csv")
rownames(LogR)<-LogR$Protein##MAKE A COLUMN W. ROW names
LogR$Protein<-NULL
library(clValid)
clmethods <- c("hierarchical","kmeans","pam")
intern <- clValid(LogR, nClust = 2:6,
                  clMethods = clmethods, validation = "internal")
summary(intern)
```

### 3.3.2.3.3 OptCluster

Another package available in R, as discussed in the introduction is the **OptCluster** package and its purpose is to find the best clustering solution in our data set.

#### R Code:

```
library(optCluster)
library(clValid)
setwd("C:/Users/Nicolaf/Desktop/MYFOLD/R1/R/LogR")
LogR<-read.csv("C:/Users/Nicolaf/Desktop/MYFOLD/R1/R/LogR/Log2R.csv")
rownames(LogR)<-LogR$Protein##MAKE A COLUMN W. ROW names
LogR$Protein<-NULL
      optclusLogR <- optCluster(LogR[,], 2:8, clMethods = c("clara","hierarchical",
      "kmeans","pam", "som"), validation="internal", seed = 123, maxitems = nrow(LogR[,]))
norm1 <- optclusLogR
aggregPlot(norm1)
print(optclusLogR)
optimalScores(optclusLogR)
```

### 3.3.2.3.4 HeatMap and Interactive HeatMap with Shiny Application

#### R Code:

```
library(d3heatmap)
library(shiny)
setwd("C:/Users/Nicolaf/Desktop/MYFOLD/SHINY/HEAT")
LogR<-read.csv("C:/Users/Nicolaf/Desktop/MYFOLD/R1/R/LogR/Log2R.csv")
rownames(LogR)<-LogR$Protein##MAKE A COLUMN W. ROW names
LogR$Protein<-NULL
dat<-LogR
runApp("C:/Users/Nicolaf/Desktop/MYFOLD/SHINY/HEAT")
```

## 3.3.3 Manual Clustering

The changes in the levels of S-nitrosylation after irradiation (compared to the control) for a protein falls into one of the following three categories: decrease, no change and increase. Since two different doses were used in the experiment, it is possible that the changes in S-nitrosylation after two different doses of irradiation should fall into a combination of three categories for each dose leading to one of 9 possible groups.

Unfortunately, this approach depends on the choice of threshold dividing between no change vs either increased or decreased S-nitrosylation. A threshold of 1.3 Fold Change

was used as criteria for clustering: proteins above 1.3 fold change were considered as increase in nitrosylation while proteins less than 1.3 fold change as decrease in nitrosylation. Nine groups were formed as depicted in the table below (+ = increase, - = decrease, 0 = no change):

Grp1	Grp2	Grp3
Inc 0.1 Gy  Inc 4 Gy	Inc 0.1 Gy  Dec 4 Gy	Inc 0.1 Gy  NC 4 Gy
++	+-	+0
Grp4	Grp5	Grp6
Dec 0.1 Gy  Inc 4 Gy	Dec 0.1 Gy  Dec 4 Gy	Dec 0.1 Gy  NC 4 Gy
-+	--	-0
Grp7	Grp8	Grp9
NC 0.1 Gy  Inc 4 Gy	NC 0.1 Gy  Dec 4 Gy	NC 0.1 Gy  NC 4 Gy
0+	0-	00

Table 2. Clustering of proteins into 9 groups

### 3.3.4 Clustering from 2 to 10: Membership Changes

Finally, Hierarchical clustering was used to cluster the data while varying the number of clusters generated from 2 to 10. The purpose of this exercise was to compare with the manual clustering results and to observe the changing membership (proteins) of each cluster as the number of clusters increased.

R Code: Membership Changes from 2 to 10

#### **Input File:**

```
setwd("C:/Users/Nicolaf/Desktop/MYFOLD/R1/R/LogR")
LogR<-read.csv("C:/Users/Nicolaf/Desktop/MYFOLD/R1/R/LogR/LogRF.csv")
rownames(LogR)<-LogR$Protein
LogR$Protein<-NULL
dat<-LogR
dat.tdy <- dat
```

#### **Calculating the Distance:**

```
Euc_Dist <- dist(dat.tdy,method = "euclidean", diag = FALSE, upper = TRUE)
c2 <- hclust(Euc_Dist, method = "ward.D2", members = NULL)
Plotting several dendrograms by changing k from 2 to 10:
dev.off(), plot.new(), par(mar=c(6, 6, 6, 0.5))
plot(c2,labels=FALSE, main = "Protein Data Clustering: (Log Ratio Filtered >=
0.5)",cex.main=0.8,xlab="Euclidean Distance", ylab= "Height/Distance between clusters")
```

```
rect.hclust(c2, k = 10, border = 1:10)
legend(locator(1), cex=0.8, legend = paste("Cl_", 1:10), pch=1, col=1:10, bty = "n")
Displaying above using the fviz function:
hc.cut <- cutree(c2, k = 10)
fviz_cluster(list(data = dat.tdy, cluster = hc.cut))
```

### 3.4 Ontology and Pathway Analysis

The groups of proteins generated by various clustering approaches were further analyzed for functional and pathway characteristics using IPA software (each group from table 2: +-, +0, ++..., uploaded to IPA, Supp file).

#### 3.4.1 Protein Functional Classification (PANTHER)

Our dataset (377) contained many proteins with different molecular and biological functions and protein class. In order to obtain the characteristic role of different groups of proteins, the dataset was uploaded to PANTHER web site<sup>156</sup> and the various functions for groups of proteins were obtained.

The file Log2R.csv (Supp) was uploaded to PANTHER web site, and *Mus musculus* was selected as the organism. Then, “functional classification viewed in gene list” option was selected before submitting the work. The result was the multiple “hit” pages and a large list of mapped IDs. The top pie chart icon has selection options for graphical display of MP, BP, CC, PC and Pie Chart Option (Molecular, Biological, Cellular Component, Protein Class and Pathways). Each color in the chart correspond to a biological function or process, *etc.* The chart was exported along with the annotation.

#### 3.4.2 Ingenuity Pathway Analysis (IPA)

To elucidate the cell signaling pathways of SNO-proteins in brains of mice treated with cesium-137  $\gamma$  rays, Ingenuity Pathway Analysis software package<sup>157</sup> was used. As we discussed in our paper,<sup>10</sup> IPA “uses a knowledge base derived from the literature to relate

the proteins to each other, through direct and indirect interactions. Identity of the proteins and their expression values were uploaded onto IPA, and canonical pathways and molecular interaction networks were generated based on the knowledge stored in the Ingenuity Pathway Knowledge Base. A ratio of the number of metabolites that map to the canonical pathway divided by the total number of molecules that map to the pathway is displayed in Results. Fisher's exact test was used to calculate a *p*-value determining the probability that the association between the metabolites and the canonical pathway was explained by chance alone.”<sup>10</sup>

The Fisher's right tailed exact test provides the  $-\log(p\text{-value})$  and the results are displayed as a diagram where the y-axis is the  $-\log(p\text{-value})$  in the bar chart; the taller the bar, the more significant the pathway is. The x-axis of the bar chart displays the names of the canonical pathways. In single analysis (for example 0.1 Gy without 4 Gy data), an orange line on the pathway graph indicates the threshold *p*-value of 0.05 and all canonical pathways that meet the threshold are displayed ( $-\log(p\text{-value}) > 1.30$  is equivalent to  $p < 0.05$ ).

The following schemes were used for IPA analysis:

1. The data (Log2R.csv, Supp.) was uploaded to IPA as a whole set to analyze the pathways, disease and network.
2. The selected groups from the manual clustering were also subjected to IPA analysis.
3. Lastly, the clusters generated by R were used to further analyze the data with IPA.

## IV Results

### 4.1 Grouping

#### 4.1.1 Whole Data Set (One Group)

The simplest way to group the proteins is having just one group using the entire data set. The data set consists of 377 proteins that showed a detectable S-nitrosylated protein in brain of C57BL/6J male mice in at least one of the three conditions: Control (0 Gy), Low Dose (0.1 Gy) and High Dose (4 Gy)  $^{137}\text{Cs}$   $\gamma$  irradiation.

##### 4.1.1.1 Data Distribution

Overall the data distribution was examined with two different data representations: i) One with spectral counts, the indicator of the amount of S-nitrosylated proteins, at three different conditions (control, low and high dose irradiations), ii) another is data derived from the spectral counts (the changes in S-nitrosylated proteins after low and high dose irradiations compared to the control).

##### 4.1.1.1.1 Distribution of Spectral Counts

The figure below shows the spectral count data for the total of 377 proteins that exhibited a detectable amount of S-nitrosylated proteins in at least one of the three conditions described above. The frequency distribution of S-nitrosylated protein spectral counts are shown in several diagrams each using a different range of spectral counts. Supplemental file/Frequency tab has the data used for creating the spectral count diagram below.

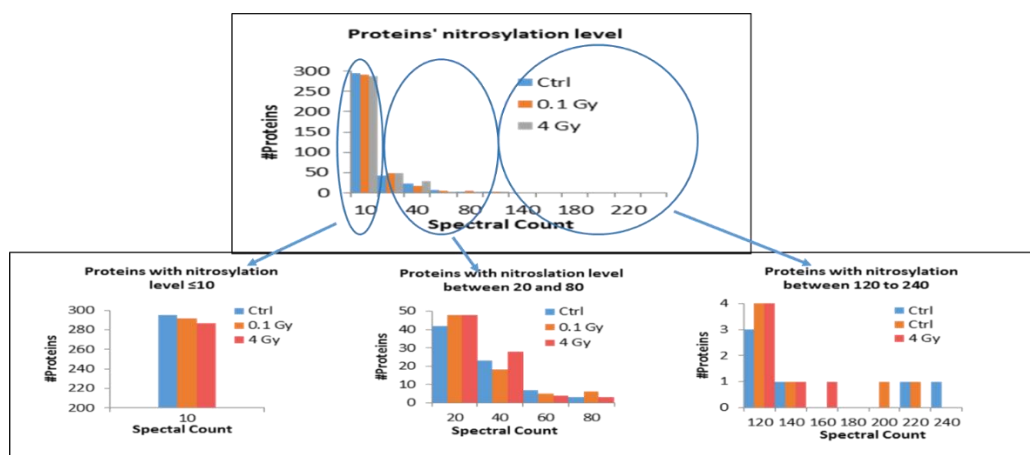


Figure 8. Frequency distribution of S-nitrosylated proteins

Top graph is representation of all 377 proteins while the bottom graph is an expansion of different ranges of spectral counts (0-10, 20-80, 120-240).

The top graph clearly showed that the majority of proteins had spectral counts of less than 10 and there were only small deviations among the three different conditions. There are only few proteins that exhibit a spectral count above 80.<sup>10</sup> More detailed distribution in three different data ranges were shown in the second row of the diagram.

#### 4.1.1.1.2 Proteins with High Nitrosylation Level

As discussed in our paper,<sup>10</sup> few proteins exhibited spectral count above 80 regardless of experimental conditions. Tubulin betas (TBB4\* and TBB2A) showed a slight decrease in spectral counts at 0.1 Gy compared to the control, while the magnitude of decrease was more enhanced at 4 Gy. Tubulin alphas on the other hand did not show appreciable changes (TBA1A, TBA1B, TBA4A) at both low and high doses compared to the control. ARF5 (ADP-ribosylation factor 5) showed almost no difference in spectral counts at 0.1 Gy, but an increase at 4 Gy. AT1B1 (Sodium/potassium-transporting ATPase subunit beta-1) showed spectral counts of 25 and 20 at 0 Gy and 4 Gy respectively, while the count rose to 120 at 0.1 Gy (not shown in Figure).<sup>10</sup>

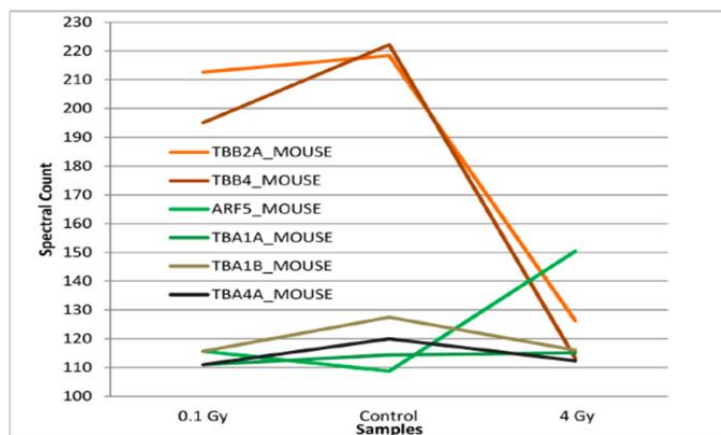


Figure 9. S-nitrosylated protein levels with spectral count above 80  
Comparison of spectral counts of SNO proteins (proteins with spectral counts above 80) showed differential modulation relative to control of  $\beta$  tubulins in brain of mice exposed to 4 Gy, while no such effect was observed at 0.1 Gy. S-nitrosylation of ADP-ribosylation factor 5 (ARF5 shown in green) increased at 4 Gy.

#### 4.1.1.1.3 Distribution of Changes in Nitrosylation Level after Irradiation

The frequency distribution showed that the majority of the proteins exhibited less than 2 fold change (increase or decrease) in nitrosylation. Most of the proteins fell in the range of -1 to +1 in log2 ratio. More proteins showed a decrease in nitrosylation at 0.1 Gy (blue bars) than at 4 Gy. In addition, the 4 Gy group had close to 83% of the proteins with less than +/- 2 fold change (data shown in 4.1.1.2.3).

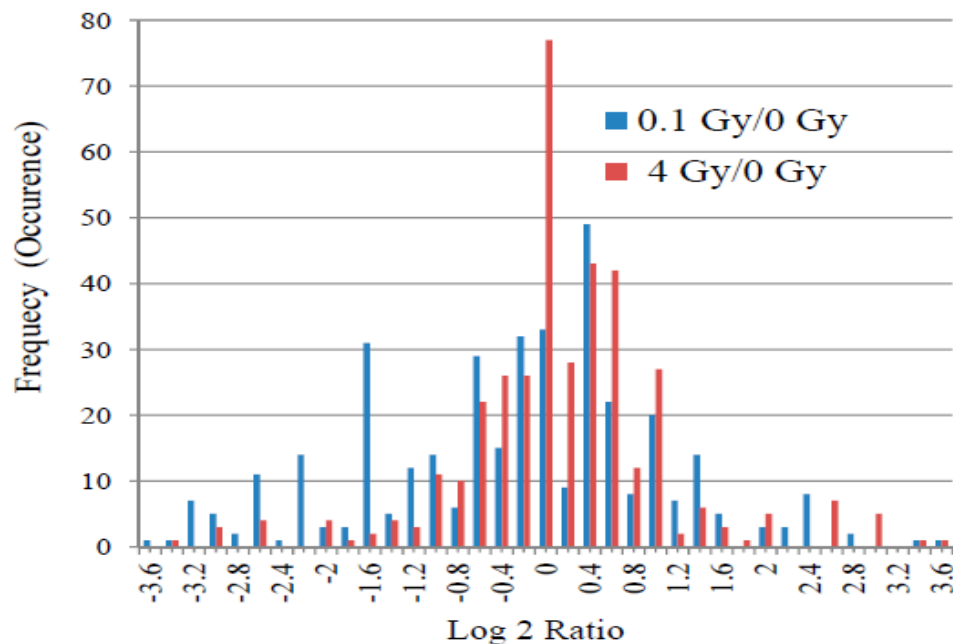


Figure 10. S-nitrosylation after exposure to low and high dose  $\gamma$  radiation  
Mass spectrometry analyses shows the changes in protein nitrosylation in brain of C57Bl/6J mice after 13 days of exposure to  $^{137}\text{Cs}$   $\gamma$  rays. X axis is the fold change expressed in log<sub>2</sub> ratio of the nitrosylated proteins after irradiation at low or high dose compared to control. Y axis is the frequency or the number of occurrences of proteins at the nitrosylation level. Blue lines show the observation at 0.1 Gy while the red lines show the observations at 4 Gy. Adapted from Nicolas *et al.* 2015.

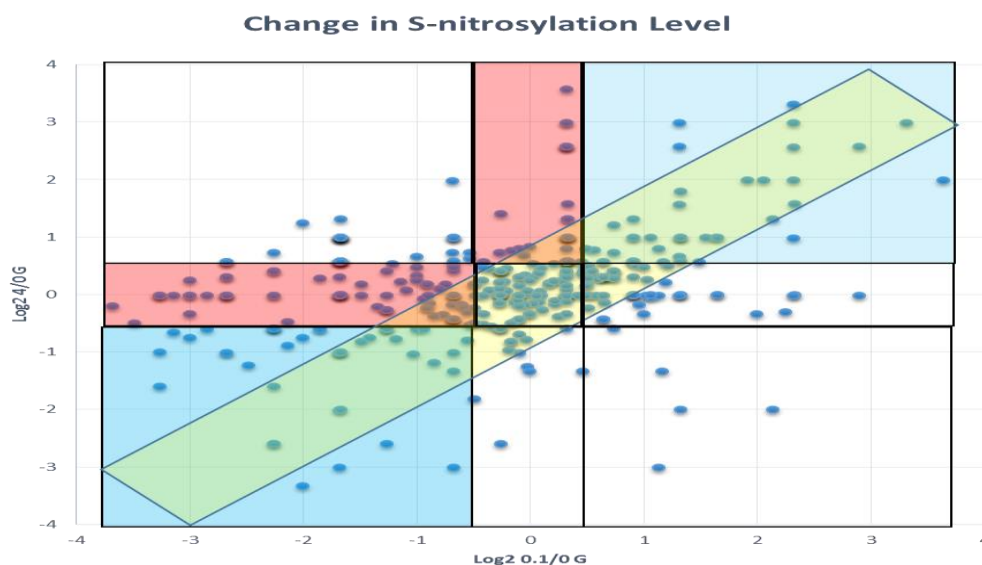


Figure 11. Scatterplot in excel showing changes in nitrosylation level

#### 4.1.1.1.4 Parametric vs. non-Parametric

The “`rquery.t.test`” function was run in order to determine whether our data follows a normal distribution and if a “t test” can be used for further analysis. For paired t test, it checks whether the difference  $d = (x - y)$  is normally distributed:

```
R Output:
Paired t-test
Data: x and y
t = -7.1064, df = 376, p-value = 6.021e-12
Alternative hypothesis: true difference in means is not equal to 0
95 percent confidence interval:
-0.6036024 -0.3419679
Sample estimates:
mean of the differences
-0.4727851
Warning message:
In rquery.t.test(x, y, paired = TRUE) :
The difference d ( = x-y) is not normally distributed : Shapiro-Wilk test p-value : 1e-06.
Use a non-parametric test like Wilcoxon test.
Using the Wilcoxon test as indicated since the mean (x-y) is not normally distributed:
```

The result above showed the value of t-test statistics is -7.1, the degrees of freedom (df) is 376, p-value is the significance level of the t-test ( $p\text{-value} = 6.02 \times 10^{-12}$ ). The confidence interval (conf.int) of the mean differences at 95% is also shown (conf.int= [-0.6, -0.3]). Finally, we have the difference of the means of the two samples (mean diff = -0.4).

However, the p-value of *Shapiro-Wilk test* is  $1 \times 10^{-6}$ , which is less than 0.05. We can then reject the null hypothesis and conclude that our data does not fit the normal distribution as indicated in the histogram discussed earlier.

```
R Output: Wilcoxon Rank Sum Test
Wilcoxon rank sum test with continuity correction
data: x and y
W = 56442, p-value = 1.002e-06
Alternative hypothesis: true location shift is not equal to 0
```

Here we have a large  $w$  value corresponding to the ranking and sum of the data in each set. The  $p$ -value indicates that there is a difference between our two data sets and since the  $p$ -value is less than the significance level of 0.05, we reject the null hypothesis. We conclude that there is enough evidence in the data to suggest that the nitrosylation levels are different under differing doses of irradiation. The Wilcoxon Rank Sum Test uses a set of observations ( $N$ ) and ranks the data from smallest value. It then adds the value of all the ranks ( $W$ ) and gives a probability  $p$  whether there is a difference between two sets of data. The Wilcoxon test results show that the hypothesis is valid and that there is a differential response in the data after irradiation with 0.1 and 4 Gy.

#### 4.1.1.2 Dose Dependent Changes in S-Nitrosylation after Irradiation

Whether a low and a high dose of irradiation exhibit different response in the levels of S-nitrosylation was examined in various approaches.

##### 4.1.1.2.1 Descriptive Statistics

R has extensive tools available for data analysis. The following section describes the results obtained from some of the useful tools used to study the effect of nitrosylation changes after irradiation. Descriptive statistic in R (Summary function and Describe) showed the smallest Log 2 value at each observation (-4.13 corresponding to protein ATP5H at 0.1 Gy and -2.99 for IFA1 protein at 4 Gy) as well as other parameters with the difference in nitrosylation at 0.1 and 4 Gy. The 25% of the data is below the 1<sup>st</sup> Quartile of -1.21 at 0.1 Gy irradiation while 25% of the data is less than -0.27 at 4 Gy irradiation. On the other hand, 75% of the data is less than 0.49 (3<sup>rd</sup> Quartile) and 0.57 at 0.1 Gy and at 4 Gy, respectively. The median also differs between the 2 observations with a negative mean for 0.1 Gy (-0.17) and positive mean for 4 Gy (0.06). The protein showing maximum

nitrosylation had a close value between the 2 observations (3.31 and 3.24 for 0.1 and 4 Gy, respectively).

### summary(LogR[vars])

	LogR10	LogR400
Min.	:-4.130	Min. :-2.9900
1st Qu.:	-1.210	1st Qu.:-0.2700
Median	:-0.170	Median : 0.0600
Mean	:-0.329	Mean : 0.1437
3rd Qu.:	0.490	3rd Qu.: 0.5700
Max.	: 3.310	Max. : 3.2400

### Describe()

<b>describe(df[vars])</b>									
<b>df[vars]</b>									
<b>2 Variables                      377 Observations</b>									
-----									
<b>LogR10</b>									
<b>n</b>	<b>missing</b>	<b>unique</b>	<b>Info</b>	<b>Mean</b>	<b>.05</b>	<b>.10</b>	<b>.25</b>	<b>.50</b>	
377	0	115	1	-0.329	-2.670	-2.250	-1.210	-0.170	
.75	.90	.95							
0.490	1.164	1.640							
<b>lowest: -4.13 -3.67 -3.47 -3.25 -3.14</b>									
<b>highest: 2.31 2.32 2.57 2.98 3.31</b>									
-----									
<b>LogR400</b>									
<b>n</b>	<b>missing</b>	<b>unique</b>	<b>Info</b>	<b>Mean</b>	<b>.05</b>	<b>.10</b>	<b>.25</b>	<b>.50</b>	
377	0	116	1	0.1437	-1.274	-0.794	-0.270	0.060	
.75	.90	.95							
0.570	0.990	1.660							
<b>lowest : -2.99 -2.67 -2.25 -2.01 -1.82</b>									
<b>highest: 2.24 2.57 2.65 2.98 3.24</b>									

Table 3. Statistical Output in R: Summary and Describe function

#### 4.1.1.2.2 Box Plot

Another useful function is the **Boxplot()**, this statistical tool groups the data through the quartiles values. The spacings between the different parts of the box indicate the degree of dispersion (spread) and skewness in the data, outliers and the quartile range ranges. The file (Box.csv) was used as input with 3 columns representing protein ID and Irr\_Dose (Log2R10 and Log2R400).

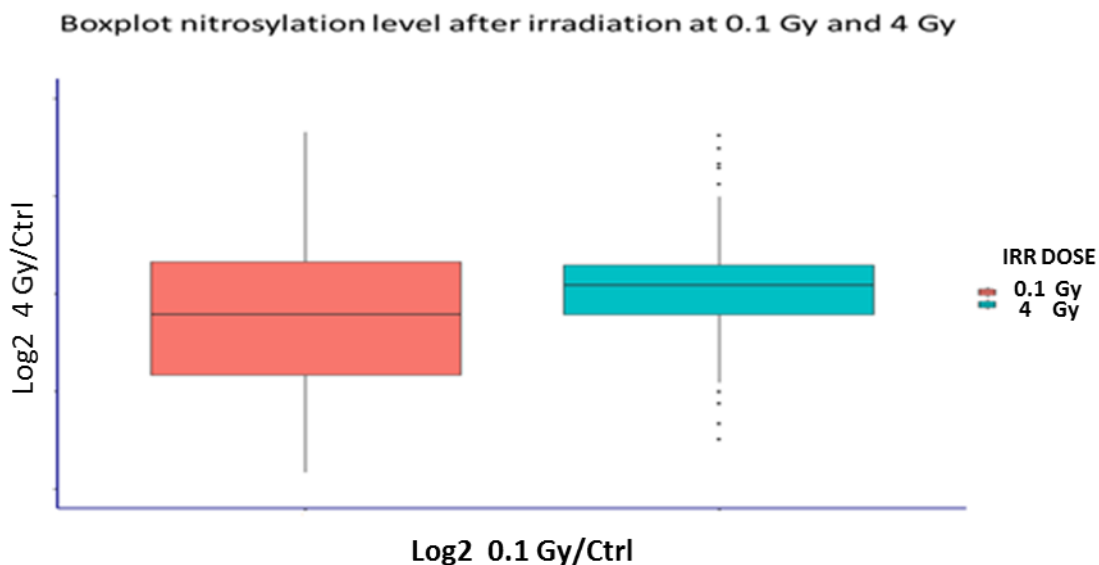


Figure 12. Boxplot displaying the data through the quartile ranges.  
Data in the Log2 (0.1/0 Gy) show more decrease and skewness in the negative range.

#### 4.1.1.2.3 Preliminary Grouping

Low dose irradiation resulted in an overall decrease in protein nitrosylation as compared to high dose (27% vs 8% respectively). A threshold of 1.3 was used: values above this threshold were considered as displaying increase in nitrosylation while values below this threshold showed decrease in nitrosylation.

Fold Change	Decrease in SNO	No Change in SNO	Increase in SNO
0.1 Gy/ Ctrl	27%	60%	12%
4 Gy/Ctrl	8%	83%	8%

Table 4. Percent of proteins with increase, no change or decrease in nitrosylation.

Most of the proteins had nitrosylation level less than 2 fold change (60% and 83%).

One protein (ATP5H) had a significant decrease (-17) in nitrosylation.

#### 4.1.1.2.4 Scatter Plots

In order to obtain a smooth scatter plot, the log2 of the ratios was taken (fold change data will show no values between -1 and 1). A scattergram was obtained showing the spread of the data between -4 and 4.

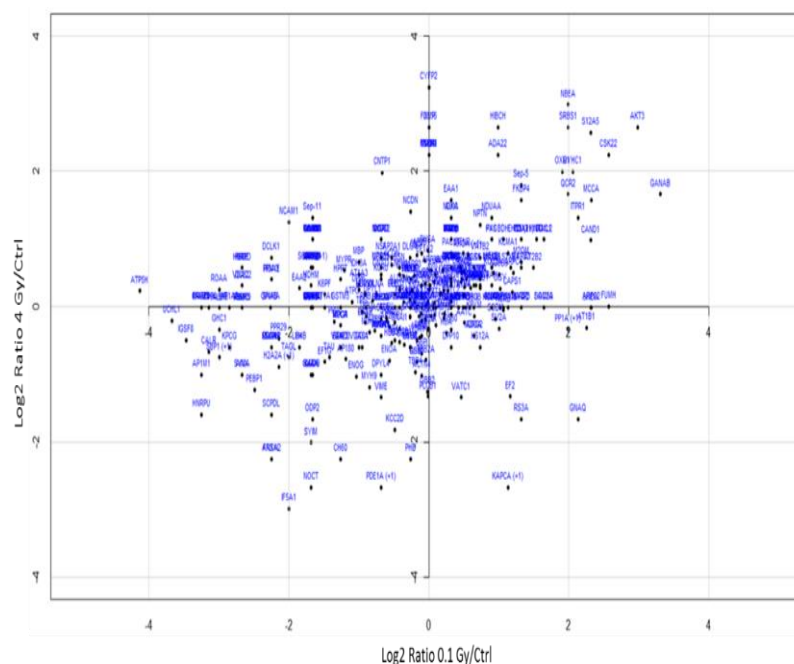


Figure 13. Log2 Scatter plot showing the spread of the data. Scattergraph generated in R: Log2 data. The dense area represents the proteins with no change in nitrosylation (-2 and 2). Areas shown are representative of differential nitrosylation between 0.1 Gy and 4 Gy irradiation.

Other plots available in R which can be used to further analyze the data are shown below

#### 4.1.1.2.5 Density plot Log Ratio

Density plot showing changes in nitrosylation after irradiation at low and high dose are displayed below.

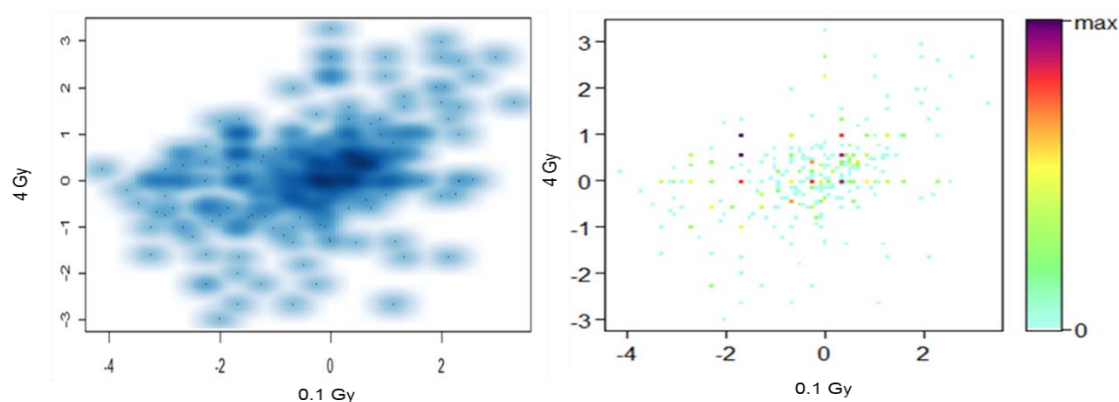


Figure 14. Various density plot displays in R

As shown in both plots the dense areas are within the no change zone between -2 and +2 log 2 Ratios. The axes were automatically generated in R.

#### 4.1.2 Clustering with R

Various tools available in R were utilized in order to obtain ‘what is the optimal number of clusters’.

##### 4.1.2.1 To Cluster or Not to Cluster: Hopkins Statistics

As discussed in the statistical section, before attempting to cluster the data we need to test whether clustering is possible as to avoid a random output from R functions.

The following code in R is meant to help in determining the tendency of the data to be clustered. Running the Hopkins test on our data resulted in a value less than 0.5 indicating that clustering is appropriate.

R Output:

```
Hopkins(df, n = nrow(df)-1)
$H
[1] 0.2524607
```

Running the Hopkins test on our random data having the same variation as the test data gave a value above 0.5 indicating that if these were random data, then they would not be appropriate for clustering.

R Output:

```
$H
[1] 0.5148587
```

It can be seen that the LogR dataset is highly clusterable (the H value = 0.5 which is above). However, the random\_df dataset is not clusterable (H= 0.25).

After showing that the data is clusterable, the next step is to determine the number of optimal clusters in the data.

#### 4.1.2.2 Prediction of the Right Number of Clusters with R

When using k-means clustering, it is important to examine where the bend in the plot is, and the best wss (within sum of squares) between the k-means choice (the total within-cluster sum of square (wss) measures the compactness of the clustering and the smallest in this value is the best choice). Using selected several clusters or groups, their wss (within sum of squares) were compared. The run with the lowest total within-cluster sum of squares was selected as the final clustering solution.

##### 4.1.2.2.1 The Elbow Method to Determine Number of Clusters: Scree Plots

The scree plot showed the within groups sum of squares by number of clusters extracted. This helped in estimating the appropriate number of clusters. A bend in the plot indicates the separation between the clusters. Here the elbow could be considered to be around 2 or 3 clusters.

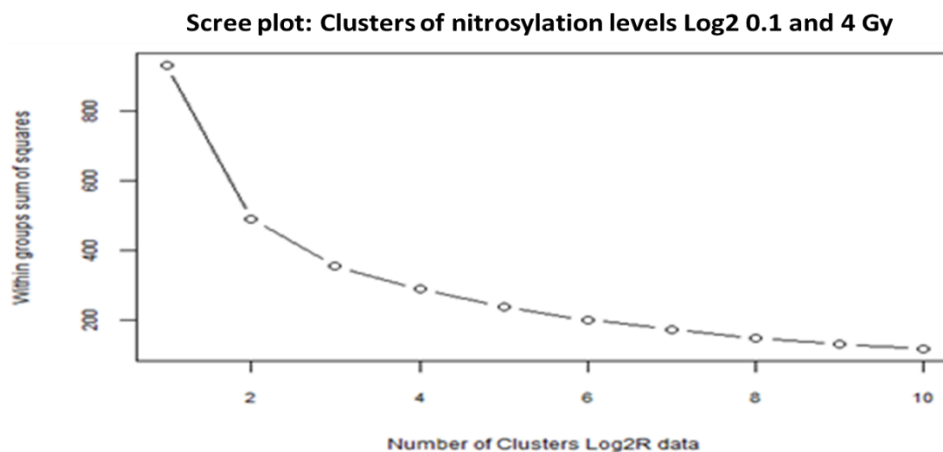


Figure 15. Scree plot  
The Scree plot showed a bend in the plot between 2 and 4.

The subsequent cluster analysis section contains the additional algorithm available in R to determine the number of appropriate clusters and appropriate grouping of the data.

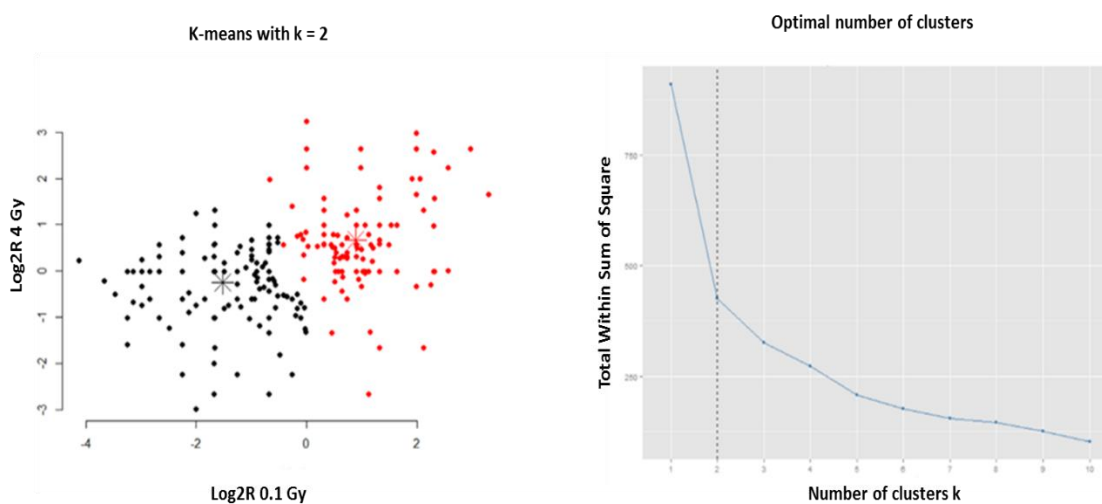


Figure 16. Plot showing the clustering by k-means algorithm.  
Clustering by 2: one cluster show decrease in nitrosylation (black), the second cluster shows an increase (red).

From the above plots, we see that the best clustering method is centered around 2 clusters solution. In k-means clustering it is necessary to specify the number of clusters.

#### 4.1.2.2.2 PAM Clustering

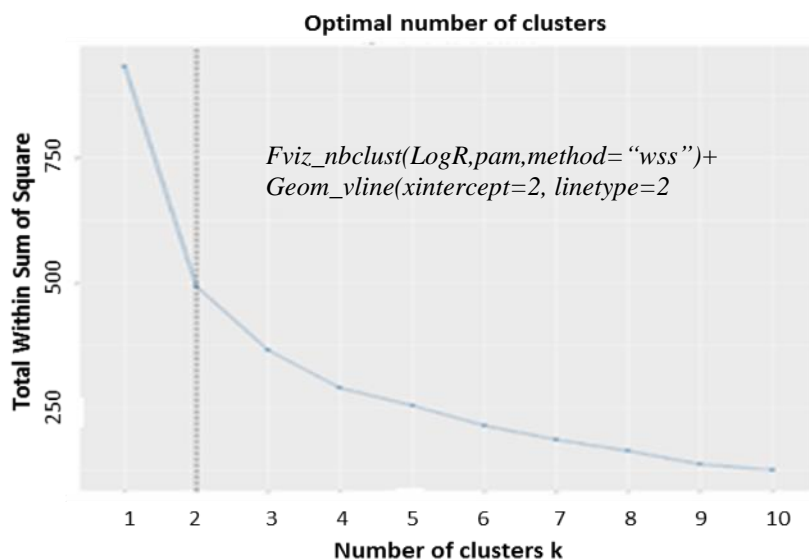


Figure 17. PAM clustering of protein data

Partition Around Medoids algorithm is also known as k-medoids clustering, a robust version of k-means clustering. It aims to minimize the average dissimilarity to all the objects in the cluster.

#### 4.1.2.2.3 Average Silhouette

The silhouette method of clustering starts by measuring how similar an object is to its own cluster (cohesion) compared to other clusters (separation). The method has a range from  $-1$  to  $+1$ , where a value near one indicates that the object belongs to its cluster. If objects in a silhouette have negative value, then the clustering configuration may have too many or too few clusters.

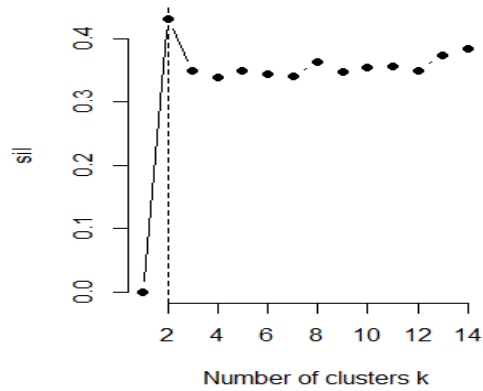


Figure 18. Average Silhouette with k cluster equals 2.

The disadvantage of the elbow methods is that it measures a global clustering characteristic only. A more sophisticated method is to use the gap statistic which provides a statistical procedure to formalize the elbow in order to estimate the optimal number of clusters.

#### 4.1.2.2.4 NbClust

NbClust package, published by Charrad *et al.* 2014,<sup>129</sup> provides 30 indices for determining the relevant number of clusters (*e.g.*, gamma, Gap, Silhouette, Hartigan).

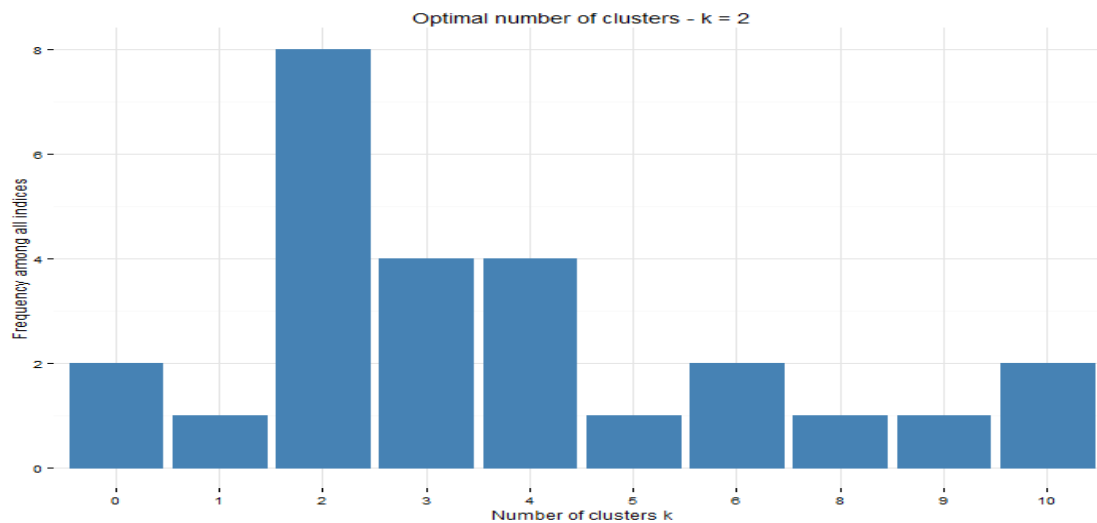


Figure 19. NbClust with frequency of indices optimal clusters K=2.

When using NbClust that uses 30 indices as criteria for clustering, the outcome is a consensus around 2 being the best selected number of clusters. When some of the separate indices were examined, a separation into 2 groups were considered to be the best solution.

#### R Output: Pam Best Clustering:

Number of clusters estimated by optimum average silhouette width: 2

The pam (partitioning around the medoids) clustering also indicates that the best cluster is 2 as shown in the graph below.

```
> plot(pam(d, pamk.best$nc))
```

```
library(fpc)
```

```
asw <- numeric(20)
```

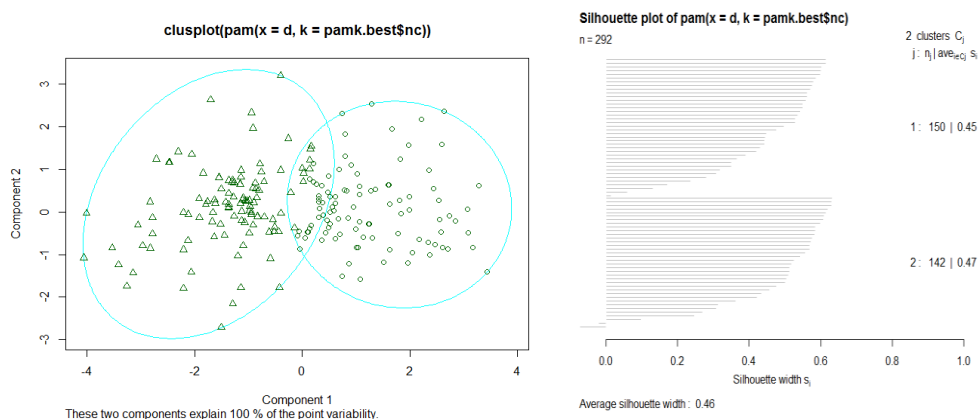


Figure 20. Best clustering solution in R using PAM.

Hierarchical clustering by 2:

Output R Code Calinski Cluster validation for (k in 2:20):

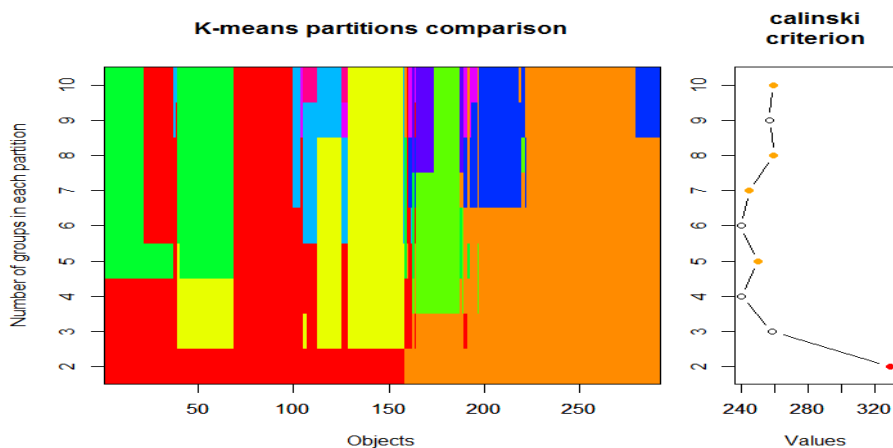
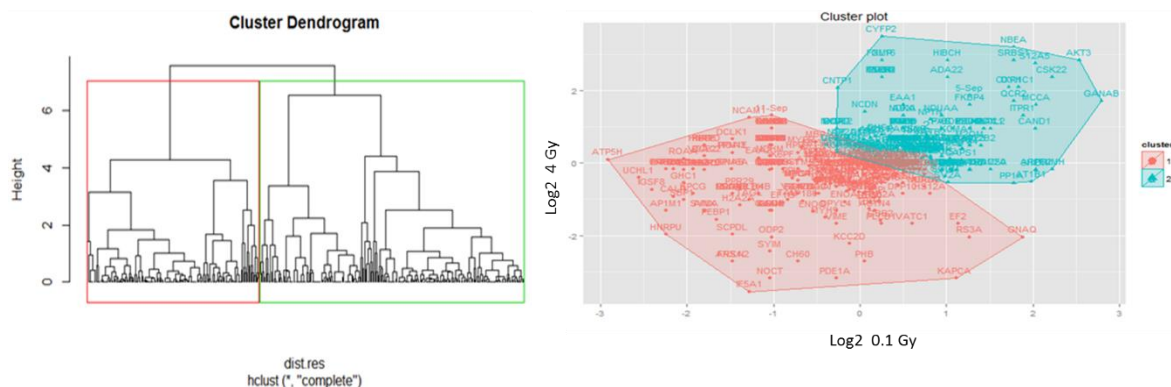


Figure 21. Best clustering solution in R using Calinski method.

We can also obtain more information on the clusters using the following R command, which gives us the number of proteins in cluster 1 (161) and cluster 2 (131). The clusters can also be saved to a file using the command write:

```
table(hc.cut)
hc.cut      1    2
           161 131
```

(Supplemental files CL1\_LogRF1 and CL2\_LgRF2)



```

dist.res <- dist(df, method = "euclidean")
# Hierarchical clustering results
hc <- hclust(dist.res, method = "complete")
# Visualization of hclust
plot(hc, labels=FALSE, hang = -1)

library(factoextra)
fviz_cluster(list(data = df, cluster =
hc.cut))

```

Figure 22. R: Identifying optimal clustering solution.

#### 4.1.2.2.5 Clustering Validity CIValid

<code>summary(intern)</code>						
Clustering Methods:						
hierarchical kmeans pam						
Cluster sizes:						
2 3 4 5 6						
Validation Measures:						
		2	3	4	5	6
hierarchical	Connectivity	8.1361	10.9468	19.9937	26.3635	31.5583
	Dunn	0.0522	0.0647	0.0647	0.0647	0.0647
kmeans	Silhouette	0.4678	0.4331	0.3942	0.3753	0.3873
	Connectivity	15.2218	28.5119	35.9909	47.1651	53.2881
pam	Dunn	0.0201	0.0409	0.0236	0.0251	0.0520
	Silhouette	0.4680	0.3912	0.3742	0.4042	0.4122
	Connectivity	24.6167	24.1266	40.3159	51.3294	69.9262
	Dunn	0.0171	0.0430	0.0470	0.0281	0.0361
	Silhouette	0.4588	0.3838	0.3726	0.3867	0.3698
Optimal Scores:						
	Score	Method	Clusters			
Connectivity	8.1361	hierarchical	2			
Dunn	0.0647	hierarchical	3			
Silhouette	0.4680	kmeans	2			

Table 5. CIValid best cluster by hierarchical and Silhouette method.

Hierarchical clustering with two clusters performs the best, with the Dunn index it gives clustering by three. K-means scores the highest with the Silhouette method (described

previously) with a score of 0.4588 giving clustering result of 2. All three plots are shown below:

```
op <- par(no.readonly=TRUE)
par(mfrow=c(2,2),mar=c(4,4,3,1))
plot(intern, legend=FALSE)
plot(nClusters(intern),measures(intern,"Dunn")[,1],type="n",axes=F,
     xlab="",ylab="")
legend("center", clusterMethods(intern), col=1:9, lty=1:9, pch=paste(1:9))
par(op)
```

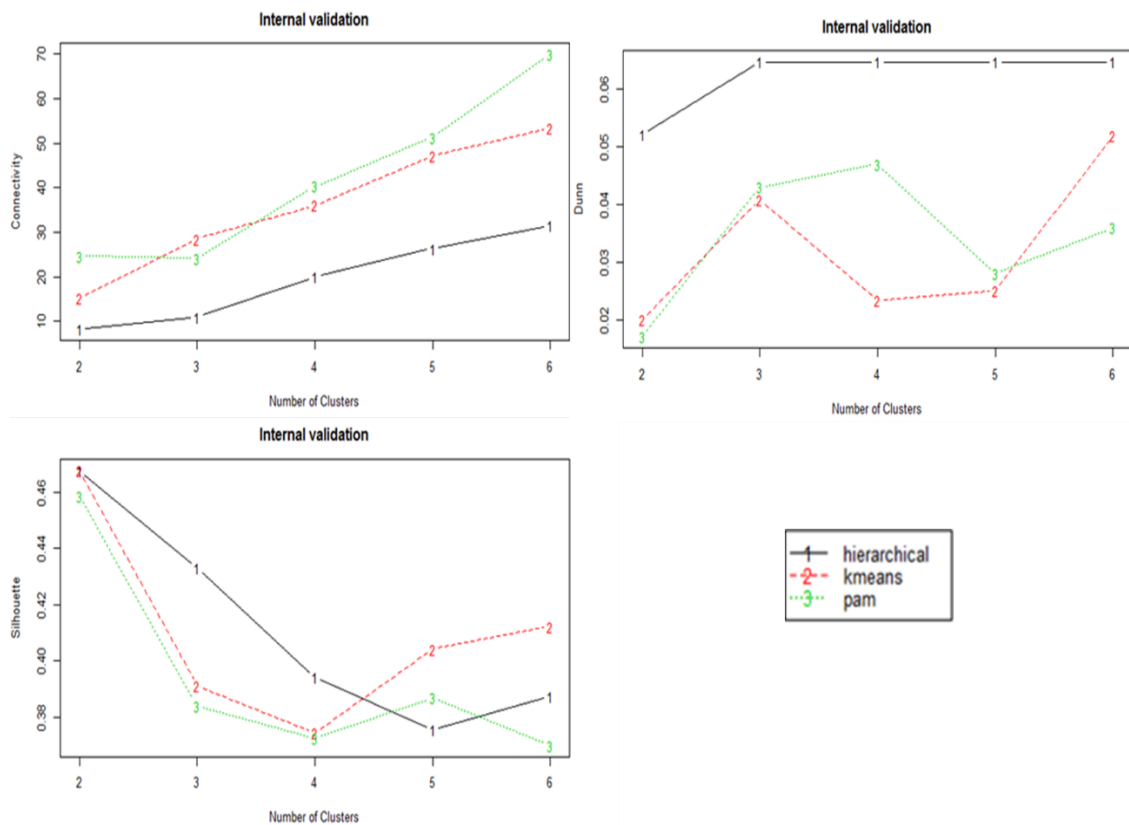


Figure 23. Plots: connectivity, Dunn Index, and Silhouette Width.

The connectivity should be minimized, while both the Dunn Index and the Silhouette Width should be maximized. Thus, it appears that hierarchical clustering (UPGMA) outperforms the other clustering algorithms. In top left graph, hierarchical

clustering has a minimized connectivity while it has a maximum Dunn and Silhouette index. For hierarchical clustering the optimal number of clusters is clearly two.

#### 4.1.2.2.6 The OptCluster Method

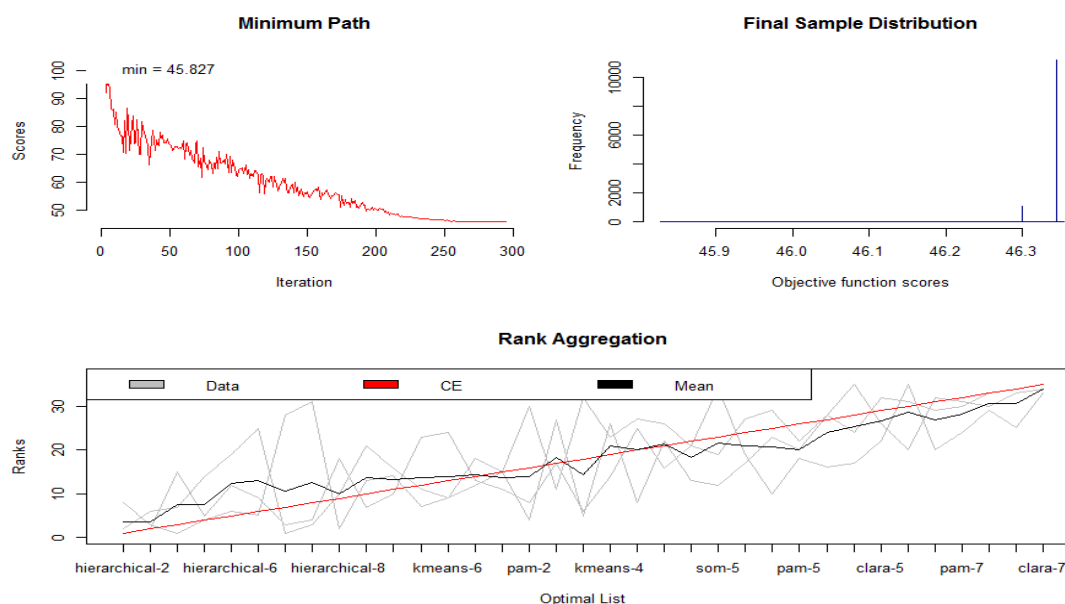


Figure 24. OptCluster: the optimal cluster solution with iterative runs.

The graph shows the statistically significant differences among the clustering methods and the iterative runs.

The overall optimal clustering method and number of clusters is: **hierarchical-2**

The optimal list is:

hierarchical-2 hierarchical-3 hierarchical-7 hierarchical-4 hierarchical-6  
hierarchical-5 kmeans-2 som-2 hierarchical-8 pam-3 som-3 kmeans-7 kmeans-6  
som-4 kmeans-3 pam-2 pam-4 clara-2 kmeans-4 som-6 clara-3 kmeans-5 som-7  
kmeans-8 pam-5 pam-6 som-8 clara-5 clara-4 pam-8 pam-7 clara-6 clara-8 clara-  
7

Algorithm: CE

Distance: Spearman

Score: 45.82707

Iterations: 295

Optimal Scores:

	Score	Method	Clusters
<b>Connectivity</b>	<b>8.1361</b>	<b>hierarchical</b>	<b>2</b>
Dunn	0.0714	hierarchical	7
Silhouette	0.4680	kmeans	2

### Heatmap: Shiny App and Interactive d3heatmap Demo

Heatmap and Dendrogram showing nitrosylation level at 0.1 Gy and 4 Gy:

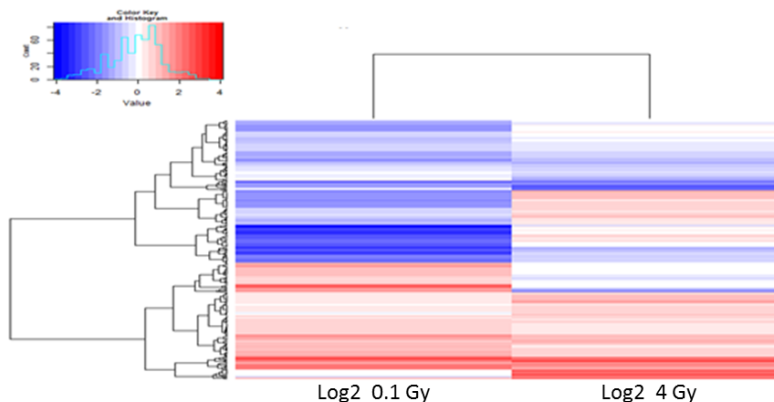


Figure 25. HeatMap data showing differential nitrosylation.  
Increase (Red) and decrease (Blue) in nitrosylation at Log2 0.1 and 4 Gy

There is a clear cut clustering in the data for irradiation at 0.1 Gy. If we look at Log2 0.1 Gy data, we see one cluster showing increase in nitrosylation (red) and one cluster showing decrease in nitrosylation. The Log2 4 Gy data (irradiated at 4 Gy) does not have the same clear division, i.e. decrease and increase in nitrosylation show about 4 clusters (groups of red blue). The blue on the left indicates that more proteins exhibited a decrease in nitrosylation after irradiation at 0.1 Gy as compared to 4 Gy. The dendrogram also shows that the best clustering is indicative of 2 as shown by previous algorithms.



Figure 26. Shiny Interactive HeatMap application

The Heatmap is a web based application displaying an interactive map where rolling the mouse over the image will list the name and values of proteins involved.

#### 4.1.3 Cluster Analysis with R: Membership Changes

The data was clustered with varying the number of clusters ranging from two to 9 using Hierarchical clustering. The purpose of such exercise was to see how the proteins were changing membership as the number of clusters increased.

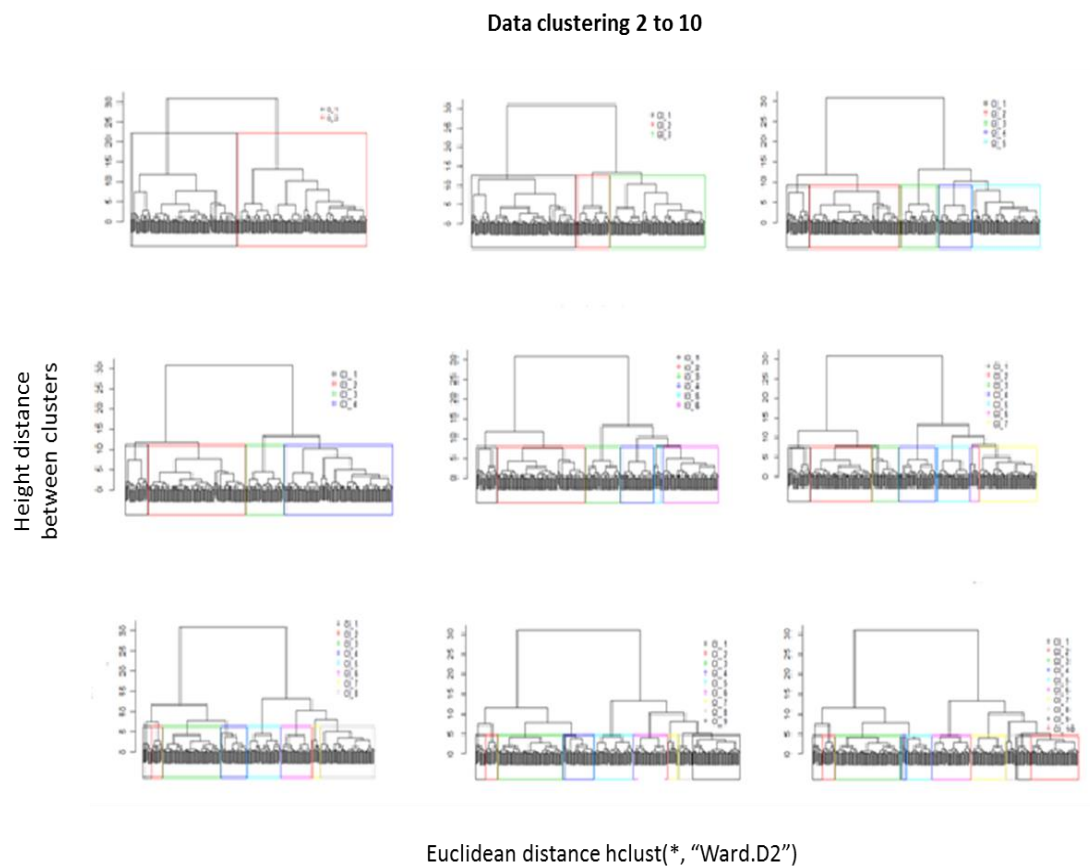


Figure 27. Membership changes as the number of clusters is increased.

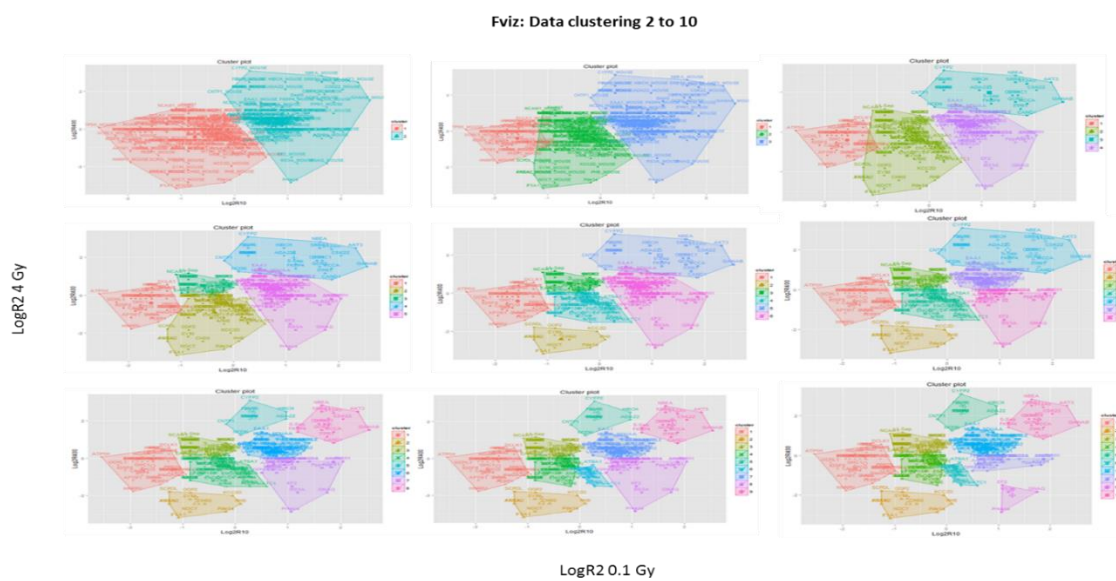


Figure 28. fviz function displaying membership changes

The aggregate function gives the table below:

```
a3 = aggregate(LogR,list(hc.cut),median)
data.frame(Cluster=a3[,1],Freq=as.vector(table(hc.cut)),a3[,-1])
```

Cluster	Freq	Log2R10	Log2R400	Cluster	Freq	Log2R10	Log2R400	Cluster	Freq	Log2R10	Log2R400
1	161	-1.49	-0.15	1	43	-2.670	-0.020	1	43	-2.670	-0.020
2	131	0.73	0.57	2	118	-0.975	-0.175	2	118	-0.975	-0.175
				3	131	0.730	0.570	3	25	1.320	2.240
								4	106	0.730	0.485
Cluster	Freq	Log2R10	Log2R400	Cluster	Freq	Log2R10	Log2R400	Cluster	Freq	Log2R10	Log2R400
1	43	-2.67	-0.020	1	43	-2.670	-0.020	1	43	-2.670	-0.02
2	79	-0.85	-0.560	2	11	-1.680	-2.250	2	11	-1.680	-2.25
3	39	-1.66	0.580	3	39	-1.660	0.580	3	39	-1.660	0.58
4	25	1.32	2.240	4	68	-0.785	-0.430	4	68	-0.785	-0.43
5	106	0.73	0.485	5	25	1.320	2.240	5	25	1.320	2.24
				6	106	0.730	0.485	6	73	0.640	0.58
								7	33	1.060	-0.02
Cluster	Freq	Log2R10	Log2R400	Cluster	Freq	Log2R10	Log2R400	Cluster	Freq	Log2R10	Log2R400
1	43	-2.670	-0.020	1	43	-2.670	-0.020	1	43	-2.670	-0.020
2	11	-1.680	-2.250	2	11	-1.680	-2.250	2	11	-1.680	-2.250
3	39	-1.660	0.580	3	39	-1.660	0.580	3	39	-1.660	0.580
4	68	-0.785	-0.430	4	52	-0.950	-0.280	4	52	-0.950	-0.280
5	11	0.000	2.240	5	11	0.000	2.240	5	11	0.000	2.240
6	73	0.640	0.580	6	16	-0.170	-0.740	6	16	-0.170	-0.740
7	33	1.060	-0.020	7	73	0.640	0.580	7	73	0.640	0.580
8	14	2.095	1.895	8	33	1.060	-0.020	8	29	1.000	-0.020
				9	14	2.095	1.895	9	4	1.240	-1.660
								10	14	2.095	1.895

Table 6. Protein membership changes per number of clusters

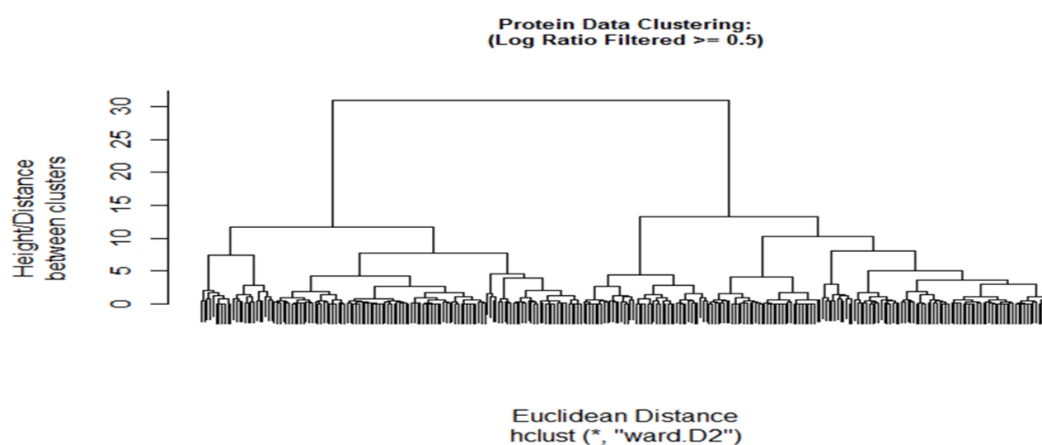


Figure 29. Dendrogram of the hierarchical clustering of proteins

#### 4.1.4 Manual Clustering

The aim of manual grouping was to detect groups of nitrosylated proteins showing the characteristic nitrosylation under low and high dose irradiation. The data was manually clustered into 9 groups according to the threshold of 1.3 fold change: nitrosylation values above 1.3 were considered to show an increase, and values below 1.3 reflected a decrease in nitrosylation. After many attempts at selecting the most suitable fold change to cluster the data, 1.3 was selected as it was shown to preserve data integrity and this fold change corresponded to a log ratio of  $\sim 0.5$ . The use of threshold aimed to separate the data with very small changes in nitrosylation to the proteins with significant change in nitrosylation level. The graphs generated by R showed the results of the log data, while the spectral representation with the fold change table was done in excel.

The following table shows the number of proteins in each of the 9 groups generated.

<b>Group #</b>	<b>Increase or decrease according to threshold of 1.3 Inc=increase, Dec=decreased, NC=no change</b>	<b># Proteins</b>
1	Inc10/Inc400	51
2	Inc10/Dec400	8
3	Inc10/NC400	38
4	Dec10/Dec400	52
5	Dec10/Inc400	41
6	Dec10/NC400	63
7	NC10/Inc400	41
8	NC10/Dec400	17
9	NC10/NC400	56

Table 7. Protein groups with increase/decrease in SNO.

#### 4.1.4.1 No Change in Nitrosylation at LDIR

##### 4.1.4.1.1 No Change after LDIR and Increase at HDIR

Graph on the left is output from R using function ggplot. Right diagram is scatterplot in excel.

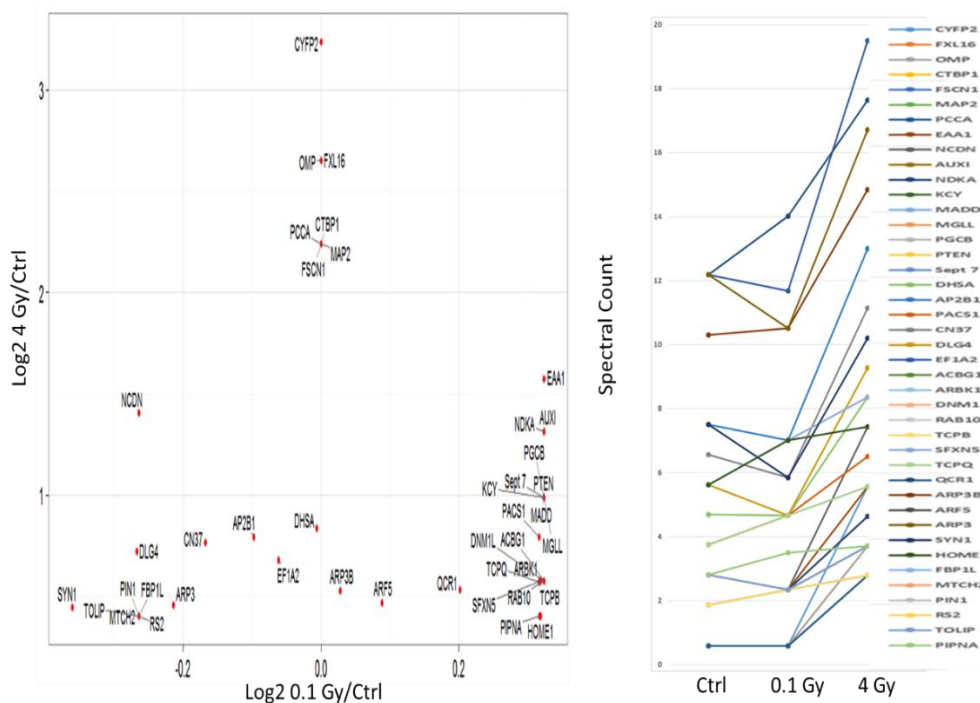


Figure 30. Scatter plot: No change in SNO at 0.1 Gy with an increase at 4 Gy

ID	Ctrl	0.1 Gy	4 Gy	SparkPlot	0.1 Gy/Ctrl	4Gy/Ctrl	ID	Ctrl	0.1 Gy	4 Gy	Spark Plot	0.1 Gy/Ctrl	4Gy/Ctrl
CYFP2	0.59	0.59	5.57		1.00	9.44	DLG4	5.62	4.67	9.28		-1.20	1.65
FXL16	0.59	0.59	3.71		1.00	6.29	EF1A2	12.19	11.68	19.5		-1.04	1.60
OMP	0.59	0.59	3.71		1.00	6.29	ACBG1	1.87	2.34	2.79		1.25	1.49
CTBP1	0.59	0.59	2.79		1.00	4.73	ARBK1	1.87	2.34	2.79		1.25	1.49
FSCN1	0.59	0.59	2.79		1.00	4.73	DNM1L	1.87	2.34	2.79		1.25	1.49
MAP2	0.59	0.59	2.79		1.00	4.73	RAB10	1.87	2.34	2.79		1.25	1.49
PCCA	0.59	0.59	2.79		1.00	4.73	TCPB	1.87	2.34	2.79		1.25	1.49
EAA1	1.87	2.34	5.57		1.25	2.98	SFXN5	5.62	7.01	8.36		1.25	1.49
NCDN	2.81	2.34	7.43		-1.20	2.64	TCPQ	3.75	4.67	5.57		1.25	1.49
AUX1	1.87	2.34	4.64		1.25	2.48	QCR1	12.19	14.02	17.64		1.15	1.45
NDKA	1.87	2.34	4.64		1.25	2.48	ARP3B	10.31	10.51	14.85		1.02	1.44
KCY	1.87	2.34	3.71		1.25	1.98	ARF5	108.74	115.64	150.4		1.06	1.38
MADD	1.87	2.34	3.71		1.25	1.98	ARP3	12.19	10.51	16.71		-1.16	1.37
MGLL	1.87	2.34	3.71		1.25	1.98	SYN1	7.5	5.84	10.21		-1.28	1.36
PGCB	1.87	2.34	3.71		1.25	1.98	HOME1	5.62	7.01	7.43		1.25	1.32
PTEN	1.87	2.34	3.71		1.25	1.98	FBP1L	2.81	2.34	3.71		-1.20	1.32
Sept 7	1.87	2.34	3.71		1.25	1.98	MTCH2	2.81	2.34	3.71		-1.20	1.32
DHSA	4.69	4.67	8.36		-1.00	1.78	PIN1	2.81	2.34	3.71		-1.20	1.32
AP2B1	7.5	7.01	13		-1.07	1.73	RS2	2.81	2.34	3.71		-1.20	1.32
PACS1	3.75	4.67	6.5		1.25	1.73	TOLIP	2.81	2.34	3.71		-1.20	1.32
CN37	6.56	5.84	11.14		-1.12	1.70	PIPNA	2.81	3.5	3.71		1.25	1.32

Table 8. Heat table: No change in SNO at 0.1 Gy, increase at 4 Gy.

The scatter graph generated by R (top left) clearly shows the central group of protein cluster showing ~ 4x increase in nitrosylation at 4 Gy with no change at 0.1 Gy (CYFP2, FXL16, OMP, CTBP1, FSCN1, MAP2, PCCA and EAA1) with protein CYFP2 showing the greatest increase at 4 Gy. ARF 5 was included in this group as it showed a slight increase in nitrosylation at high dose radiation.

#### 4.1.4.1.2 No Change in Nitrosylation at LDIR and No Change at HDIR

ID	Ctrl	0.1 Gy	4 Gy	Spark	0.1 Gy/Ctrl	4 Gy/Ctrl	ID	Ctrl	0.1 Gy	4 Gy	Spark	0.1 Gy/Ctrl	4 Gy/Ctrl
COF2	4.69	4.67	3.7		-1.00	-1.26	CNTP2	5.62	5.84	5.57		1.04	-1.01
ERF3A	4.69	4.67	3.7		-1.00	-1.26	BTBDH	2.81	2.34	2.79		-1.20	-1.01
C560	4.69	5.84	3.7		1.25	-1.26	DDX3L	2.81	2.34	2.79		-1.20	-1.01
ACTB	68.4	73.59	57		1.08	-1.21	MGST3	2.81	2.34	2.79		-1.20	-1.01
ODPB	7.5	7.01	6.5		-1.07	-1.15	TALDO	2.81	2.34	2.79		-1.20	-1.01
AT8A1	8.44	8.18	7.4		-1.03	-1.14	TBA1A	114.4	111	115		-1.03	1.01
ADT2	27.2	31.54	24		1.16	-1.13	SYT1	44.06	46.73	45.5		1.06	1.03
SPTB2	19.7	16.35	18		-1.20	-1.12	SPTA2	36.56	31.54	38.1		-1.16	1.04
CY1	10.3	10.51	9.3		1.02	-1.11	ARP2	17.81	17.52	18.6		-1.02	1.04
COF1	11.3	9.35	10		-1.20	-1.10	EF1A1	15	11.68	15.8		-1.28	1.05
TBA1B	127	115.6	116		-1.10	-1.10	DPYL2	27.18	33.88	28.8		1.25	1.06
AATM	12.2	12.85	11		1.05	-1.09	RAB3A	11.25	9.35	12.1		-1.20	1.07
GABT	13.1	16.35	12		1.25	-1.09	2AAA	7.5	7.01	8.36		-1.07	1.11
SV2B	14.1	16.35	13		1.16	-1.08	S6A17	7.5	9.35	8.36		1.25	1.11
TBA4A	120	111	112		-1.08	-1.07	VATA	27.18	30.37	30.6		1.12	1.13
NT5D3	3.75	3.5	3.7		-1.07	-1.01	HS90B	47.81	53.73	54.8		1.12	1.15
TEBP	3.75	3.5	3.7		-1.07	-1.01	VP26A	5.62	4.67	6.5		-1.20	1.16
GLU2B	3.75	4.67	3.7		1.25	-1.01	G3P	20.62	17.52	24.1		-1.18	1.17
HYOU1	3.75	4.67	3.7		1.25	-1.01	DYN1	25.31	29.2	29.7		1.15	1.17
KS6A3	3.75	4.67	3.7		1.25	-1.01	HS90A	63.74	77.1	75.2		1.21	1.18
OCAD2	3.75	4.67	3.7		1.25	-1.01	CMC1	9.37	9.35	11.1		-1.00	1.19
RP3A	3.75	4.67	3.7		1.25	-1.01	RL5	3.75	3.5	4.64		-1.07	1.24
SUCB1	3.75	4.67	3.7		1.25	-1.01	ROA1	3.75	3.5	4.64		-1.07	1.24
SYNJ1	3.75	4.67	3.7		1.25	-1.01	ODO1	3.75	4.67	4.64		1.25	1.24
SMD3	7.5	7.01	7.4		-1.07	-1.01	DX39B	15	15.19	18.6		1.01	1.24
VATH	6.56	7.01	6.5		1.07	-1.01	VPP1	16.87	16.35	21.4		-1.03	1.27
ACTY	5.62	4.67	5.6		-1.20	-1.01	VATE1	6.56	8.18	8.36		1.25	1.27
AL1L1	5.62	4.67	5.6		-1.20	-1.01	HXK1	12.19	12.85	15.8		1.05	1.29

Table 9. Heat table: No change in SNO at 0.1 Gy, no change at 4 Gy.

As shown in ([Table 7](#)), 56 proteins belonged to the group where there was no significant change in nitrosylation under irradiation at either low dose (0.1 Gy) or high dose (4 Gy). Similarly, to the first group (no change at low dose but increase at high dose), this group was also found to have a high percentage of the function related to catalytic and binding activity.

#### 4.1.4.1.3 No Change after LDIR and Decrease at HDIR

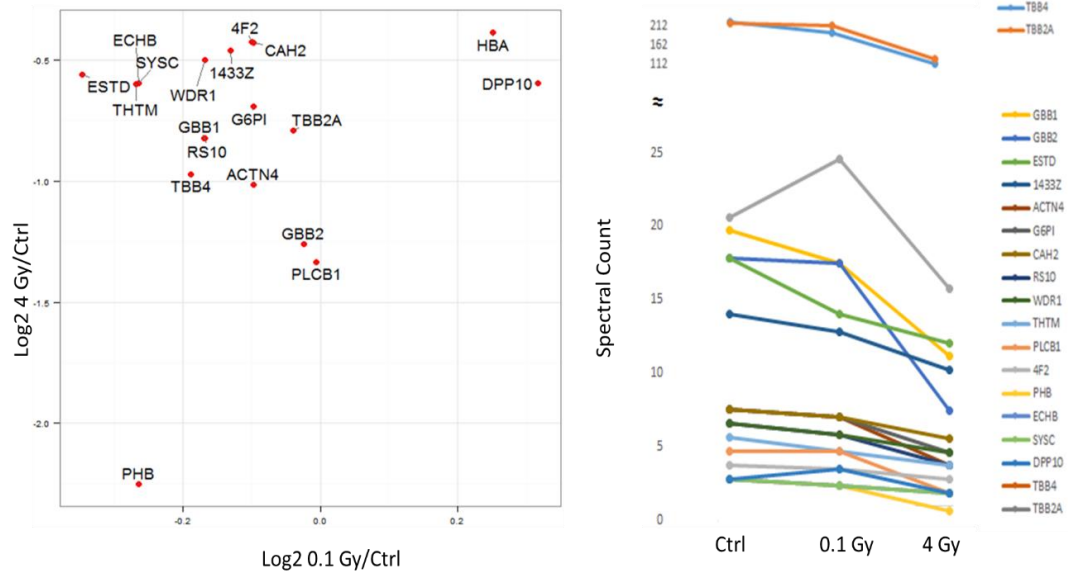


Figure 32. Scatter plot: No change in SNO at 0.1 Gy, decrease at 4 Gy.

ID	Ctrl	0.1 Gy	4 Gy	Spark Plot	0.1 Gy/Ctrl	4 Gy/Ctrl
TBB4	222.2	195.08	113.26		-1.14	-1.96
TBB2A	218.4	212.6	126.26		-1.03	-1.73
HBA	20.62	24.53	15.78		1.19	-1.31
GBB1	19.69	17.52	11.14		-1.12	-1.77
GBB2	17.81	17.52	7.43		-1.02	-2.40
ESTD	17.81	14.02	12.07		-1.27	-1.48
1433Z	14.06	12.85	10.21		-1.09	-1.38
ACTN4	7.5	7.01	3.71		-1.07	-2.02
G6PI	7.5	7.01	4.64		-1.07	-1.62
CAH2	7.5	7.01	5.57		-1.07	-1.35
RS10	6.56	5.84	3.71		-1.12	-1.77
WDR1	6.56	5.84	4.64		-1.12	-1.41
THTM	5.62	4.67	3.71		-1.20	-1.51
PLCB1	4.69	4.67	1.86		-1.00	-2.52
4F2	3.75	3.5	2.79		-1.07	-1.34
PHB	2.81	2.34	0.59		-1.20	-4.76
ECHB	2.81	2.34	1.86		-1.20	-1.51
SYSC	2.81	2.34	1.86		-1.20	-1.51
DPP10	2.81	3.5	1.86		1.25	-1.51

Table 10. Heat Table: No change in SNO at 0.1 Gy, decrease at 4 Gy.

Nineteen (19) proteins belonged to this group with protein PHB showing the greatest decrease at 4 Gy.

#### 4.1.4.2 Decrease in Nitrosylation after LDIR

##### 4.1.4.2.1 Decrease after LDIR and Increase at HDIR

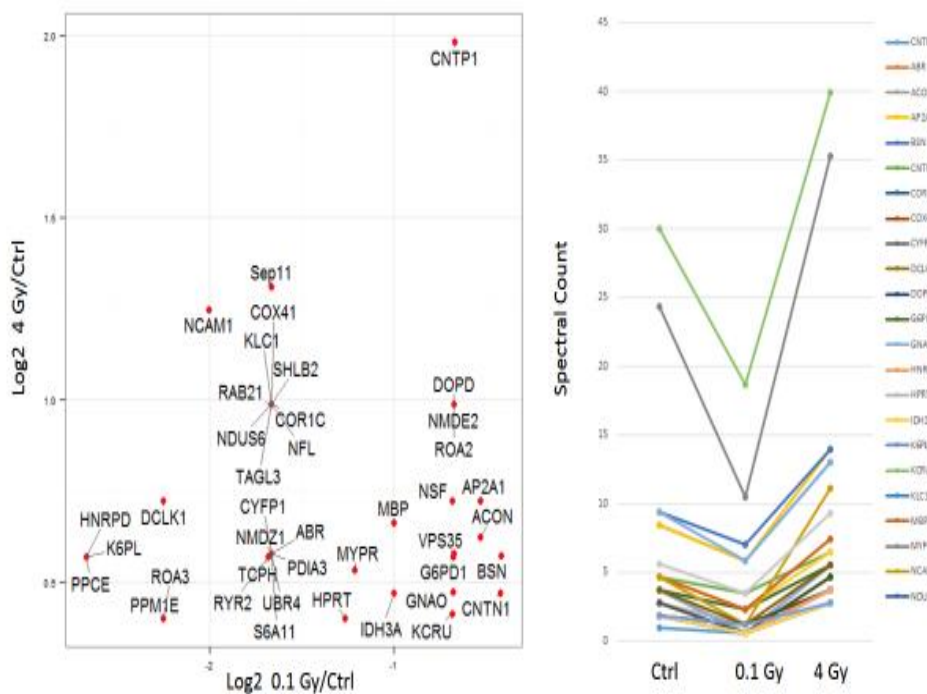


Figure 33. Scatter plot: Decrease in SNO at 0.1 Gy, increase at 4 Gy. Proteins showing a decrease at 0.1 Gy and an increase at 4 Gy (nitrosylation level represents the raw spectral count).

ID	Ctrl	0.1 Gy	4 Gy	Spark	0.1 Gy/Ctrl	4 Gy/Ctrl	ID	Ctrl	0.1 Gy	4 Gy	Spark	0.1 Gy/Ctrl	4 Gy/Ctrl
CNTP1	0.9	0.59	3.71		-1.59	3.95	NCAM1	4.69	1.17	11.14		-4.01	2.38
ABR	1.9	0.59	2.79		-3.17	1.49	NDUS6	1.87	0.59	3.71		-3.17	1.98
ACON	8.4	5.84	13		-1.45	1.54	NFL	1.87	0.59	3.71		-3.17	1.98
AP2A1	8.4	5.84	13.9		-1.45	1.65	NMDE2	1.87	1.17	3.71		-1.60	1.98
BSN	9.4	7.01	13.9		-1.34	1.49	NMDZ1	1.87	0.59	2.79		-3.17	1.49
CNTN1	4.7	3.5	6.5		-1.34	1.39	NSF	5.62	3.5	9.28		-1.61	1.65
COR1C	1.9	0.59	3.71		-3.17	1.98	PDIA3	1.87	0.59	2.79		-3.17	1.49
COX41	1.9	0.59	3.71		-3.17	1.98	PPCE	3.75	0.59	5.57		-6.36	1.49
CYFP1	1.9	0.59	2.79		-3.17	1.49	PPM1E	2.81	0.59	3.71		-4.76	1.32
DCLK1	2.8	0.59	4.64		-4.76	1.65	RAB21	1.87	0.59	3.71		-3.17	1.98
DOPD	1.9	1.17	3.71		-1.60	1.98	ROA2	1.87	1.17	3.71		-1.60	1.98
G6PD1	3.8	2.34	5.57		-1.60	1.49	ROA3	2.81	0.59	3.71		-4.76	1.32
GNAO	9.4	5.84	13		-1.60	1.39	RYR2	3.75	1.17	5.57		-3.21	1.49
HNRPD	3.8	0.59	5.57		-6.36	1.49	S6A11	1.87	0.59	2.79		-3.17	1.49
HPRT	2.8	1.17	3.71		-2.40	1.32	Sep11	1.87	0.59	4.64		-3.17	2.48
IDH3A	4.7	2.34	6.5		-2.00	1.39	SHLB2	1.87	0.59	3.71		-3.17	1.98
K6PL	3.8	0.59	5.57		-6.36	1.49	TAGL3	1.87	0.59	3.71		-3.17	1.98
KCRU	30	18.69	39.9		-1.61	1.33	TCPH	1.87	0.59	2.79		-3.17	1.49
KLC1	1.9	0.59	3.71		-3.17	1.98	UBR4	1.87	0.59	2.79		-3.17	1.49
MBP	4.7	2.34	7.43		-2.00	1.58	VPS35	1.87	1.17	2.79		-1.60	1.49
MYPR	24	10.51	35.3		-2.32	1.45							

Table 11. Heat table: decrease in SNO at 0.1 Gy, increase at 4 Gy.

A comparison of proteins showing decrease in nitrosylation (fold change less than 1.3) after irradiation at 0.1 Gy while the same proteins experienced an increase in nitrosylation at 4 Gy. HNRPD, K6PL and PPCE showed greater than 6 fold decrease in nitrosylation.

This group of proteins ( $\downarrow$ 0.1 Gy,  $\uparrow$ 4 Gy) had a change in nitrosylation ranging from 6 fold decrease to ~4 fold increase as shown in the above table. The 3 proteins with a significant decrease of 6 fold include HNRPD, K6PL and PPCE. Other proteins showing greater than 4 fold decrease, although the increase was moderate, include NCAM1, DCLK1, PPM1E and ROA3. The protein SEP-11 protein showed a slight decrease in nitrosylation; however, the nitrosylation at HDIR was significant (~4 fold).

#### 4.1.4.2.2 Decrease after LDIR and Decrease at HDIR

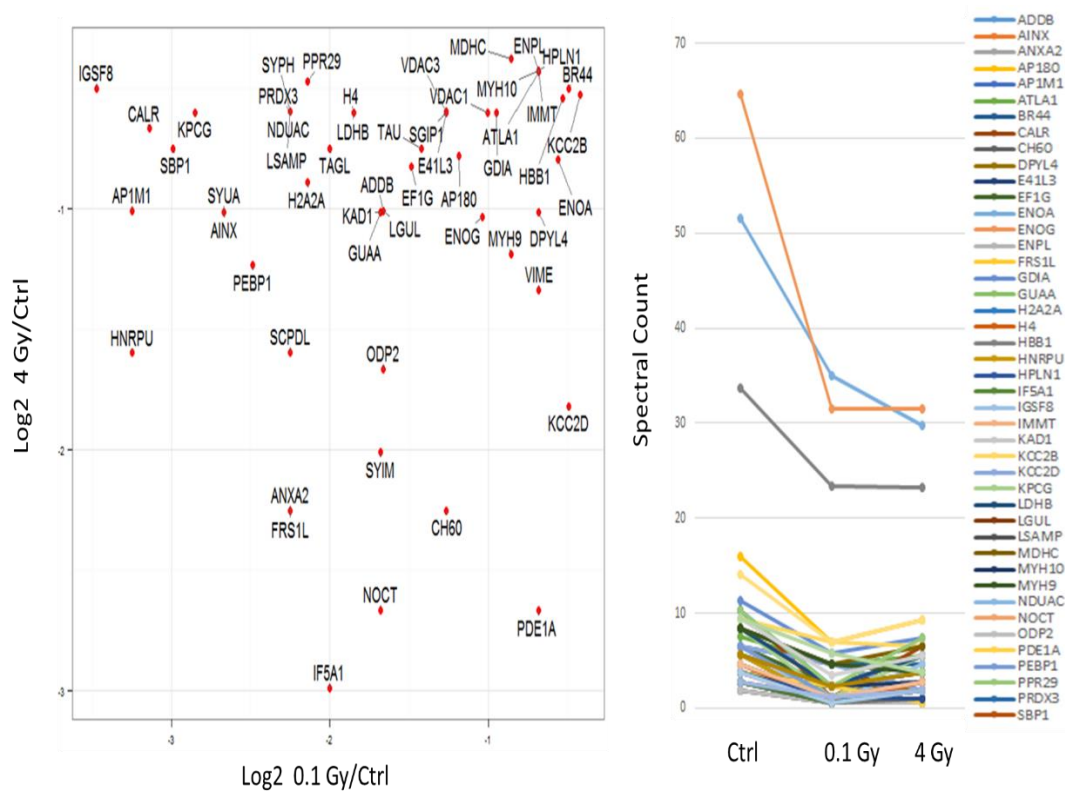


Figure 34. Decrease in nitrosylation after 0.1 Gy and 4 Gy irradiation.

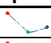
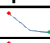
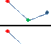
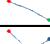
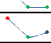


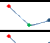



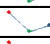
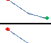
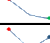
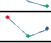
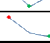
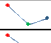
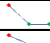

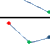
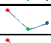
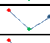


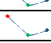
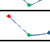
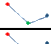
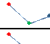

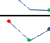
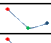
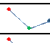
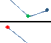

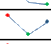
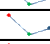
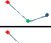
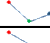




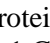
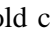
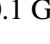



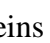
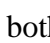


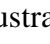
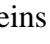
ID	Ctrl	0.1 Gy	4 Gy	Spark	0.1 Gy/Ctrl	4 Gy/Ctrl	ID	Ctrl	0.1 Gy	4 Gy	Spark	0.1 Gy/Ctrl	4 Gy/Ctrl
ADDB	1.87	0.59	0.93		-3.17	-2.01	KCC2B	9.37	7.01	6.5		-1.34	-1.44
AINX	3.75	0.59	1.86		-6.36	-2.02	KCC2D	6.56	4.67	1.86		-1.40	-3.53
ANXA2	2.81	0.59	0.59		-4.76	-4.76	KPCG	8.44	1.17	5.57		-7.21	-1.52
AP180	15.94	7.01	9.28		-2.27	-1.72	LDHB	8.44	2.34	5.57		-3.61	-1.52
AP1M1	5.62	0.59	2.79		-9.53	-2.01	LGUL	1.87	0.59	0.93		-3.17	-2.01
ATLA1	7.5	4.67	5.57		-1.61	-1.35	LSAMP	2.81	0.59	1.86		-4.76	-1.51
BR44	6.56	4.67	4.64		-1.40	-1.41	MDHC	8.44	4.67	6.5		-1.81	-1.30
CALR	10.31	1.17	6.5		-8.81	-1.59	MYH10	3.75	2.34	2.79		-1.60	-1.34
CH60	2.81	1.17	0.59		-2.40	-4.76	MYH9	8.44	4.67	3.71		-1.81	-2.27
DPYL4	3.75	2.34	1.86		-1.60	-2.02	NDUAC	2.81	0.59	1.86		-4.76	-1.51
E41L3	5.62	2.34	3.71		-2.40	-1.51	NOCT	3.75	1.17	0.59		-3.21	-3.21
EF1G	6.56	2.34	3.71		-2.80	-1.77	ODP2	1.87	0.59	0.59		-3.17	-3.17
ENOA	51.56	35.04	29.71		-1.47	-1.74	PDE1A	3.75	2.34	0.59		-1.60	-6.36
ENOG	64.68	31.54	31.57		-2.05	-2.05	PEBP1	6.56	1.17	2.79		-5.61	-2.35
ENPL	3.75	2.34	2.79		-1.60	-1.34	PPR29	10.3	2.34	7.43		-4.41	-1.39
FRS1L	2.81	0.59	0.59		-4.76	-4.76	PRDX3	2.81	0.59	1.86		-4.76	-1.51
GDIA	11.25	5.84	7.43		-1.93	-1.51	SBP1	4.69	0.59	2.79		-7.95	-1.68
GUAA	3.75	1.17	1.86		-3.21	-2.02	SCPD1	2.81	0.59	0.93		-4.76	-3.02
H2A2A	10.31	2.34	5.57		-4.41	-1.85	SGIP1	5.62	2.34	3.71		-2.40	-1.51
H4	8.44	2.34	5.57		-3.61	-1.52	SYIM	3.75	1.17	0.93		-3.21	-4.03
HBB1	33.75	23.36	23.21		-1.44	-1.45	SYPH	2.81	0.59	1.86		-4.76	-1.51
HNRPU	5.62	0.59	1.86		-9.53	-3.02	SYUA	3.75	0.59	1.86		-6.36	-2.02
HPLN1	3.75	2.34	2.79		-1.60	-1.34	TAGL	4.69	1.17	2.79		-4.01	-1.68
IF5A1	4.69	1.17	0.59		-4.01	-7.95	TAU	9.37	3.5	5.57		-2.68	-1.68
IGSF8	6.56	0.59	4.64		-11.12	-1.41	VDAC1	14.1	7.01	9.28		-2.01	-1.52
IMMT	3.75	2.34	2.79		-1.60	-1.34	VDAC3	2.81	1.17	1.86		-2.40	-1.51
KAD1	3.75	1.17	1.86		-3.21	-2.02	VIME	9.37	5.84	3.71		-1.60	-2.53

Table 12. Nitrosylation decrease at 0.1 Gy and 4 Gy.

A comparison of proteins showing decrease in nitrosylation (fold change less than 1.3) after irradiation at 0.1 Gy and decrease in nitrosylation at 4 Gy.

A total of 52 proteins showed a decrease in nitrosylation at both observations (0.1 and 4 Gy, [Table 9](#)). As illustrated in the heat chart above, more proteins showed significant decrease under 0.1 Gy as opposed to the 4 Gy treatment (more blue): AP1M1, HNRPU, IGSF8, KPCG, SBP1 and SYUA. It is interesting to see that protein ANXA2 and FRS1L showed similar decrease in nitrosylation at both observations (-4.76) while IF5A1 and PDE1A showed significant decrease at 4 Gy. Protein IGSF8 showed the greatest decrease in nitrosylation at 0.1 Gy.

#### 4.1.4.2.3 Decrease after LDIR and No Change at HDIR

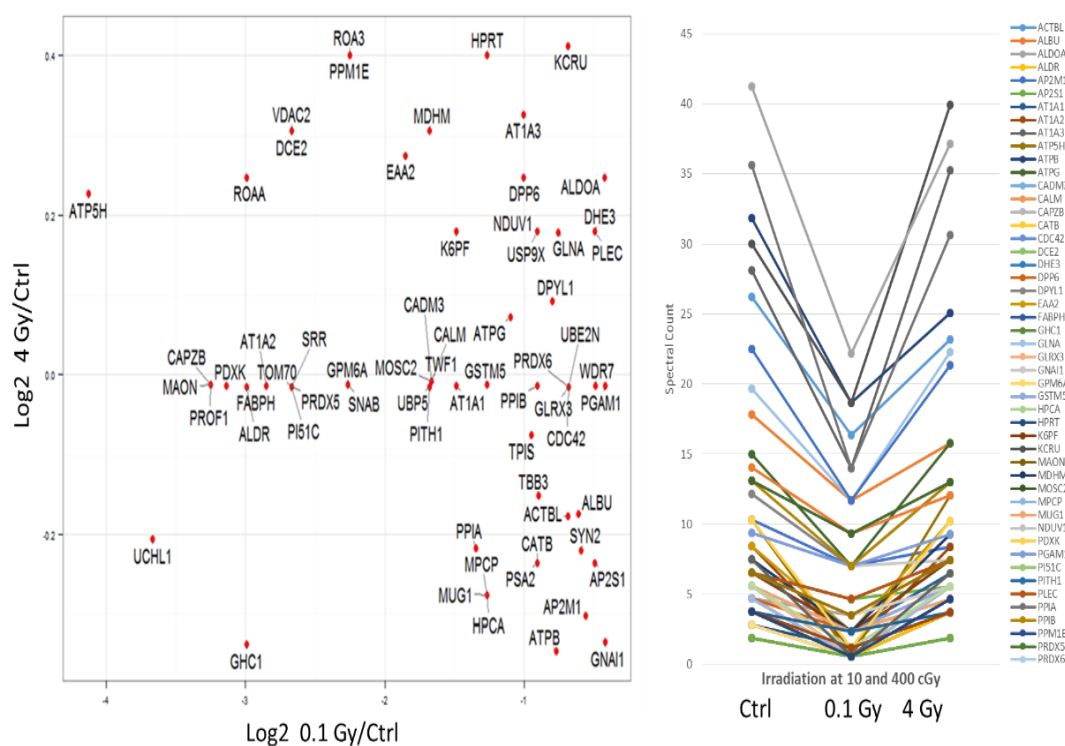


Figure 35. Decrease in nitrosylation at 0.1 Gy and no change at 4 Gy irradiation.

ID	Ctrl	0.1 Gy	4 Gy	Spark	0.1 Gy/Ctrl	4 Gy/Ctrl	ID	Ctrl	0.1 Gy	4 Gy	Spark	0.1 Gy/Ctrl
ACTBL	26.3	16.35	23.21		-1.61	-1.13	MAON	5.62	0.59	5.57		-9.53
ALBU	17.8	11.68	15.78		-1.52	-1.13	MDHM	7.5	2.34	9.28		-3.21
ALDOA	4.69	3.5	5.57		-1.34	1.19	MOSC2	1.87	0.59	1.86		-3.17
ALDR	4.69	0.59	4.64		-7.95	-1.01	MPCP	5.62	2.34	4.64		-2.40
AP2M1	10.3	7.01	8.36		-1.47	-1.23	MUG1	5.62	2.34	4.64		-2.40
AP2S1	6.56	4.67	5.57		-1.40	-1.18	NDUV1	6.56	3.5	7.43		-1.87
AT1A1	6.56	2.34	6.5		-2.80	-1.01	PDXK	10.31	1.17	10.21		-8.81
AT1A2	8.44	1.17	8.36		-7.21	-1.01	PGAM1	9.37	7.01	9.28		-1.34
AT1A3	28.1	14.02	35.28		-2.01	1.25	PI51C	3.75	0.59	3.71		-6.36
ATP5H	10.3	0.59	12.07		-17.47	1.17	PITH1	3.75	1.17	3.71		-3.21
ATPB	31.9	18.69	25.07		-1.71	-1.27	PLEC	6.56	4.67	7.43		-1.40
ATPG	15	7.01	15.78		-2.14	1.05	PPIA	35.62	14.02	30.64		-2.54
CADM3	1.87	0.59	1.86		-3.17	-1.01	PPIB	13.12	7.01	13		-1.87
CALM	1.87	0.59	1.86		-3.17	-1.01	PPM1E	2.81	0.59	3.71		-4.76
CAPZB	5.62	0.59	5.57		-9.53	-1.01	PRDX5	3.75	0.59	3.71		-6.36
CATB	6.56	3.5	5.57		-1.87	-1.18	PRDX6	3.75	2.34	3.71		-1.60
CDC42	3.75	2.34	3.71		-1.60	-1.01	PROF1	5.62	0.59	5.57		-9.53
DCE2	3.75	0.59	4.64		-6.36	1.24	PSA2	6.56	3.5	5.57		-1.87
DHE3	6.56	4.67	7.43		-1.40	1.13	ROA3	2.81	0.59	3.71		-4.76
DPP6	4.69	2.34	5.57		-2.00	1.19	ROAA	4.69	0.59	5.57		-7.95
DPYL1	12.2	7.01	13		-1.74	1.07	SNAB	5.62	1.17	5.57		-4.80
EAA2	8.44	2.34	10.21		-3.61	1.21	SRR	3.75	0.59	3.71		-6.36
FABPH	4.69	0.59	4.64		-7.95	-1.01	SYN2	14.06	9.35	12.07		-1.50
GHC1	4.69	0.59	3.71		-7.95	-1.26	TBB3	41.25	22.19	37.14		-1.86
GLNA	19.7	11.68	22.28		-1.69	1.13	TOM70	3.75	0.59	3.71		-6.36
GLRX3	3.75	2.34	3.71		-1.60	-1.01	TPIS	22.5	11.68	21.35		-1.93
GNAI1	9.37	7.01	7.43		-1.34	-1.26	TWF1	1.87	0.59	1.86		-3.17
GPM6A	5.62	1.17	5.57		-4.80	-1.01	UBE2N	3.75	2.34	3.71		-1.60
GSTM5	5.62	2.34	5.57		-2.40	-1.01	UBP5	3.75	1.17	3.71		-3.21
HPCA	5.62	2.34	4.64		-2.40	-1.21	UCHL1	7.5	0.59	6.5		-12.71
HPRT	2.81	1.17	3.71		-2.40	1.32	USP9X	6.56	3.5	7.43		-1.87
K6PF	6.56	2.34	7.43		-2.80	1.13	VDAC2	3.75	0.59	4.64		-6.36
KCRU	30	18.69	39.92		-1.61	1.33	WDR7	13.12	9.35	13		-1.40

Table 13. Nitrosylation decrease at 0.1 Gy and no change at 4 Gy.

A comparison of proteins showing decrease in nitrosylation (fold change less than 1.3) after irradiation at 0.1 Gy and no change at 4 Gy.

A total of 63 proteins belonged to this group with almost 50% showing more than 2 fold decrease in nitrosylation.

The following proteins showed significant decrease in nitrosylation (>8 fold change): ATP5H, UCHL1, ROAA, CAPZB, MAON, PROF1, PDXK, (ATP5H having a ~17 fold decrease in nitrosylation with a 0.59 expression value at the Ctrl level). Proteins DCE2, VDAC2, ALDR, FABPH, AT1A2, PI51C, PRDX5, SRR, TOM70, and GHC1 showed also a moderate decrease in nitrosylation (>6 fold decrease).

#### 4.1.4.3 Increase in Nitrosylation at LDIR

##### 4.1.4.3.1 Increase at LDIR and Decrease at HDIR.

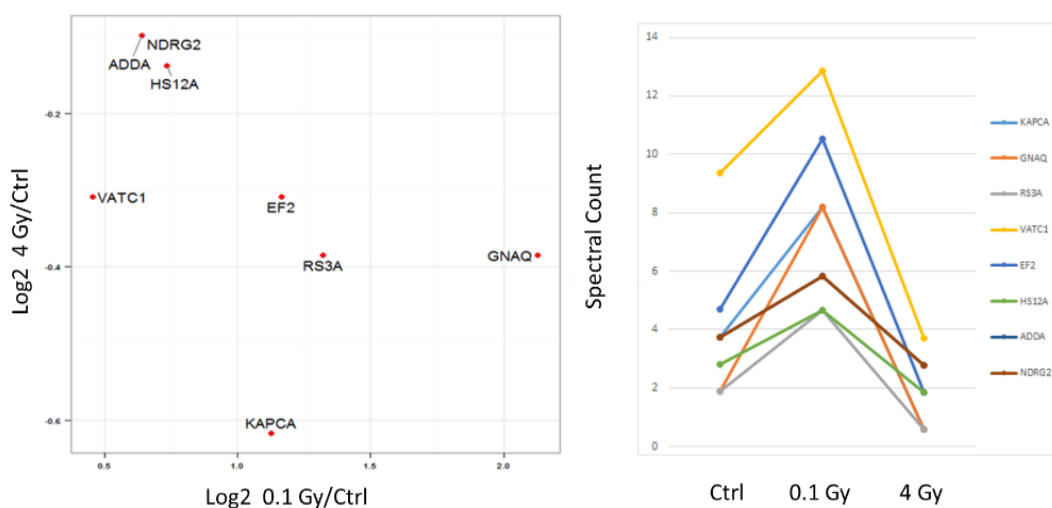


Figure 36. Increase in nitrosylation after 0.1 Gy and decrease after 4 Gy

ID	Ctrl	0.1 Gy	4 Gy	Spark	0.1 Gy/Ctrl	4 Gy/Ctrl
KAPCA	3.75	8.18	0.59		2.18	-6.36
GNAQ	1.87	8.18	0.59		4.37	-3.17
RS3A	1.87	4.67	0.59		2.50	-3.17
VATC1	9.37	12.85	3.71		1.37	-2.53
EF2	4.69	10.51	1.86		2.24	-2.52
HS12A	2.81	4.67	1.86		1.66	-1.51
ADDA	3.75	5.84	2.79		1.56	-1.34
NDRG2	3.75	5.84	2.79		1.56	-1.34

Table 14. Nitrosylation increase at 0.1 Gy and decrease at 4 Gy.

The table above is a comparison of proteins with increase in nitrosylation (fold change > 1.3) after irradiation at 0.1 Gy while the same proteins experienced a decrease in nitrosylation at 4 Gy. GNAQ, RS3A, KAPCA and EF2 have greater than 2 fold increase in nitrosylation.

## 4.1.4.3.2 Increase at LDIR and No Change at HDIR.

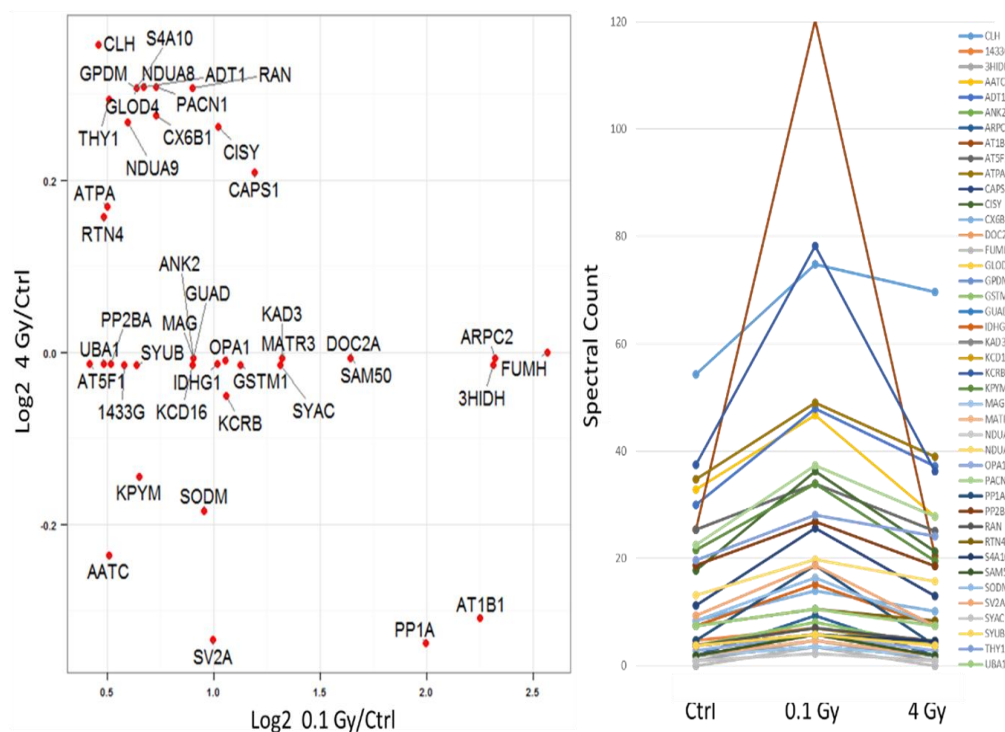


Figure 37. Scatter plot: Increase in SNO after 0.1 Gy and no change after 4 Gy exposures.

ID	Ctrl	0.1 Gy	4 Gy	Spark	0.1 Gy/Ctrl	4 Gy/Ctrl	ID	Ctrl	0.1 Gy	4 Gy	Spark	0.1 Gy/Ctrl	4 Gy/Ctrl
CLH	54.37	74.76	69.63		1.38	1.28	KCD16	3.75	7.01	3.71		1.87	-1.01
1433G	4.69	7.01	4.64		1.49	-1.01	KCRB	37.5	78.26	36.21		2.09	-1.04
3HIDH	0.94	4.67	0.93		4.97	-1.01	KPYM	21.56	33.88	19.5		1.57	-1.11
AATC	32.81	46.73	27.85		1.42	-1.18	MAG	1.87	3.5	1.86		1.87	-1.01
ADT1	30	47.89	37.14		1.60	1.24	MATR3	1.87	4.67	1.86		2.50	-1.01
ANK2	1.87	3.5	1.86		1.87	-1.01	NDUA8	3.75	5.84	4.64		1.56	1.24
ARPC2	1.87	9.35	1.86		5.00	-1.01	NDUA9	13.12	19.86	15.78		1.51	1.20
AT1B1	25.31	120.32	20.43		4.75	-1.24	OPA1	2.81	5.84	2.79		2.08	-1.01
AT5F1	25.31	33.88	25.07		1.34	-1.01	PACN1	22.5	37.38	27.85		1.66	1.24
ATPA	34.68	49.06	38.99		1.41	1.12	PP1A	4.69	18.69	3.71		3.99	-1.26
CAPS1	11.25	25.7	13		2.28	1.16	PP2BA	18.75	26.87	18.57		1.43	-1.01
CISY	17.81	36.21	21.35		2.03	1.20	RAN	3.75	7.01	4.64		1.87	1.24
CX6B1	8.44	14.02	10.21		1.66	1.21	RTN4	7.5	10.51	8.36		1.40	1.11
DOC2A	1.87	5.84	1.86		3.12	-1.01	S4A10	3.75	5.84	4.64		1.56	1.24
FUMH	0.59	3.5	0.59		5.93	1.00	SAM50	1.87	5.84	1.86		3.12	-1.01
GLOD4	3.75	5.84	4.64		1.56	1.24	SODM	8.44	16.35	7.43		1.94	-1.14
GPDM	3.75	5.84	4.64		1.56	1.24	SV2A	9.37	18.69	7.43		1.99	-1.26
GSTM1	3.75	8.18	3.71		2.18	-1.01	SYAC	0.94	2.34	0.93		2.49	-1.01
GUAD	1.87	3.5	1.86		1.87	-1.01	SYUB	3.75	5.84	3.71		1.56	-1.01
IDHG1	7.5	15.19	7.43		2.03	-1.01	THY1	19.69	28.04	24.14		1.42	1.23
KAD3	1.87	4.67	1.86		2.50	-1.01	UBA1	7.5	10.51	7.43		1.40	-1.01

Table 15. Nitrosylation increase at 0.1 Gy and no change at 4 Gy.

A comparison of proteins showing increase in nitrosylation (fold change > 1.3) after irradiation at 0.1 Gy and no change at 4 Gy

4.1.4.3.3 Increase at LDIR and Increase at HDIR

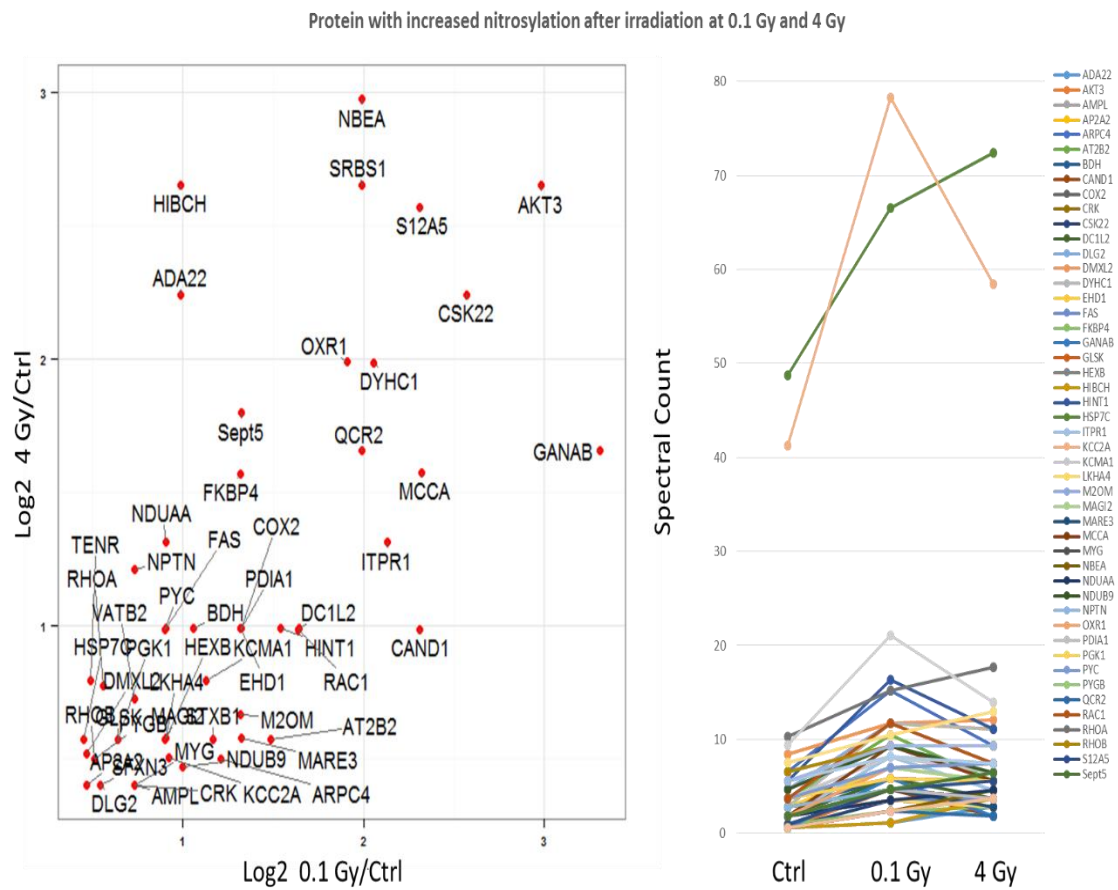


Figure 38. Increase in nitrosylation following 0.1 Gy and 4 Gy exposures

ID	Ctrl	0.1 Gy	4 Gy	Spark	0. Gy/Ctrl	4 Gy/Ctrl	ID	Ctrl	0.1 Gy	4 Gy	Spark	0. Gy/Ctrl	4 Gy/Ctrl
ADA22	0.59	1.17	2.79		1.98	4.73	LKHA4	1.87	3.5	2.79		1.87	1.49
AKT3	0.59	4.67	3.71		7.92	6.29	M2OM	4.69	11.68	7.43		2.49	1.58
AMPL	2.81	4.67	3.71		1.66	1.32	MAGI2	3.75	7.01	5.57		1.87	1.49
AP2A2	8.44	11.68	11.1		1.38	1.32	MARE3	1.87	4.67	2.79		2.50	1.49
ARPC4	6.56	15.19	9.28		2.32	1.41	MCCA	1.87	9.35	5.57		5.00	2.98
AT2B2	3.75	10.51	5.57		2.80	1.49	MYG	2.81	4.67	3.71		1.66	1.32
BDH	2.81	5.84	5.57		2.08	1.98	NBEA	0.59	2.34	4.64		3.97	7.86
CAND1	0.94	4.67	1.86		4.97	1.98	NDUAA	1.87	3.5	4.64		1.87	2.48
COX2	1.87	4.67	3.71		2.50	1.98	NDUB9	4.69	9.35	6.5		1.99	1.39
CRK	2.81	4.67	3.71		1.66	1.32	NPTN	2.81	4.67	6.5		1.66	2.31
CSK22	0.59	3.5	2.79		5.93	4.73	OXR1	1.87	7.01	7.43		3.75	3.97
DC1L2	1.87	5.84	3.71		3.12	1.98	PDIA1	1.87	4.67	3.71		2.50	1.98
DLG2	5.62	8.18	7.43		1.46	1.32	PGK1	3.75	5.84	5.57		1.56	1.49
DMXL2	8.44	11.68	12.1		1.38	1.43	PYC	3.75	7.01	7.43		1.87	1.98
DYHC1	2.81	11.68	11.1		4.16	3.96	PYGB	6.56	9.35	9.28		1.43	1.41
EHD1	2.81	7.01	5.57		2.49	1.98	QCR2	0.59	2.34	1.86		3.97	3.15
FAS	1.87	3.5	3.71		1.87	1.98	RAC1	3.75	11.68	7.43		3.11	1.98
FKBP4	0.94	2.34	2.79		2.49	2.97	RHOA	10.3	15.19	17.6		1.47	1.71
GANAB	0.59	5.84	1.86		9.90	3.15	RHOB	6.56	9.35	9.28		1.43	1.41
GLSK	3.75	5.84	5.57		1.56	1.49	S12A5	0.94	4.67	5.57		4.97	5.93
HEXB	1.87	3.5	2.79		1.87	1.49	Sept5	1.87	4.67	6.5		2.50	3.48
HIBCH	0.59	1.17	3.71		1.98	6.29	SFXN3	5.62	8.18	7.43		1.46	1.32
HINT1	5.62	16.35	11.1		2.91	1.98	SRBS1	0.59	2.34	3.71		3.97	6.29
HSP7C	48.7	66.58	72.4		1.37	1.49	STXB1	9.37	21.03	13.9		2.24	1.49
ITPR1	1.87	8.18	4.64		4.37	2.48	TENR	7.5	10.51	13		1.40	1.73
KCC2A	41.3	78.26	58.5		1.90	1.42	VATB2	5.62	9.35	9.28		1.66	1.65
KCMA1	3.75	8.18	6.5		2.18	1.73							

Table 16. Nitrosylation increase at 0.1 Gy and increase at 4 Gy.

A comparison of proteins showing increase in nitrosylation (fold change > 1.3) after irradiation at either 0.1 Gy or 4 Gy.

## 4.2 Molecular Function and Biological Process

In order to evaluate the appropriateness of grouping, the biological pathway and processes were examined for various groups generated by different approaches using PANTHER and IPA.

### 4.2.1 Whole Data Set (One Group)

#### 4.2.1.1 PANTHER (Protein ANALysis THrough Evolutionary Relationships)

PANTHER classifies proteins and identify their function. It is part of the GO reference genome project (gene ontology: protein attributes, annotation, function and enrichment).

The data was uploaded to PANTHER as protein ID without the expression values. Analysis was done in 2 ways:

**Functional Classification Viewed in Gene/Protein List:** The IDs from our list were mapped to the database and the percent of genes/proteins from our data participating in each function was obtained.

**PANTHER Overrepresentation Test:** This test uses the binomial distribution statistics (where the probability of the gene from our list is the same as the reference list, i.e. NULL hypothesis). P value would be the probability of proteins from our list mapping to the reference list. The distribution of 377 proteins in Gene Ontology Molecular Function is given in the following figure. The highest occurrence is catalytic activity (184 proteins), followed by binding (110 proteins). It should be noted that structural molecule activity shows as third highest occurrence with 63 proteins. Among these proteins, structural constituent of cytoskeleton is the majority (50 proteins).

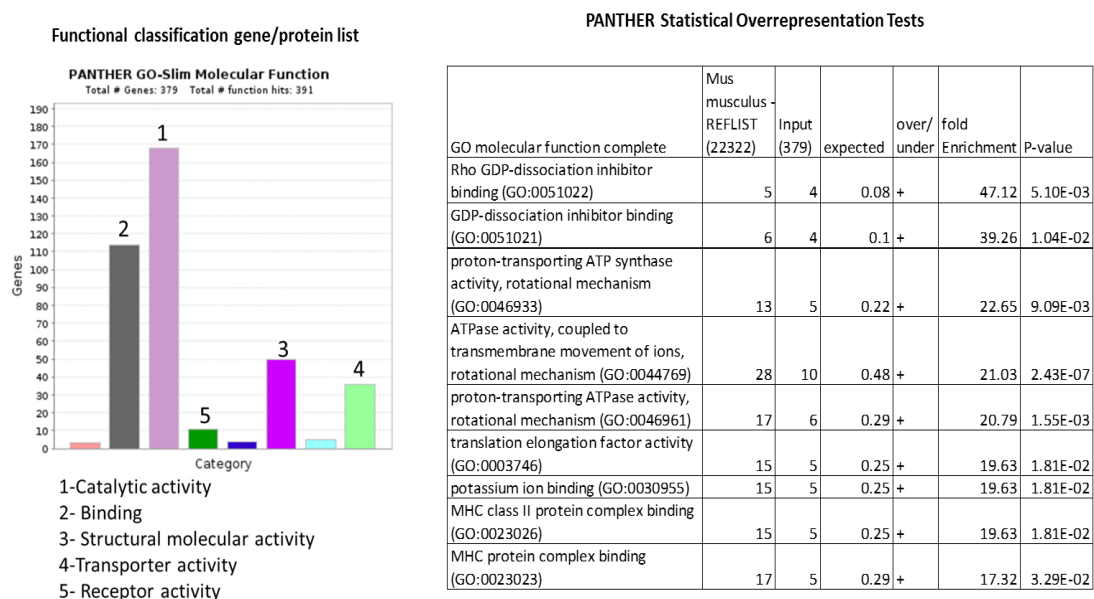


Figure 39. PANTHER's Molecular Function classification  
The molecular function was viewed as functional classification and statistical overrepresentation.

The functional classification showed ‘catalytic activity and binding’ as the highest ranking. The statistical overrepresentation graph showed Rho GDP as the highest p value with high fold enrichment. The proportion of catalytic activity in mouse proteins is 4020 genes out of 22000 or 18% compared to 142/377 or ~38% in our dataset. For the Biological process, we see that metabolic, cellular and localization are the top 3 processes that the protein groups are involved in.

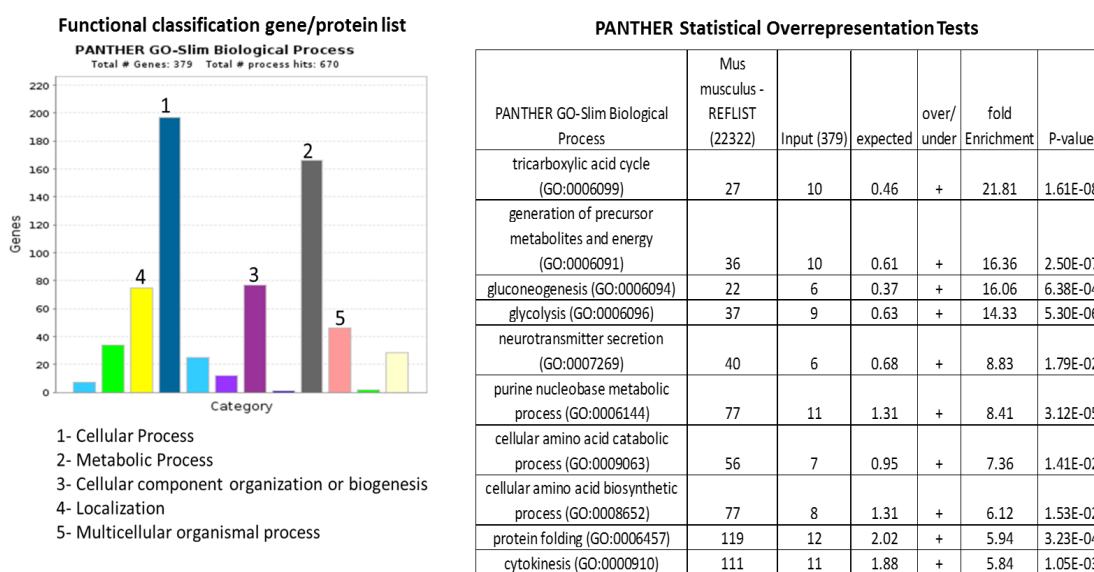


Figure 40. PANTHER's Biological Process classification  
 The Biological process of proteins viewed as functional classification and overrepresentation.

The functional classification showed ‘cellular process and metabolic’ as the highest ranking. The statistical overrepresentation graph showed TCA as having the highest p value with high fold enrichment. ‘Cellular Process’ was identified as the highest with 229 proteins followed by ‘Metabolic process’ with 146 proteins. Within cellular processes, more than a half (81 proteins) belongs to ‘cell communication’ [AKT3 belong to this group], ‘Cell cycle’ with 40 proteins follows as second largest group as shown below.

#### 4.2.1.2 Ingenuity Pathway Analysis (IPA)

The complete data set was uploaded into IPA as fold change and analysis was run. nNOS was identified as the most differentially nitrosylated pathway by IPA. As the figure below shows, nNOS signaling was greatly inhibited (activation score) at 0.1 Gy while it showed an increased activation at 4 Gy.

Fold change data set (377) uploaded to IPA and nNOS identified as the major differentially nitrosylated pathway.

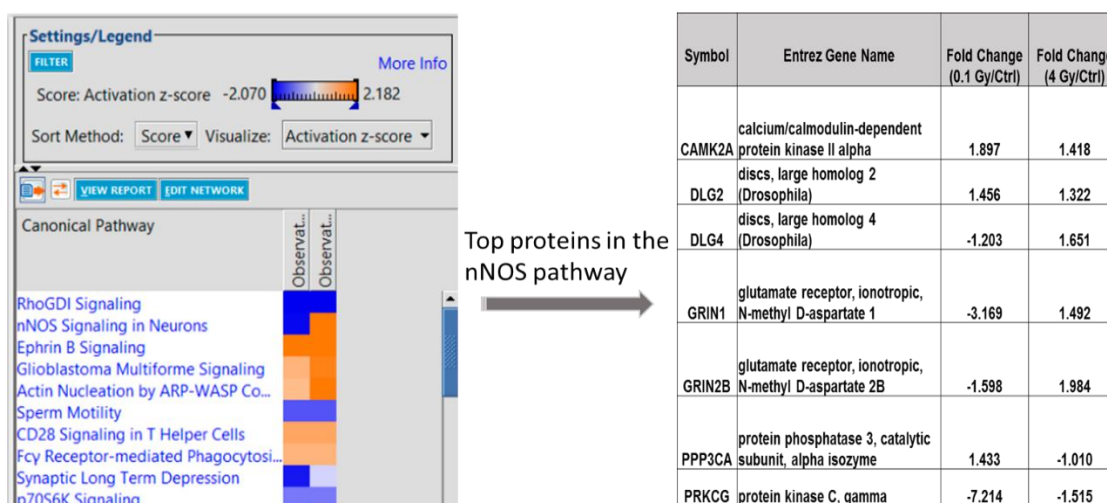


Figure 41. nNOS Pathway Heat Map

The different pathways enriched under each observation are shown. Whereas nNOS is apparently inhibited by 0.1 Gy (blue color), it is activated by 4 Gy (orange color). The table to the right lists the proteins involved in the nNOS signaling pathway.

Protein Kinase C and Grin1 are 2 proteins with significant differential nitrosylation in nNOS pathway as has been generated by IPA (see below). The graph on the left shows the proteins involved in the pathway at 0.1 Gy while the graph on the right shows the ones involved at 4 Gy. Green color depicts proteins with decrease in nitrosylation while red color corresponds to proteins with increase in nitrosylation. NMDAR subunits GRIN1 and GRIN2B belong to this pathway and are involved in synapse plasticity.

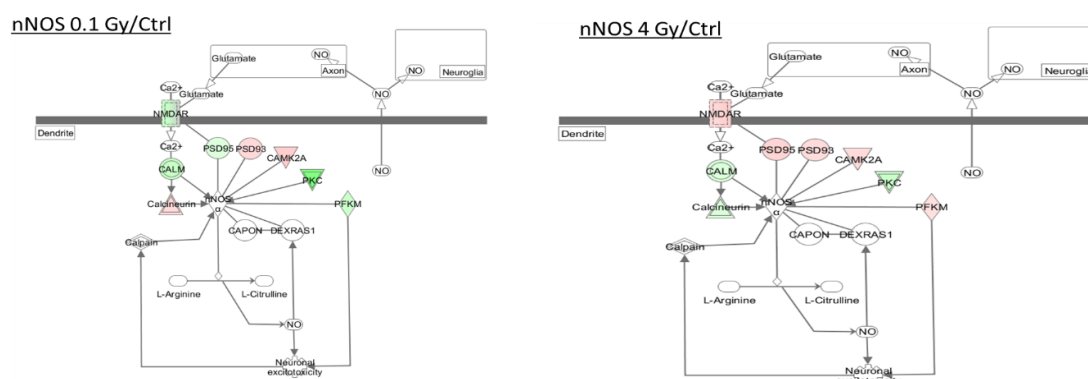


Figure 42. IPA generated nNOS signaling pathway

NMDAR activity is inhibited by nitrosylation during moderate stress (low dose) while an increase in NO production leads to increased nitrosylation, hyperactivating NMDAR (high dose) and resulting in toxicity.

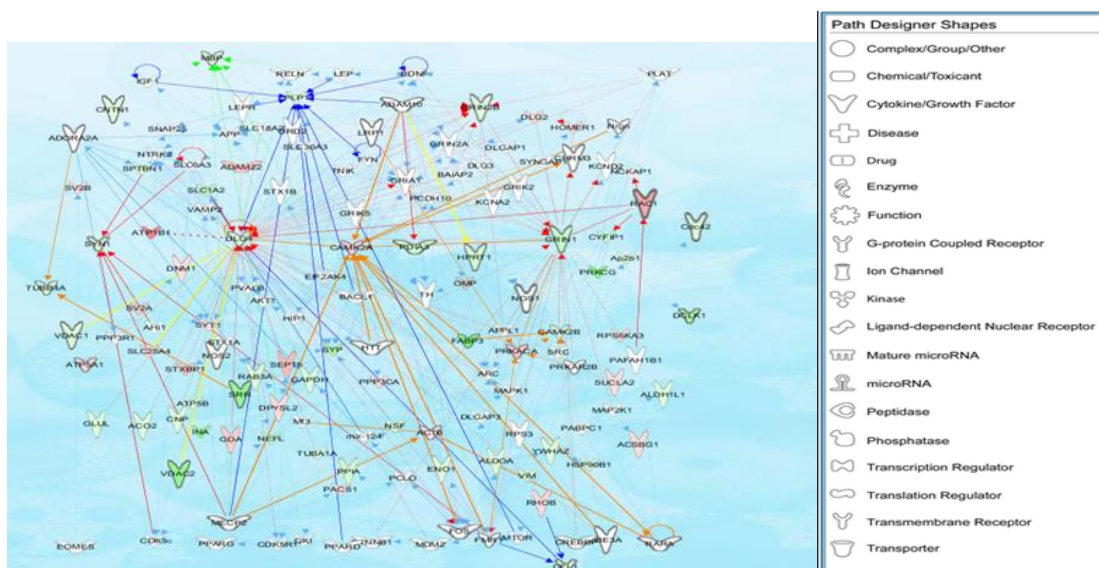


Figure 43. Cell to cell signaling, nervous system development network  
Cell to Cell Signaling Network. The network had 66 focus molecules (proteins bolded) participating in the cell to cell interaction and nervous system development.

Out of 140 total protein predicted by IPA, the majority of our proteins belong to the cytokine growth factor family. We also have hubs of densely connected proteins like CAMK2A, DLG4, PLP1 and BDNF.

#### 4.2.2 Optimum Cluster of 2 from R

The output of the clustering solution by R resulted in grouping the proteins into 2 major clusters (the output files generated CL1\_LogRF2 and CL2\_LogRF2, Supp files). Each cluster was uploaded into IPA for comparative analysis.

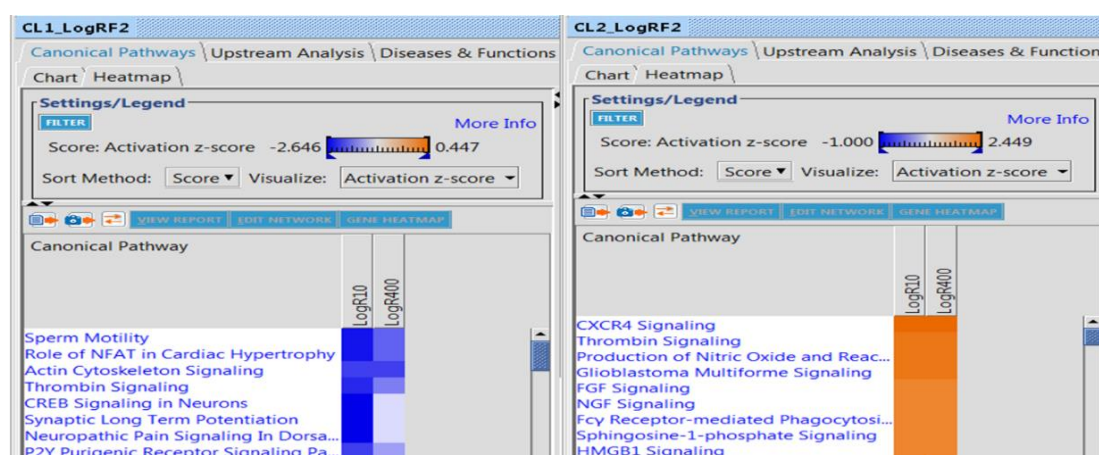


Figure 44. R two cluster solution at low and high dose  $\gamma$ -irradiation

Cluster 1 showing a decrease in nitrosylated proteins seems to be involved in reduction in activation of the major pathways displayed above (Figure 41, pathways with activation score  $< -2$  were selected). On the other hand, cluster 2 where protein nitrosylation was increased showed an enhancement in activation of many pathways. Both experimental conditions (0.1 Gy and 4 Gy) resulted in the same effect indicating that this grouping focused on the dose independent radiation effects, whereas cluster 1 showed a more reduced pathway activity at 0.1 Gy as compared to 4 Gy.

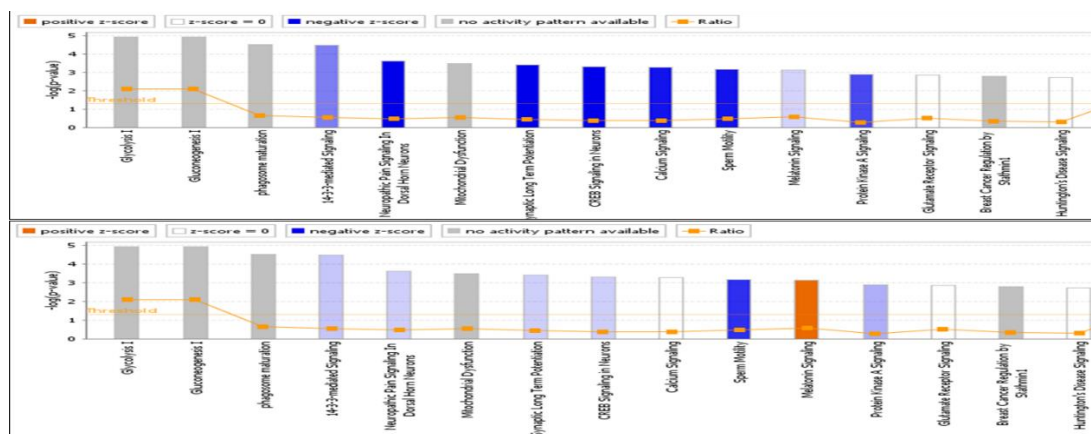


Figure 45. Bar Chart of Cluster 1 (decrease in nitrosylation).

Pathways generated under 0.1 Gy (LogR10 CL1) and 4 Gy (LogR400 CL1) irradiation, are shown in top and bottom panels, respectively.

(See Supp. Files: LogR10\_CL1 pathway and LogR10\_CL2 pathway)

The orange line indicates the threshold p-value of 0.05 and all canonical pathways that meet the threshold are displayed. The y-axis displays the  $-\log$  of p-value which is calculated by Fisher's exact test (right-tailed). Thus, the taller bars represent an increased significance. For the single analysis, the various pathways are presented from largest ratio to smallest ratio. The orange and blue colored bars indicate predicted pathway activation or inhibition, respectively (by z-score). The white bars are those with a z-score at or very close to 0. The gray bars indicate pathways where no prediction can currently be made, and the orange points connected by a thin line represent the Ratio that is calculated by the number of genes in a given pathway that meet the cutoff criteria, divided by the total number of genes in that pathway. The “Expected” column (in the table that is displayed when you select one of the bar charts) indicates the state that a gene is predicted to have if the pathways were activated.

From the above graph, it was shown that in cluster 1 most pathways experienced a decrease in activation with a significant decrease at LDIR as opposed to HDIR. In the

melatonin signaling pathway, we have a decrease in nitrosylation at LDIR with a significant increase in activation at HDIR. In addition, the CREB, LTP and pain signaling showed differential nitrosylation under 0.1 Gy and 4 Gy.

Cluster 1 pathways showing differential activation at 0.1 Gy and 4 Gy						
Pathways				0.1 Gy	4 Gy	
CREB Signaling in Neurons				-2.65	-0.38	
Synaptic Long Term Potentiation				-2.65	-0.38	
Neuropathic Pain Signaling in Dorsal Horn				-2.65	-0.38	
Symbol	0.1 Gy	4 Gy	Network*	CREB Signaling	Synaptic LTP	Neuropathic
CAMK2B	-0.42	-0.53	1,2	X	X	X
CAMK2D	-0.49	-1.82	2	X	X	X
GNB1	-0.17	-0.82	3	X		
GRIN1	-1.66	0.58	2	X	X	X
GRIN2B	-0.68	0.99	2	X	X	X
PDIA3	-1.66	0.58	2	X	X	X
PLCB1	-0.01	-1.33	1	X	X	X
PRKCG	-2.85	-0.6	2	X	X	X

\*Networks: 1- Behavior, Neurological Disease, Cell Death and Survival, 2- Cell-To-Cell Signaling and Interaction, Nervous System Development and Function, Behavior, 3- Behavior, Neurological Disease, Cell Morphology

#### 4.2.2.1 Neuropathic Pain Signaling Pathway

The decrease in protein expression observed in our results showed an inhibition/suppression of neuropathic pain signaling pathway.

IPA knowledge base<sup>158</sup> describes that “Peripheral nerve injury induces release of the Neurotransmitter Glutamate and the Neuromodulators: Tac1 (Tachykinin-1) and BDNF (Brain Derived Neurotrophic Factor) from the central terminals of Primary Afferents. Glutamate is the major excitatory neurotransmitter in the Spinal Cord and it acts on ionotropic AMPA (Glutamate Receptor, Ionotropic, AMPA), and NMDARs (N-Methyl D-Aspartate Receptors) as well as on MGLURs (Glutamate Receptor, Metabotropic) (Ref.4 & 5). Whereas AMPA receptors are important for the rapid excitatory synaptic transmission of physiological nociception, NMDARs play a critical role in plasticity in the CNS.”

According to Qiagen Pathway Knowledge base<sup>159</sup>, “Long-Term Potentiation (LTP) is the increase of synaptic strength between two neurons following high frequency stimulation of the synapse. A majority of synapses that experience LTP (*e.g.* in the hippocampus) involve a postsynaptic increase in calcium, which is mediated through activation of the

According to Qiagen Pathway Knowledge base<sup>159</sup>, “Long-Term Potentiation (LTP) is the increase of synaptic strength between two neurons following high frequency stimulation of the synapse. A majority of synapses that experience LTP (*e.g.* in the hippocampus) involve a postsynaptic increase in calcium, which is mediated through activation of the

ionotropic glutamate receptor, N-methyl-D-aspartic acid (NMDA) receptor. Activation of NMDA receptors by glutamate released from the presynaptic neuron results in  $\text{Ca}^{2+}$  influx, which coactivates the extracellular regulated signal kinase (ERK) and cyclic adenosine monophosphate (cAMP) signal transduction pathways.”

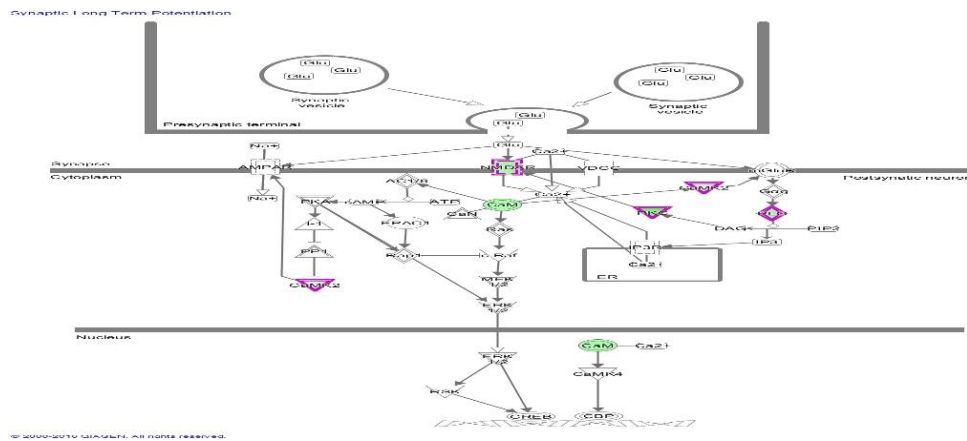


Figure 47. Synaptic Long Term Potentiation Pathway

#### 4.2.2.3 CREB Signaling in Neurons

According to the Qiagen Pathway Knowledge base,<sup>160</sup> “The process of consolidating a new memory, and the dynamic complexity of information processing within neuronal networks, is greatly increased by activity-dependent changes in gene expression within individual neurons. A leading paradigm of such regulation is the activation of the nuclear transcription factor CREB (cAMP responsive element binding protein) and its family members the ATF (activating transcription factor) and CREM (cAMP response element modulator).”

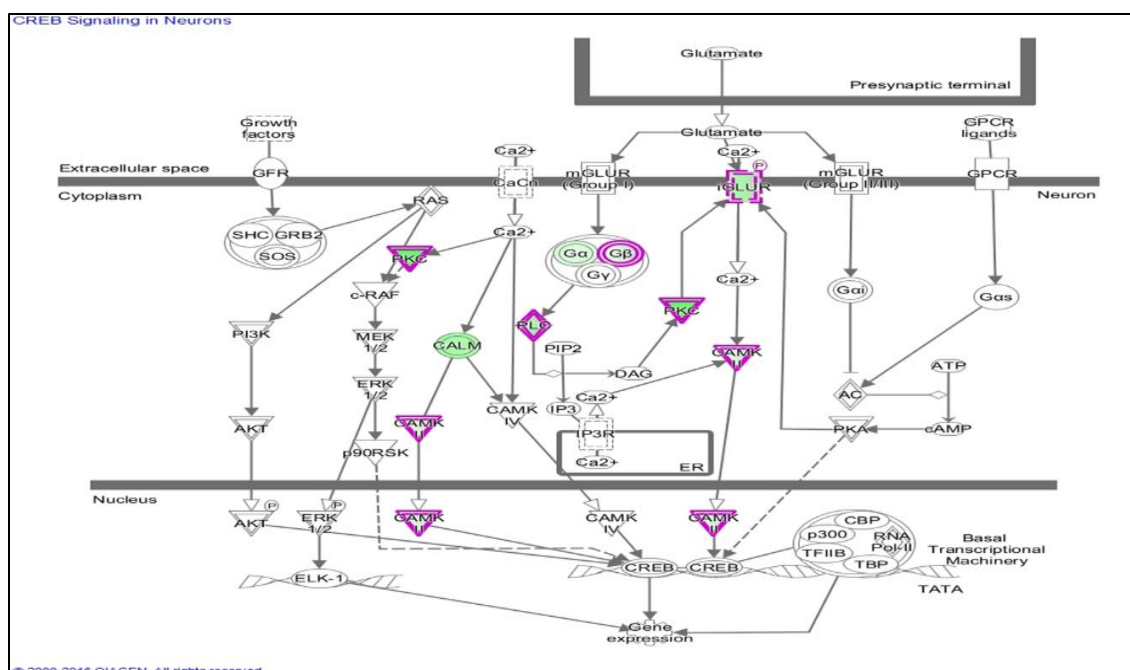


Figure 48. CREB Signaling in neurons

“CREB can form homodimers or heterodimers with other members of the ATF family, including ATF1 and CREM. However, heterodimerization of CREB with other members of the ATF family decreases its stability and CRE (cAMP Responsive Element) binding affinity. Changing levels of cAMP,  $\text{Ca}^{2+}$  and TGF-Beta (Transforming Growth Factor-Beta) regulate CREB and its closely related proteins (SHC, GRB2, SOS, HRas, cRaf, etc.) that implicate in a variety of biological responses such as neuronal excitation, long-term memory formation, neural cell proliferation, and opiate tolerance.”

#### 4.2.2.4 Melatonin Signaling

Our mass spectrometry results revealed modulation of several proteins implicated in melatonin signaling as highlighted in the Table below.

Symbol	Expr Log Ratio	Expected
CAMK2B	-0.53	Down
CAMK2D	-1.82	Down
PDIA3	0.58	Up
PLCB1	-1.33	Up
PRKCG	-0.6	Up

Table 17. Proteins participating in the Melatonin Signaling Pathway

The melatonin pathway showed an increase in activation at 0.1 Gy as compared to 4 Gy (0.44 and -0.44 respectively). From the table above, it is noted that some of the proteins, specifically PLCB1 and PRKCG are expected to increase in expression, however the results obtained indicate a decrease in their nitrosylation levels.

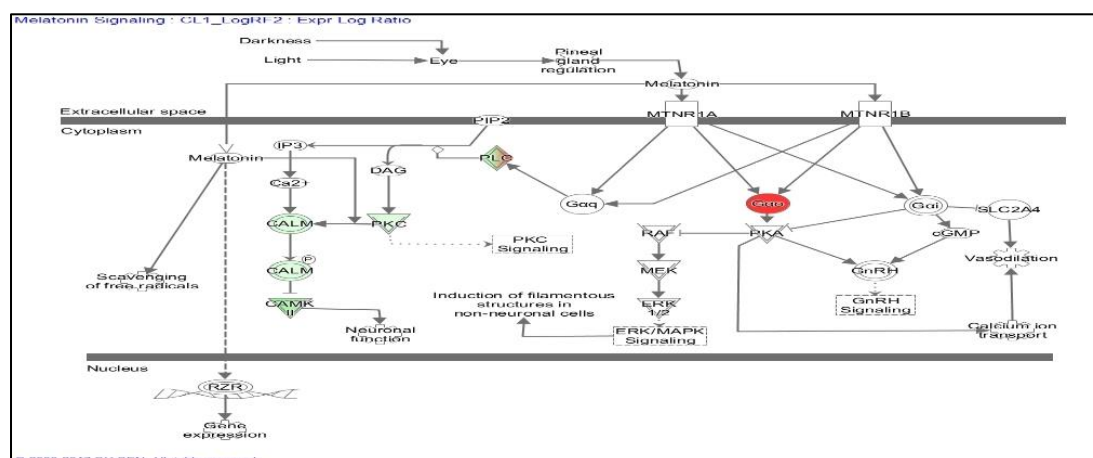
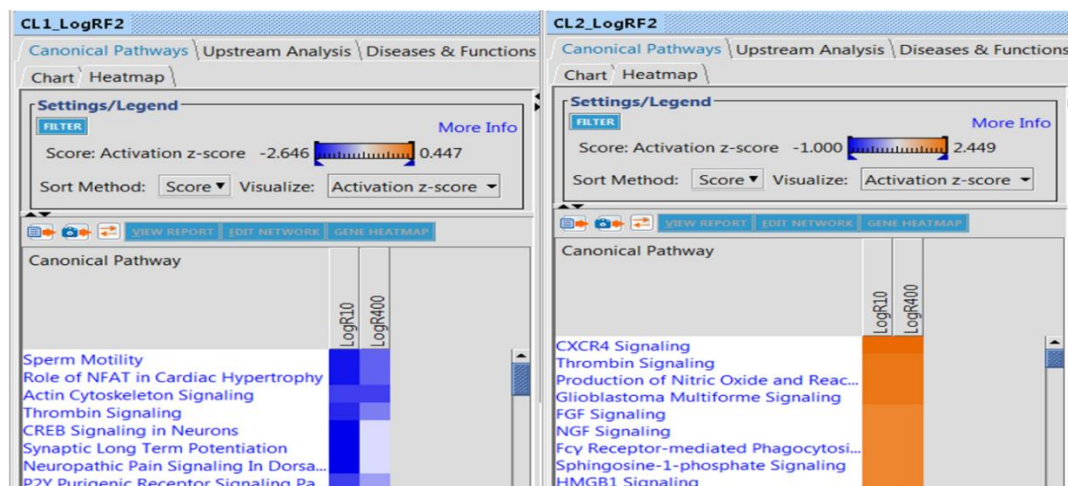


Figure 49. Melatonin Signaling Pathway

Melatonin plays a role in a variety of conditions, from insomnia to cancer, to acting as an anti-aging agent. Melatonin acts as scavenger of free radicals, especially highly toxic hydroxyl radicals.



The cluster above showing decrease in nitrosylation seem to be involved in decrease in activation of major pathways (pathways with activation/deactivation scores greater or less than 2 were selected).

#### 4.2.2.5 Insulin Receptor Signaling

Cluster 2 where the proteins were overall increased in nitrosylation showed an enhancement in activation of many pathways. Both experimental conditions resulted in this effect (0.1 Gy and 4 Gy) although cl1 showed a more reduced pathway activity at 0.1 Gy as compared to 4 Gy.

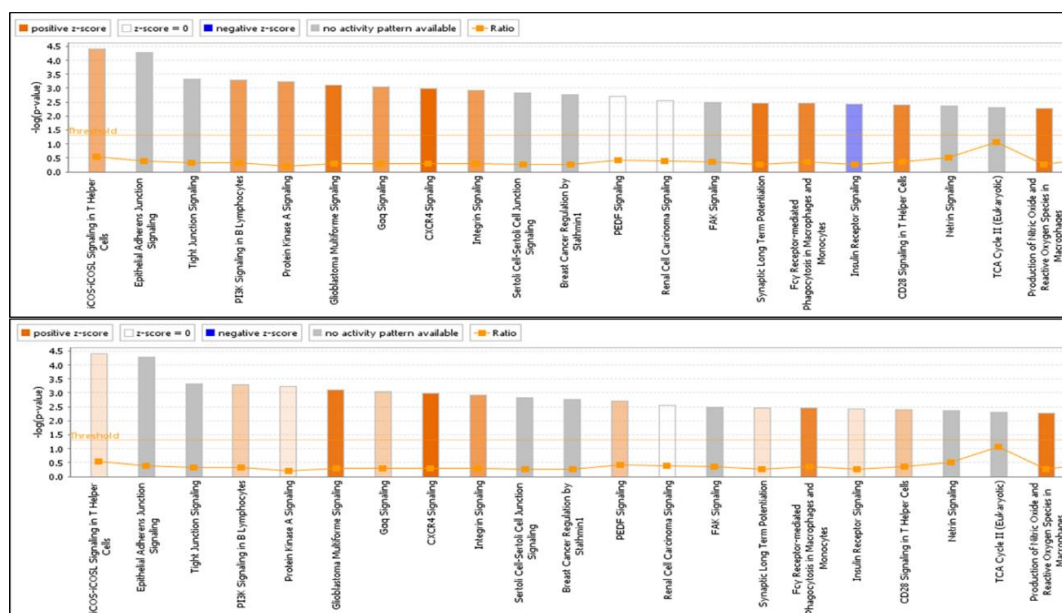


Figure 50. LogR10 Pathway from CL2 (Top) and LogR400 CL2 (bottom). Cluster 2 represents the overall increase in nitrosylation. (See sup file LogR400\_CL1\_Pathway and LogR400 CL2\_Pathway for data)

It is interesting to see that in Cluster 2 where there is an increase in nitrosylation, there is an abundant involvement of cells implicated in the immune response: T-cell, B-cell and macrophages.

Analyses of the results show that three top pathways are differentially activated under the two irradiation conditions: These pathways are iCOS-iCOSL signaling in T Helper Cells, PI3K Signaling in B Lymphocytes and Protein Kinase A signaling. The pathways with activation score greater than 2 include: Synaptic LTP, production of nitric oxide and reactive oxygen species and thrombin signaling. Insulin receptor signaling is the only pathway showing a decrease at 0.1 Gy and an increase at 4 Gy.

### 4.2.3 Hierarchical Clustering

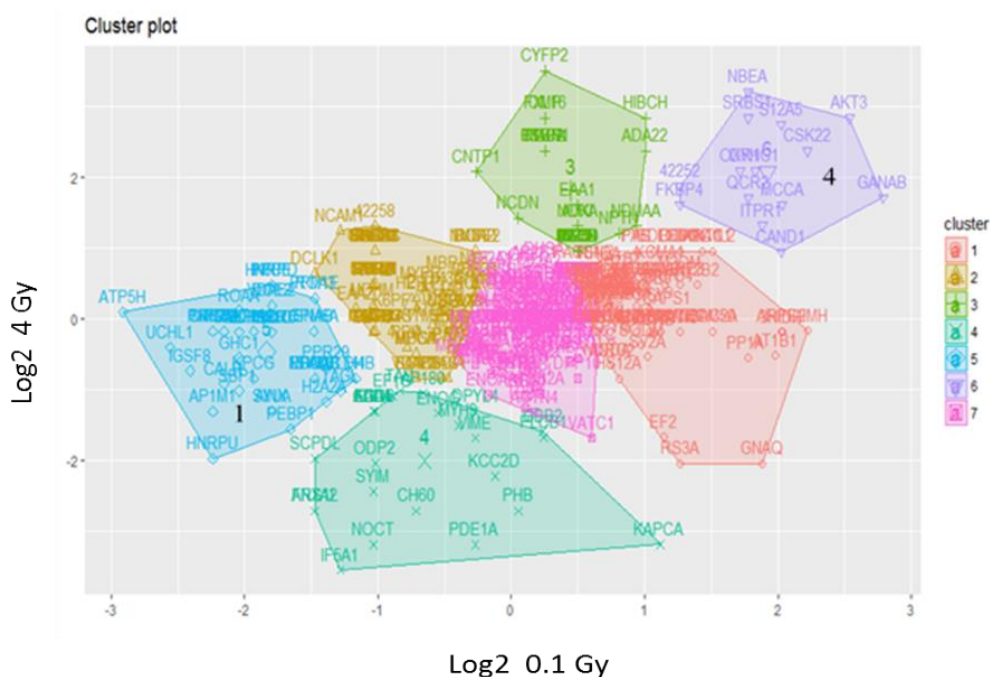


Figure 51. Consistent clusters showing differential effect of irradiation

Previously, Fig. 28 has shown that certain clusters remained consistent regardless of further subdivisions after 6. Two regions of interest are region 1 and 4 (Fig 51): Cluster 4 is showing increase in nitrosylation at 0.1 Gy and 4 Gy. While cluster one shows decrease in nitrosylation at 0.1 Gy. Upload and analysis of these 2 groups by IPA identified the following top pathways in each group.

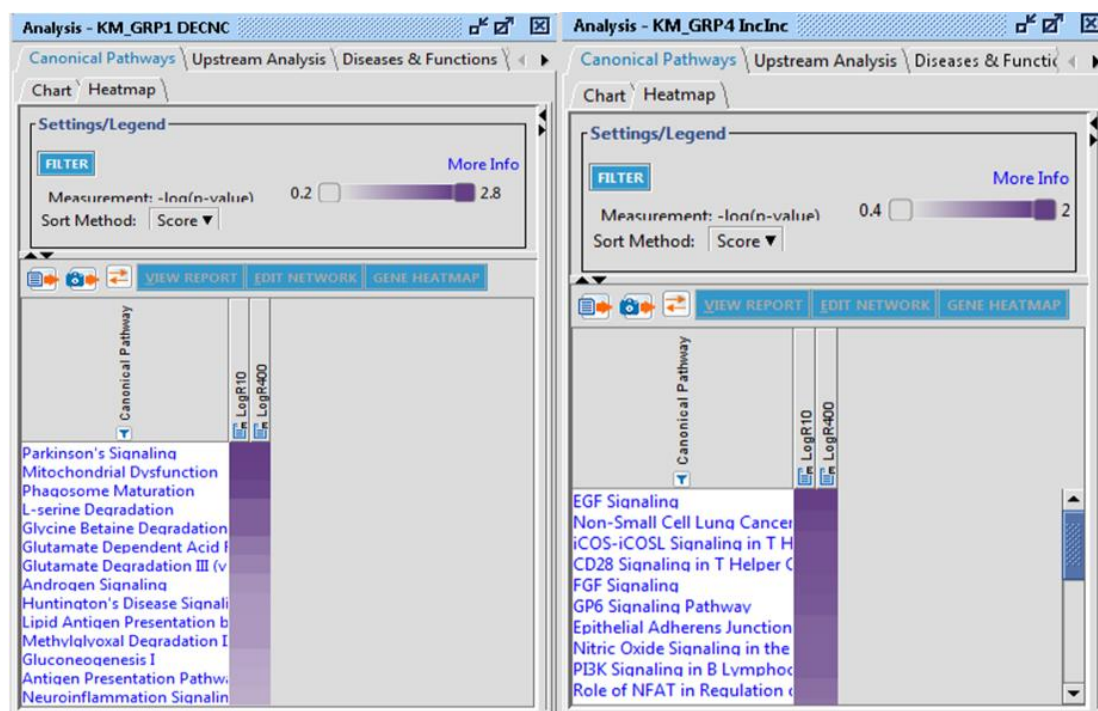


Figure 52. Different pathways identified with different clusterings of proteins  
Parkinson Signaling is top pathway in cluster of proteins showing decrease in nitrosylation at 0.1 Gy and no change at 4 Gy, while EGF signaling is top pathway in proteins showing increase in nitrosylation at 0.1 and 4 Gy irradiation.

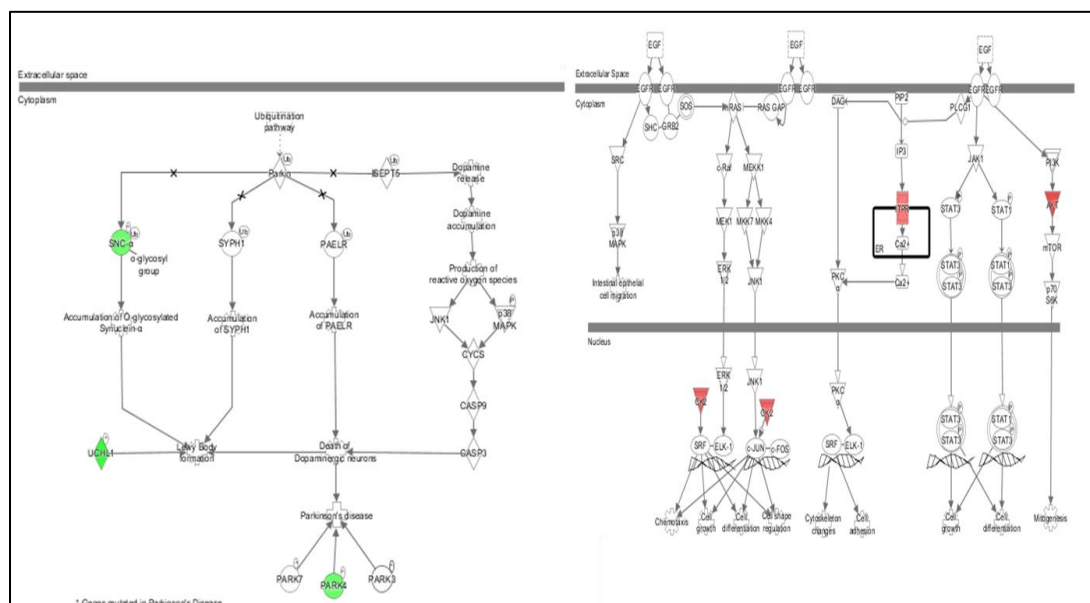


Figure 53. Parkinson and EGF Pathways

## 4.2.4 Manual Clustering

### 4.2.4.1 Proteins Showing No Change in Nitrosylation after LDIR

#### 4.2.4.1.1 No Change after LDIR and Increase at HDIR: Glutamate Receptor Signaling Pathway and the Nervous System

The table in supp file (table IPA output 9 grps) showed that this group had the glutamate receptor as the most significant pathway (p-value  $0.7 \times 10^{-4}$ ). The proteins are involved in neurological disease and form a network of cell to cell signaling and interactions.

Three proteins DLG4 (PSD-95), HOME1 and SLC1A3 (EAA1) were identified by IPA (IPA output table in index) as key players in the glutamate receptor signaling pathway. In addition, the proteins are involved in cellular brain death and the degeneration of the cerebellum. The following proteins (SYN1, DLG4, CNP, AP2B1, OMP, HOMER1, DNM1L, PTEN) were identified to be involved in the primary network for Cell-To-Cell Signaling and Interaction, Nervous System Development and Function, and Behavior.

#### 4.2.4.1.2 No Change after LDIR and HDIR

No significant pathways were identified in this group of proteins.

#### 4.2.4.1.3 No Change after LDIR and Decrease after HDIR: G Protein Signaling and Neurological Disease

The primary pathway for this group is G Protein Signaling mediated by TUBB and the 2 proteins involved are PLCB1 and GNB1 (GBB1). The prominent network in this group is Hereditary Disorder, Neurological Disease and Psychological Disorders with 3 focus proteins (GPI, HBA1/HBA2, and PLCB1). The function of the proteins in this group is related to maintenance of neuronal cells.

The top network above had a score of 18 with 17 focus molecules and a total of 116 molecules participating in the network. The score is a value used to rank networks according to their degree of relevance. The FAQs about using IPA document<sup>161</sup> describes that “The score takes into account the number of Network Eligible molecules in the network and its size, as well as the total number of network eligible molecules analyzed

and the total number of molecules in the Ingenuity Knowledge Base that could potentially be included in networks. Networks are ordered according to their score, with the highest scoring network displayed at the top of the page. The network Score is based on the hypergeometric distribution and is calculated with the right-tailed Fisher's Exact Test. Another feature noticeable in the network are the hub proteins.” A "hub" in the network connects a higher fraction of Network Eligible molecules relative to all molecules. Again, GRIN1/GRIN2B from our dataset are highly connected proteins along PLP1, MBP and NCAM1.

4.2.4.2.2 Decrease at LDIR and Decrease at HDIR

Calcium Signaling was the top selected pathway. The proteins CALR, MYH9, MYH10, CAMK2D, and Camk2b have a role in the Calcium Signaling Pathway while the following proteins (PRKCG, SNCA, SYP, EIF5A, MAPT, VDAC1, GDI1, CAMK2D, Camk2b) were found to participate also in Cell-To-Cell Signaling and Interaction, Nervous System Development and Function, and Behavior.

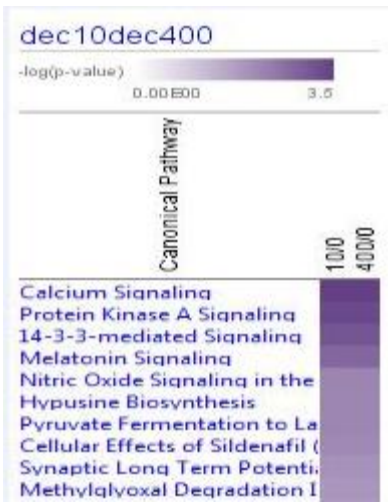


Table 18. Top Pathways: decrease in nitrosylation at 0.1 and 4 Gy

Figure 55. Phagosome Maturation Pathway

Phagosomes are involved in the degradation of bacteria, as well as apoptotic and senescent cells. Phagosome maturation involves steps of fusion with the lysosome in order to create a mature phagolysosome for host defense. Failure to complete the phagosome maturation results in the inability of the host to defend itself against bacteria or clearing of senescent cells.

#### 4.2.4.3 Proteins Showing Increase in Nitrosylation at LDIR

##### 4.2.4.3.1 Increase at LDIR and Decrease at HDIR: Diphtamide Biosynthesis and Nervous System

The following proteins (PRKACA, EEF2, FMR1, GRIN1) were found to be involved in the Nervous System Development and Function, Cell-To-Cell Signaling and Interaction, and Behavior network pathways, while EEF2 participated in the Diphtamide Biosynthesis pathway.

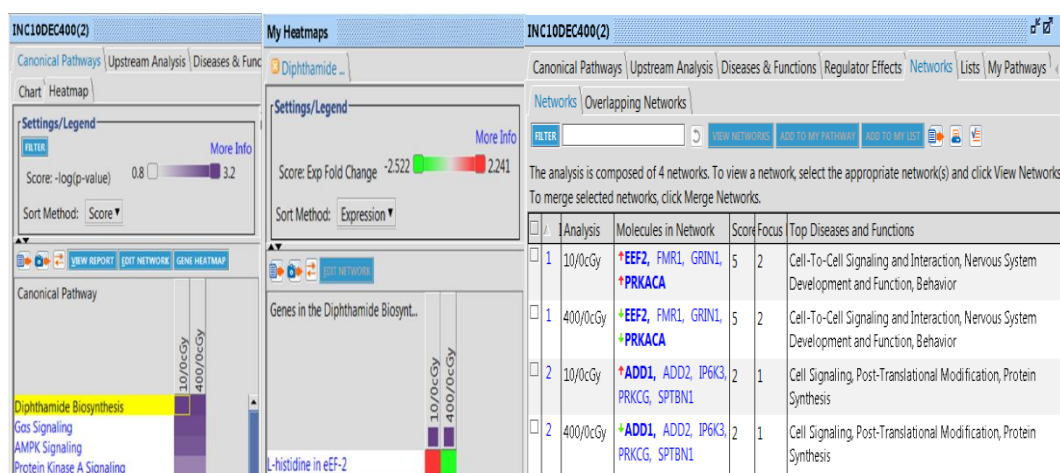


Figure 56. Pathway analysis, heatmap and networks (Cluster increase at 0.1 Gy and decrease at 4 Gy).

Since this group contains a limited number of proteins, most of the pathways are generated from either a single protein or combination of 2 to 3 proteins. The first 2 pathways displayed had a  $-\log(p\text{-value}) > 3$ . For example, the highest ranking pathway in this group is for Dipthamide Biosynthesis and it is generated because of the molecule EF2 (eukaryotic translation factor). The EF2 protein is encoded in humans by the *EEF2* gene. According to NCBI Gene site<sup>162</sup>, “This gene encodes a member of the GTP-binding translation elongation factor family. This protein is an essential factor for protein synthesis. It promotes the GTP-dependent translocation of the nascent protein chain from the A-site to the P-site of the ribosome. This protein is completely inactivated by EF-2 kinase phosphorylation.” The second ranking pathway Gas Signaling, is the result of involvement of the 2 proteins ADD1 and PRKACA.

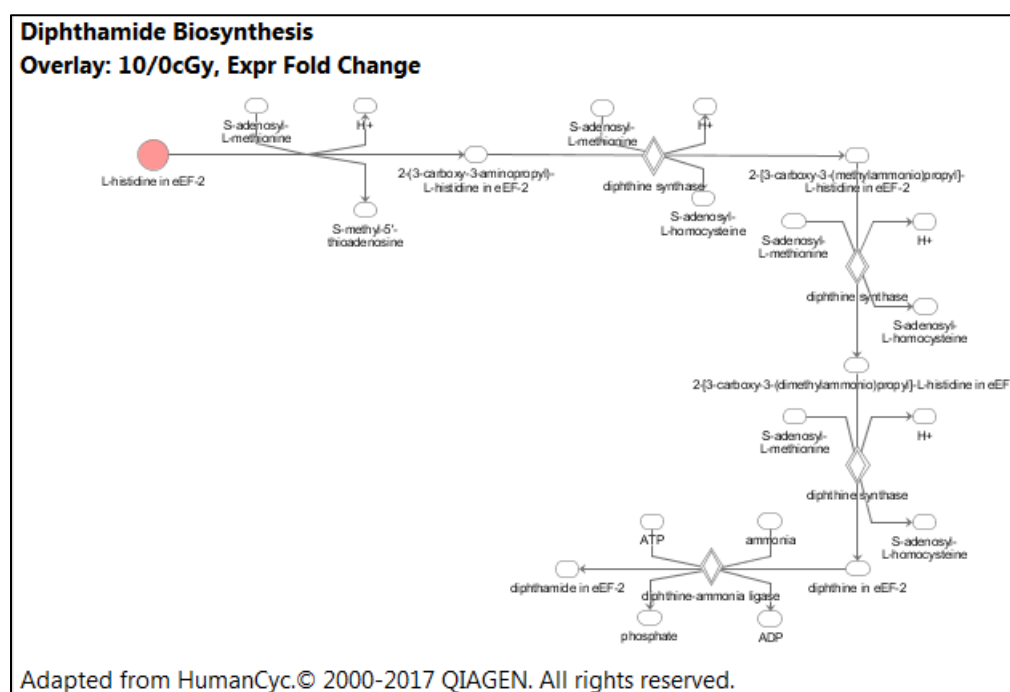


Figure 57. Dipthamide Biosynthesis Pathway.

DIPHTHAMIDE is a unique post-translationally modified histidine residue found only in the translation elongation factor 2 protein (eEF-2). Mutant mice defective in its biosynthesis are retarded in their growth and development, and almost always die before birth. Diphthamide is a target for bacterial toxins (diphtheria and pseudomonas) since the bacteria lack this uniquely modified amino acid and are able to shut down the eukaryotic machinery.

#### 4.2.4.3.2 Increase at LDIR and No Change at HDIR: TCA Cycle II Pathway and the Nervous System

Again, the following network “Cell-To-Cell Signaling and Interaction, Nervous System Development and Function, Cell Morphology” was found to be highly activated with 7 focus molecules/proteins involved (ATP5A1, PPP3CA, SLC25A4, GDA, MAG, SOD2, and CADPS). The TCA Cycle II (Eukaryotic) pathway was top pathway involved with IDH3G, FUMH inclusion.

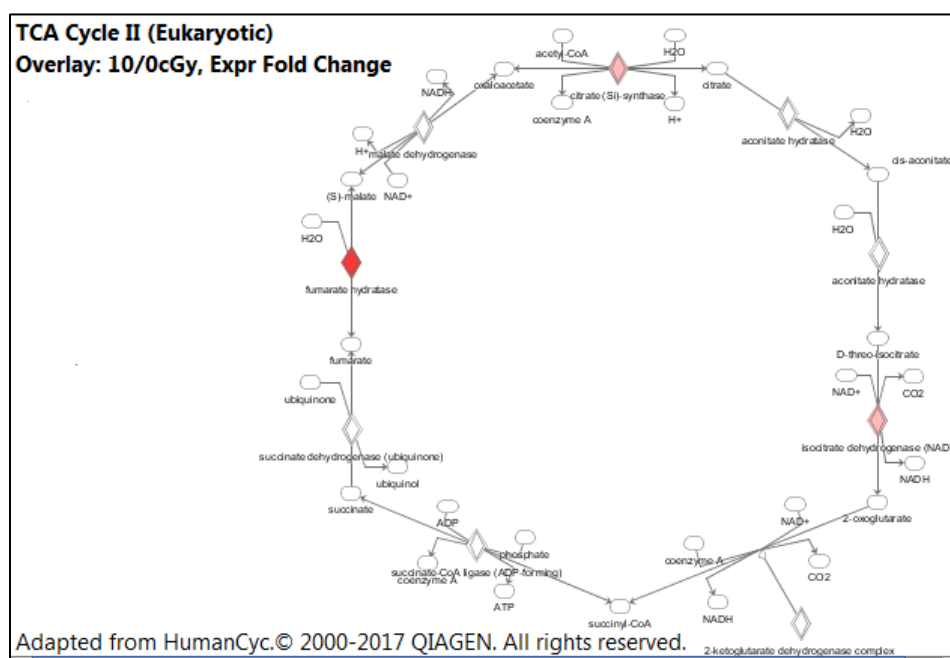


Figure 58. TCA Cycle II Pathway

#### 4.2.4.3.3 Increase at LDIR and Increase at HDIR: ALS Signaling and the Nervous System

The 3 main proteins, GRIN1, GRIN2B, and NEFL, are involved in the ALS signaling pathway (Amyotrophic Lateral Sclerosis Signaling), while 15 focus proteins were involved in the “Cell-To-Cell Signaling and Interaction, Nervous System Development and Function, Hereditary Disorder” network: BSN, CNTN1, ACO2, CNTNAP1, GRIN2B, NSF, MBP, PLP1, HPRT1, GRIN1, KLC1, NEFL, PDIA3, NCAM1, DCLK1.

The illustration depicted in Figure 53 shows the top pathways identified by IPA when the cluster ( $\downarrow 10$ ,  $\uparrow 400$ ) was uploaded for analysis. The 3 top pathways are involved in neuronal development and control, and again nNOS signaling pathway is selected as one of the pathways generated by our set of proteins. The table of p values shows the significance of each pathway ( $p < 0.05$ ).

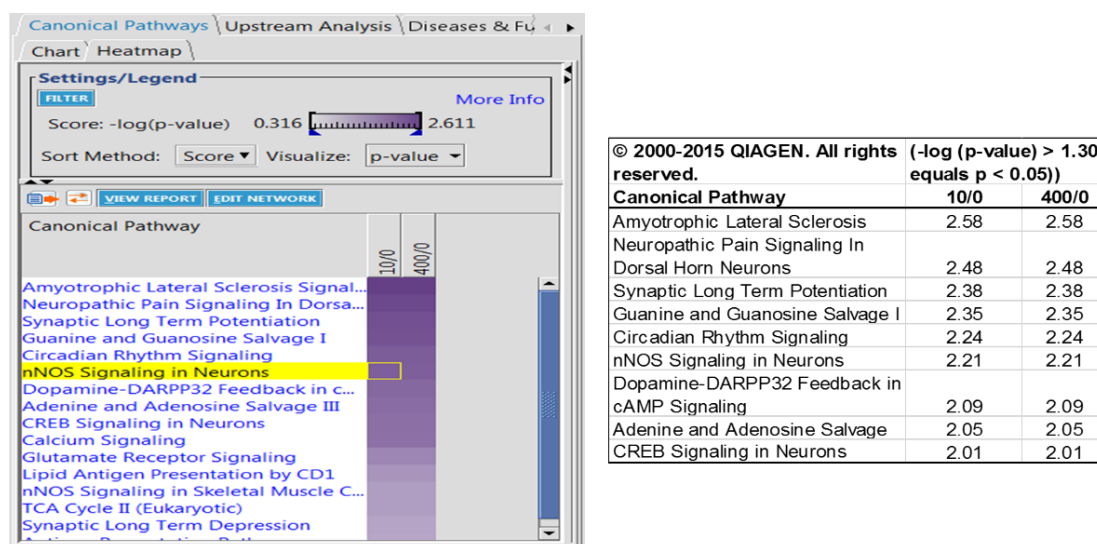


Figure 59. Top pathways: decrease in SNO at 0.1 Gy and increase at 4 Gy

ALS is shown as top pathway along with Neuropathic, synaptic and nNOS signaling.

Glutamate receptor as well as NMDA receptor are proteins involved in the pathway along with the Neurofilament peptide.

NMDAR (N-methyl D-aspartate receptors) is composed of 2 subunits, namely Grin1 and Grin2 b. S-nitrosylation of NMDARs downregulates its excessive activity providing neuroprotection. The complexing of NMDAR with nNOS regulates the S-nitrosylation of NMDARs. NitroMemantine is a drug used to diminish NMDAR hyperactivation by nitrosylating the NMDAR protein.<sup>88</sup>

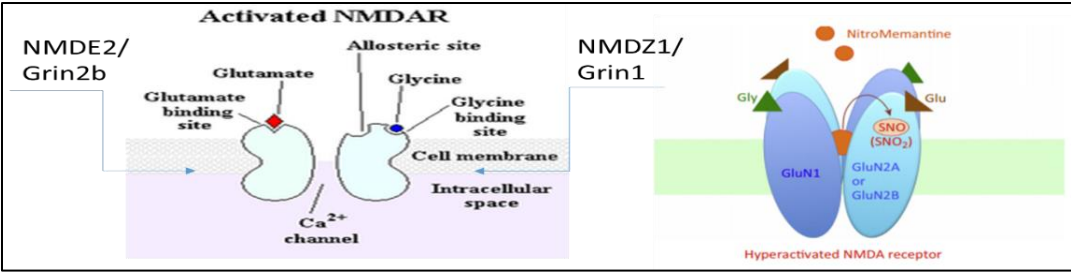


Figure 61. Pharmacological drugs to control the activity of NMDAR

A look at our nitrosylation values reveals that the 2 subunits, Grin1 and Grin2b show a decrease in nitrosylation at 0.1 Gy with a corresponding increase at 4 Gy.

Protein descriptions	Protein name (Swissprot)	Molecular Weight	Quantitative value		
			Ctrl	0.1 Gy	4 Gy
Glutamate receptor ionotropic, NMDA GN=Grin2b	NMDE2_MOUSE	166 kDa	1.87	1.17	3.71
Glutamate receptor ionotropic, NMDA GN=Grin1	NMDZ1_MOUSE	105 kDa	1.87	0	2.79

Table 20. NMDAR subunits with their nitrosylation levels in brain of mice exposed to 0.1 or 4 Gy

4.2.4.4 Disease and Functions Analysis

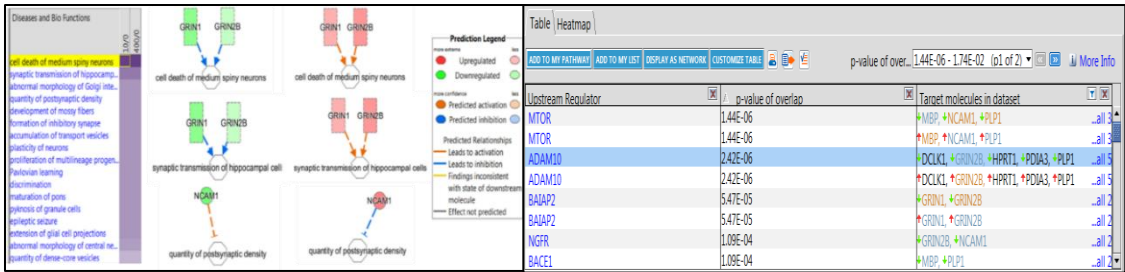


Figure 62. Disease and Functions and Upstream Regulators (Decrease in nitrosylation at 0.1 Gy and increase at 4 Gy).

Left: GRIN 1 & 2 are main players in the activation or inhibition of the biological function. NCAM (neural cell adhesion molecule) differential effect on the synaptic

function is also observed. Right: Top upstream regulators associated with clusters of differential nitrosylation - mTOR (mechanistic target of rapamycin) is shown as the upstream regulator with a high p value followed by the ADAM10 protein regulating a larger number (5) of proteins (orange color: predicted activation, blue predicted inhibition).

IPA gives information about the biological function and the diseases associated with our cluster. As can be seen from above, GRIN1/2 (NMDZ1/NMDE2) have differential nitrosylation at LDIR vs. HDIR and differential biological function: A decrease in the level of the proteins (not necessarily the nitrosylation level) results in an inhibition of cell death and the hippocampal transmission of neurons while the opposite is true. On the other hand, a decrease in the level of NCAM1 leads to the activation of postsynaptic density at 0.1 Gy, while elevated levels of NCAM1 perturbs postsynaptic density.

The “upstream regulator” in IPA refers to the molecule that can affect the expression of another molecule. The analysis examines the known targets of each upstream regulator in our dataset, compares the targets’ actual direction of change to expectations derived from the literature, and then issues a prediction for each upstream regulator. mTOR (mechanistic target of rapamycin) activates NCAM1 and PLP1 while it inhibits MBP. ADAM10 on the other hand has a broader effect targeting 5 proteins from our dataset.

## V Discussion

### 5.1 Irradiation Alters the Level of Protein S-Nitrosylation

The *in vivo* effect of exposure to low dose ionizing radiation on S-nitrosylation was investigated in order to assess and better understand adverse health outcomes resulting from such exposures.<sup>71,72</sup> In particular, post-translational modifications events by S-nitrosylation have not been well characterized.<sup>163,164</sup> However, recently S-nitrosylation has gained increased attention, especially in neurobiology and brain research.<sup>24</sup> Especially, S-nitrosylation was found exert an effect on phosphorylation, acetylation, ubiquitination, sumoylation and redox modifications of proteins.<sup>76</sup> In our study, altered levels of SNO proteins were detected in brain tissue at 13 days after whole body exposure of young-adult C57BL/6J mice to 0.1 Gy or 4 Gy of <sup>137</sup>Cs  $\gamma$  rays, which highlights induction/persistent effects long after irradiation to low or high doses of radiation received during diagnostic procedures or radiotherapy, respectively.

#### 5.1.1 Levels and Changes in S-Nitrosylation following <sup>137</sup>Cs $\gamma$ Ray Irradiation

From the data distribution and descriptive statistics of the whole data set (section 4.1.1.1 & 4.1.1.2), it is clear that most of the brain proteins identified by mass spectrometry exhibited small spectral counts (less than 10). The data also showed that there are other proteins with high spectral counts in the control sample and in both the low and high dose radiation samples. Our data showed various tubulin proteins belong to this latter group where S-nitrosylation of tubulins at physiological conditions is well documented.<sup>165</sup> Only a small number of proteins exhibited a large change in spectral count after irradiation. As we discussed in our paper,<sup>10</sup> most of the proteins exhibited a small magnitude of change

(less than 2 fold) relative to sham-treated mice, but a greater decrease in nitrosylation occurred at 0.1 Gy compared to 4 Gy exposure. This decrease was also consistent with the decrease observed in the western blot depicted in Figure 55 shown below for 50kD proteins.

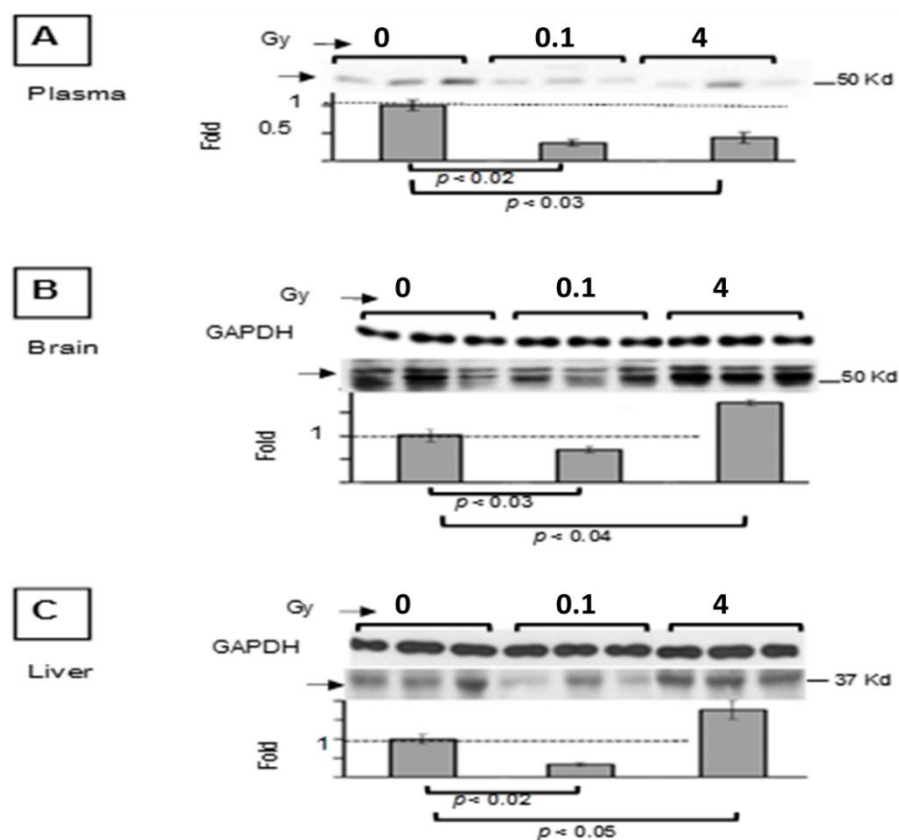


Figure 63. Western Blot: Modulation of S-nitrosylation by ionizing radiation

Western blot analyses, following biotin-switch assay, of nitrosylated proteins from organs of C57Bl/6J mice exposed 13 days earlier to  $^{137}\text{Cs}$   $\gamma$  rays. Proteins from mouse organs were freshly extracted and subjected to the biotin switch assay. The biotinylated proteins were detected with anti-biotin antibody. Protein aliquots (15  $\mu\text{g}$ ), before enrichment, were used as input standard and the expression level of GAPDH was used as loading control. In case of plasma, staining of the membrane with Ponceau S Red (not shown) indicated equal loading.<sup>10</sup>

## 5.2 Clustering of S-Nitrosylated Proteins

Mathematically, it was shown that our data distribution warrants the clustering of proteins into different groups. The difficult question to address was to determine how many different groups should be created. According to various tools available in R packages the optimum number of group should be two groups. The results from the two groups reflected dose independent changes in S-nitrosylation due to  $\gamma$  ray irradiation. One group of proteins is characterized by an increase in S-nitrosylation after irradiation, while another group belong to the proteins with decreased S-nitrosylation after irradiation. In addition, groups were created based on the intuition that proteins belong to three different groups after  $\gamma$ -ray-irradiation. Two groups of proteins exhibited either an increase or a decrease in S-nitrosylation, respectively, while another group of proteins showed no significant change in the levels of S-nitrosylation. Since there were two different doses, combination of three groups for each dose resulted in a total of nine different groups. Unfortunately, the group memberships were affected by the specific threshold value marking the boundary between no changes in S-nitrosylation level vs increased/decreased S-nitrosylation. This bias in threshold assignment may be avoided by use of k-means clustering or hierarchical clustering with a specified number of clusters of 9. Using manual clustering, it is clear that the 9 groups fall into several categories. First, the 3 groups that fall into a diagonal belong to dose independent radiation effects on S-nitrosylation (Figure 11). Upper right and lower left groups showed significant increase or decrease in S-nitrosylation respectively regardless of the irradiation dose applied. The group in the middle showed no changes in S-nitrosylation after irradiation regardless of the dose applied. The most interesting groups fall under the reverse diagonal. The group at the upper left and lower right showed

significant increase/decrease in S-nitrosylation similar to the previous groups, but the effects of irradiation is dose dependent and reveal opposite effects. Namely in the upper left corner group, the proteins showed significant increase in S-nitrosylation after high dose (4 Gy) irradiation but significant decrease in S-nitrosylation was observed after low dose (0.1 Gy) irradiation. The lower right corner group exhibited the opposite behavior. Unfortunately, a small number of proteins belonged to this group.

The remaining four groups, upper center, lower center, left center, and right center correspond to a significant increase or decrease in S-nitrosylation with one dose of irradiation, but very small changes in S-nitrosylation under another dose. In our data, the proteins showing significant decrease in S-nitrosylation at low dose irradiation but no significant changes in S-nitrosylation after high dose of irradiation are shown in the left center group. Similarly, the proteins with a significant increase in S-nitrosylation after high dose of irradiation while no changes after low dose irradiation are shown in the upper center group. Unfortunately, if one changes the threshold value to separate the no change from increased/decreased S-nitrosylation, this affects the membership of these groups and as there is no unique way to set the thresholds, thus there is no unique way to create these groups. This difficulty could be overcome by specifying several number of clusters with standard cluster analysis (k-means or hierarchical clustering). For example, clustering with the cluster number 7 seemed to show the two groups discussed above without any artificially defined threshold.

### **5.3 Characterization of Protein Clusters through Ingenuity Pathway Analysis**

Ingenuity Pathway Analysis software package was used to obtain biological characteristics of groups of proteins acquired from various clustering approaches. In order to determine

the effect of the differential nitrosylation level, the output table from IPA which summarizes changes for each group for pathways, diseases and networks were examined.

### 5.3.1 Pathways Identified Decreases in Nitrosylation at Low Dose IR

Taking the 3 groups of decreased nitrosylation at 4 Gy, we notice that majority of the pathways involved neuronal signaling (ALS, Neuropathic, Synaptic LTP, nNOS, Glutamate synthesis, degradation and calcium signaling).

As we discussed in our paper,<sup>10</sup> “following exposure to either 0.1 Gy or 4 Gy, AKT3 (RAC-gamma serine/threonine-protein kinase) was one of the proteins with the highest fold increase, since no nitrosylated AKT3 was observed in control samples. AKT3 is a member of PI3K/AKT signaling proteins that also include PTEN whose nitrosylation was also found to be modulated by  $\gamma$  rays in our data set (Supplementary Table 1). Interestingly, S-nitrosylation of PTEN has recently been reported to act as an on-off system for PI3-kinase-Akt signaling”. Notably, PI3K/AKT signaling has a key role in brain development.<sup>166</sup> The modulation of PI3K/AKT has been shown to affect cell proliferation and survival in irradiated cells.<sup>167</sup> S-nitrosylation of PTEN (another protein with an important function in the cellular responses to ionizing radiation)<sup>166</sup> by low concentrations of NO at Cys-83 inhibited its enzymatic activity<sup>165</sup> and consequently stimulated the downstream Akt cascade, which is essential for cell survival.<sup>168</sup> Therefore, our results add to the wealth of knowledge related to another post-translational event, namely phosphorylation, that controls activation of signaling by Akt.<sup>10</sup>

Other proteins showing significant increase in nitrosylation include the CSK22, DYHC1, GANAB, MCCA, NBEA, OXR1, QCR2 S12AS, and SRBS1. NBEA is the product of the *NEUROBEACHIN* gene, which is associated with autism and is expressed

in the forebrain, stem and cerebellum. NBEA is involved in the postsynaptic activity and controls synapse formation and dendritic transport.<sup>169</sup> GANAB (neutral alpha-glucosidase AB) is involved in glucose metabolism and is part of a complex responsible for dissociating and regulating glycoproteins to promote correct protein folding. This protein was found to be highly susceptible to an increase in S-glutathionylation under nitrosative stress. The product of nitrosative stress can be a mix of GSH (glutathionylation) and RNS/ROS products. There is an interplay between the PDI system (protein disulfide isomerases) and the endoplasmic reticulum (ER) role in accumulating misfolded proteins under stressful conditions. Increase in nitrosylation of GANAB can lead to the inhibition of its chaperone and isomerase activity and promotes a misfolded protein response in the ER.<sup>170</sup> OXR1 is the oxidation resistance protein 1 and is involved in protection from oxidative damage, in negative regulation of cysteine S-nitrosylation, and in the neuronal apoptotic process. On the other hand, cytoplasmic Dynein heavy chain (DYHC1) is a protein that is target for nitrosylation and denitrosylation by the thioredoxin enzyme, and can achieve a two fold increase<sup>171</sup> in nitrosylation under nitrosative stress. Its role is like a motor propelling the vesicles and organelles along the microtubules. CSK22 Casein kinase II subunit alpha is a protein involved in many cellular processes, including progression through the cell cycle, apoptosis and transcription. Methylocrotonoyl-CoA carboxylase subunit alpha and mitochondrial MCCA are involved in amino acid degradation pathway (Leucine). SORBS1 Sorbin and SH3 domain-containing protein 1 play a role in insulin-stimulated glucose transport. They are involved in the formation of actin stress fibers and focal adhesions processes that modulate the radiation response.<sup>172</sup>

As discussed in our paper<sup>10</sup>, “a salient finding of our study was that relative to control, nitrosylated tubulin betas (TBB4 and TBB2A) were decreased as a function of dose in brain, whereas nitrosylated tubulin alphas were essentially unchanged. Interestingly, the most recently discovered post-translational modification of tubulin was the S-nitrosylation of  $\alpha$ - and  $\beta$ -tubulins in the murine brain.<sup>173</sup> Three cysteine residues in  $\alpha$ -tubulin and 4 in  $\beta$ -tubulin have been identified to be susceptible to this modification.<sup>174</sup> Further, it has been reported that S-nitrosylation of tubulin alters its polymerization.<sup>175</sup> Importantly, dysfunction of the cytoskeleton has been associated with numerous neurodegenerative conditions, including Alzheimer’s and Parkinson’s disease.<sup>176</sup>”

“Our results<sup>10</sup> have also shown that the level of nitrosylated ARF-5 was increased in brain of mice exposed to 4 Gy. The ARFs are a family of small guanine nucleotide-binding proteins known to play a role in vesicular trafficking and organelle structure by recruiting coat proteins, regulating phospholipid metabolism and modulating the structure of actin at membrane surfaces.<sup>177</sup> They influence actin assembly at the Golgi to facilitate vesicle fission.<sup>178</sup> The exact functions of ARF5 are unclear, however, some studies have indicated that it might have a role in early Golgi transport and in recruiting coat components to *trans*-Golgi membranes.<sup>179</sup>” Interestingly, ARF accumulates in response to persistent radiation-induced DNA damage and plays an important role in orchestrating up-regulation of the p53 protein (a central player in many responses to ionizing radiation), modulation of DNA repair, and induction of cell-cycle delays.<sup>180</sup>

Further, in our paper,<sup>10</sup> we report that “relative to control, the expression level of nitrosylated sodium/potassium-transporting ATPase subunit beta-1 was increased by ~ 5-fold in brain of mice exposed to 0.1 Gy, but was unchanged following irradiation with 4

Gy. This protein maintains transmembrane electrochemical gradients in all mammalian cells through the transport of extracellular  $K^+$  in exchange for intracellular  $Na^+$ .<sup>181</sup> Modifications that affect this function would result in important physiological perturbations: The concentration gradients of  $Na^+$  and  $K^+$  ions across the plasma membrane is essential for maintaining cellular homeostasis,<sup>182</sup> and early studies have investigated inactivation of the Na,K-pump following exposure to ionizing radiation.<sup>183</sup>

The output from IPA also revealed an indication of additional differential effect on the brain cells when there was an increase in nitrosylation at 4 Gy. For example, the group showing increase at 4 Gy were involved in pathways related to cell morphology and nervous system development (diphthamide signaling, protein kinase, TCA Cycle II and epithelial adherens). Also, the network of cell to cell signaling and interaction was dominant among this group.

#### 5.3.1.1 nNOS Pathway Differential Activation

Exposing cells to a low dose of 0.1 Gy initiates a process that may ultimately lead to enhanced tolerance to harmful effects of subsequent exposures to other environmental agents, including subsequent exposure to radiation.<sup>66</sup> This study suggested that upregulation of proteins (nitrosylated proteins) implicated in protective biological pathways (*e.g.* DNA repair, antioxidation) following exposure to 0.1 Gy may equip C57Bl/6J male mice with a capacity to resist the damaging effects of a subsequent exposure to ionizing radiation, or to oxidative stress from normal metabolism.

As discussed in our paper<sup>10</sup>, “neuronal nitric oxide synthase (nNOS) signaling was inhibited by low dose  $\gamma$  rays and activated by high dose (Fig. 41). Whereas total NOS activity was reported to be increased in brain shortly (within 30-60 min) after exposure of

pregnant Wistar rats to 1 Gy dose of  $\gamma$  rays,<sup>184</sup> studies on the regulation of nNOS activation as a function of time following *in vivo* irradiation are lacking. Such studies would be important, since nNOS inhibitors are being investigated as a novel strategy for the treatment and prevention of human melanoma,<sup>184</sup>; in particular, melanoma patients are often treated with radiation.<sup>185</sup> However, the statistical significance of our results (P value and Z score) needs to be interpreted cautiously since ‘IPA Knowledge Base’ is based on gene/protein expression and not on the amount of nitrosylated protein. Although the identity of canonical pathways and networks involving the uploaded proteins should remain unchanged, statistical significance calculations need to be modified to accommodate the fact that not all proteins contain free cysteine that can be nitrosylated”.

#### 5.3.1.2 Amyotrophic Lateral Sclerosis

Denitrosylation at 4 Gy (for example HNRPD, K6PL, PPCE, NMDZ1, NMDEz, NFL) involved the Amyotrophic Lateral Sclerosis signaling network. This pathway (ALS, also called Maladie the Charcot or Lou Gehrig's disease) is a progressive, usually fatal paralytic disorder caused by the degeneration of motor neurons. The cause of ALS is unclear, but appears to involve cascades of events including oxidative damage, excitotoxicity, aberrant protein aggregation, mitochondrial defects, and caspase activation, which can lead to death of motor neurons in ALS patients. Nitrosative stress caused by high doses of radiation results in increased NO production<sup>32</sup> and increased nitrosylation activity. This in turn can lead to hyperactivation of the NMDAR causing cell death. In our study, the proteins involved in ALS showed a decrease in nitrosylation at low dose and increase at high dose radiation. S-nitrosylation studies have indicated that increase in nitrosylation is usually associated with inhibition of the NMDAR and in neurodegenerative diseases,<sup>111</sup> while

physiological and reduced nitrosylation resulted in neuroprotection. Further studies have also shown that apoptotic responses to ionizing radiation can be mediated by NMDAR in immature neuronal cells.<sup>2</sup>

#### 5.3.1.3 Calcium Signaling

Calcium has a pivotal role in signal transduction and the cellular responses to ionizing radiation.<sup>186</sup> Cell signaling pathways are initiated when plasma membrane receptors are activated due to external signals (neurotransmitters, hormones or growth factors). This results in the flow of calcium ions from the extracellular space to the cytosol (through the NMDAR) or the freeing of sequestered intracellular stores from the endoplasmic reticulum.<sup>186</sup> The de-nitrosylated proteins at both observations (0.1 and 4 Gy) included the calcium / calmodulin kinases, the MAPT (microtubule associated protein tau) kinase, the voltage dependent anion channel (VDAC), PRKCG (protein kinase C gamma), GDP dissociation inhibitor, EIF5A (eukaryotic translation factor), SNCA (synuclein alpha) and the transporter protein synaptophysin. In the brain, activated NMDAR becomes permeable to  $\text{Ca}^{2+}$  and activates nNOS to produce NO and ROS. Denitrosylation of NMDAR inhibits this process, and denitrosylation of the proteins involved in calcium signaling leads to reduced influx of calcium into the cell playing a protective role against neurodegeneration cascade.<sup>186</sup>

#### 5.3.1.4 Synaptic Long Term Potentiation

According to the IPA knowledgebase,<sup>159</sup> “Long-term potentiation (LTP) is the increase of synaptic strength between two neurons following high frequency stimulation of the synapse. A majority of synapses that experience LTP (*e.g.* in the hippocampus) involve a postsynaptic increase in calcium that is mediated through activation of the ionotropic

glutamate receptor, the N-methyl-D-aspartic acid (NMDA) receptor. Activation of NMDA receptors by glutamate released from the presynaptic neuron results in  $\text{Ca}^{2+}$  influx which coactivates the extracellular regulated signal kinase (ERK) and cyclic adenosine monophosphate (cAMP) signal transduction pathways. Activation of these two regulatory pathways increases the transcription of a family of genes via the cAMP responsive element binding (CREB) protein activation. CREB mediated transcriptional activation in the post synaptic neuron is believed to be an important event in LTP.” It is noteworthy that CREB plays a major role in the cellular responses to ionizing radiation (*e.g.* activation of cell cycle checkpoints and induction of apoptosis) and may contribute to neurodegeneration in ataxia telangiectasia (AT) patients who are known to be highly radiosensitive.<sup>166</sup>

The NMDA receptor mediated  $\text{Ca}^{2+}$  flux activates calmodulin dependent adenylyl cyclases, which play a critical role in generating the cAMP that in turn activates protein kinase A (PKA). The activation of PKA has a major role in supporting the nuclear translocation of ERK.<sup>187</sup> The activation of ERK is highly sensitive to regulation by ionizing radiation.<sup>187</sup> It leads to indirect activation of CREB by coupling to ribosomal protein S6 kinase (RSK), which then phosphorylates and activates CREB. The activation of PKA also results in the activation of I-1, an inhibitor of protein phosphatase 1 (PP1). In the absence of activated I-1, calmodulin kinase II (CaMKII) is dephosphorylated and inactivated by PP1. The NMDA receptor dependent PKA mediated phosphorylation of I-1 thus results in activation of CaMKII, one of the most abundant proteins in neurons. Activated CaMKII plays a role in the activation and phosphorylation of the ionotropic glutamate receptor alpha-amino-3-hydroxy-5-methylisoxazole-4-propionic acid (AMPA) receptor. This covalent modification of AMPA receptors results in a modulation of receptor numbers and

therefore to an increased response to glutamate which is an important postsynaptic event in LTP. The NMDA mediated  $\text{Ca}^{2+}$  flux also activates CaMKIV, which triggers CREB/CREB binding protein (CBP)-dependent transcription by phosphorylating CBP.

In addition to the ionotropic glutamate receptors, the metabotropic glutamate receptors mGluR also play a role in LTP. The mGluR via coupled G protein, activates the phospholipase C (PLC)/protein kinase C (PKC) pathway which triggers the NMDA receptor, thus increasing  $\text{Ca}^{2+}$  influx. Furthermore, the inositol triphosphate (IP3) generated as a result of PLC activation increases  $\text{Ca}^{2+}$  release from intracellular sources, further activating calmodulin dependent pathways. Irradiation can cause the deregulation of  $\text{Ca}^{2+}$  homeostasis and triggers programmed cell death by regulating death specific enzymes.<sup>188</sup> Furthermore, activated PKC is involved in numerous cellular responses, including the sphingomyelin/ceramide signal transduction pathway.<sup>189</sup>

It was interesting to see that the group of proteins with decrease in nitrosylation at 0.1 Gy and increase at 4 Gy, which included the 2 glutamate receptors (GRIN2B and GRIN1) as main players, has disease related to cell death and survival. Other major common disease and functions in the group with decrease at 4 Gy were related to cell signaling and neurological disease. The common network being the cell to cell signaling and nervous system development.

### **5.3.2 Cell Death and Apoptotic Pathways Identified Increased in Nitrosylation**

#### **5.3.2.1 Diphtamide**

According to InterPro Zinc finger, DPH-type (IPR007872),<sup>190</sup> “Diphtamide is a unique post-translationally modified histidine residue found only in translation elongation factor 2 (eEF-2).” Mutant mice defective in its biosynthesis are retarded in growth and

development, and almost always die before birth. Also, InterPro<sup>190</sup> states, “It is conserved from archaea to humans and serves as the target for the diphtheria toxin and the *Pseudomonas* exotoxin A. These two toxins catalyze the transfer of ADP-ribose to diphthamide on eEF-2, thus inactivating eEF-2, halting cellular protein synthesis, and causing cell death.” By targeting this unique modified amino acid which does not exist in bacteria, these pathogens are able to shut down the eukaryotic protein synthesis machinery without jeopardizing their own system.<sup>191</sup>

#### 5.3.2.2 Actin Cytoskeletal signaling

Zareba-Kozioł et al. (2014)<sup>86</sup> wrote “The synaptic cytoskeleton is particularly important for synaptic plasticity and plays a role in rapid activity-dependent changes of synapse volume or shape. Disruptions in the synaptic cytoskeleton affect the stability and maturation of synapses and subsequently disturb neuronal communication. Actin cytoskeletal pathology may be an early cause of transport defects in AD. ” “Okamoto & Lipton (2015)<sup>192</sup> discussed “An axon is the neuronal process that serves to relay afferent signals via action potential propagation. Axonal guidance, outgrowth, and retraction are coordinated by dynamic rearrangements of the actin and microtubule cytoskeletons. The coordinated remodeling of the cytoskeleton is essential for brain development. Missense and splice-site mutations in  $\alpha$ - and  $\beta$ -tubulin isotypes, constituents of neuronal microtubules, which can cause human neurodevelopmental disorders such as lissencephaly.<sup>193</sup> Additionally, the quality control or proteostasis of actin and tubulin proteins is strictly regulated during neuronal maturation in the developing brain. Abnormal expression or mutation in cytoskeletal proteostasis genes causes a spectrum of neurological disorders.<sup>194</sup> Notably, one key regulator of the dynamics of actin filaments and

microtubules involves NO signaling.. Microtubule-associated proteins (MAPs), a group of filamentous proteins, control the integrity and dynamics of microtubules.<sup>195</sup> MAP1B is highly expressed in the developing brain and, along with tau, is the main member of the neuronal MAPs.<sup>196</sup> MAP1B protein undergoes proteolytic cleavage to generate MAP1B heavy chain (HC) and light chain (LC1), and forms a protein complex (HC/LC1). MAP1B is an essential regulator of the axonal cytoskeleton,<sup>197</sup> controlling assembly and stability of both actin filaments and microtubules.<sup>198</sup> MAP1B has been reported to mediate nNOS-dependent axon retraction.<sup>199</sup> nNOS physically interacts with LC1, but not HC, and cysteine-2457 on LC1 is S-nitrosylated. This S-nitrosylation reaction changes the conformation of LC1 and results in increased binding of the HC/LC1 MAP1B complex to microtubules. This leads to axonal retraction, possibly by inhibiting the action of dynein, which is necessary for axonal extension.<sup>199</sup>

### 5.3.2.3 Gas Signaling

The G-proteins are heterotrimers, consisting of  $\alpha$ ,  $\beta$ , and  $\gamma$  subunits. They are involved in signal transduction for numerous types of ligands such as hormones, neurotransmitters and chemokines. These extracellular signals are received by members of a large superfamily of receptors. The G-protein-coupled receptors (GPCRs), activate the G-proteins and route the signals to several distinct intracellular signaling pathways thus initiating changes in cell behavior. Cabrera-Vera et al. (2003) wrote “In the inactive heterotrimeric state, GDP is bound to the  $G\alpha$  subunit. Upon activation, GDP is released, GTP binds to  $G\alpha$ , and subsequently  $G\alpha$ -GTP dissociates from the  $G\beta\gamma$  and from the receptor. Both  $G\alpha$ -GTP and  $G\beta\gamma$  are then free to activate downstream effectors. The duration of the signal is determined by the intrinsic GTP hydrolysis rate of the  $G\alpha$ -subunit and the subsequent re-association of

G $\alpha$ -GDP with G- $\beta\gamma$ .” The G-proteins have been reported to regulate cellular survival and other functions following exposure to ionizing radiation.<sup>200</sup>

## **5.4 Irradiation in the Treatment of Neurodegenerative Diseases**

In the preceding discussions, we briefly outlined how the neuronal pathways involved in brain function and physiology are perturbed by irradiation. The gateway through which these perturbations are taking place is through NMDAR-associated ion channels. Nakamura<sup>24</sup> studied the effect of nitrosylation on neurodegenerative disease. He concluded, and as was highlighted above, that under nitrosative stress (seen in old age), there is an increase in the level of NO and a concurrent increase in the level of nitrosylation leading to neurodestruction. Here, we show that high dose irradiation mimics the results seen under increased nitrosative stress, while exposure to the low dose radiation corresponded to the observation seen under moderate stress (protection of brain cells).

### **5.4.1 Low Dose Radiation and Moderate Increase in SNO/Adaptation Process**

Although Nakamura *et al.*<sup>24</sup> described the process of a moderate increase in nitrosylation as a protective pre-neurodestruction step, our results indicated that under moderate or mild nitrosative stress some proteins also undergo de-nitrosylation steps as a neuroprotection strategy. We have seen this as a decrease in activation of the nNOS pathway at low dose irradiation (0.1 Gy) while the pathway was hyperactivated at high dose (4 Gy). Another pathway identified in our study and implicated in neuronal disease is the ALS (Amyotrophic Lateral Sclerosis). Again, this was one of the neurodegenerative diseases caused by an increase in nitrosylation, and in our study this pathway similarly belonged to the proteins with a decrease in nitrosylation under mild stress and an increase under high stressful conditions (radiation).

## **5.5 Biomarker Discovery**

As stated in section 2.4, an effort is underway by the European project (MELODI) to study the biological and health effects of low dose radiation. The dedication of specific database (BIDE) to house low dose ionizing radiation mechanistic data is another focused effort emphasizing the importance of biomarkers in studies of the health effects of low dose radiation. A limitation in the development of Biomarkers centers on the development of sensitive and specific biomarkers of exposure to ionizing radiation. The challenge remains in identifying biomarkers that modulate radiation sensitivity for further investigation. Most research on biomarker discovery remain in the discovery stage. Recent update has shown that only one group of biomarkers has so far been rather investigated to a large extent and it is the radiation specific mRNA transcript profiles. Further concerted research is needed in order to discover biomarkers of exposure to ionizing radiation that may predict long term adverse outcomes such as cancer, and neurodegenerative diseases.<sup>154,201</sup>

## VI Conclusion and Future Directions

Optimal number of clustering resulted in 2 groups showing dose independent changes. Biological significance of the groups was not clear. On the other hand, manual clustering with an artificial threshold identified one group of proteins in the ALS signaling pathway that exhibited differential dose response. K-means clustering without artificial cutoff identified two groups of proteins with dose dependent responses, one in Parkinson disease and the other one in the glutamate receptor signaling.

Whole data analysis showed a significant decrease in S-nitrosylated proteins at low dose (0.1 Gy) while a slight increase was observed at high dose (4 Gy). RhoGDI pathway was identified to be inactivated in a dose independent manner, while nNOS signaling pathway was differentially regulated by low and high doses. The results clearly show dose dependent S-nitrosylation effect leading to activation or inactivation of certain pathways and the analyses suggest a protective low dose effect, which needs further investigation. In addition, together with other studies, this project supports continuous re-evaluation of current radiation protection models as new mechanistic and epidemiological results become available.

Our study demonstrated a differential effect of radiation on S-nitrosylation after low and high dose exposures of mice to  $^{37}\text{Cs}$   $\gamma$  rays. In addition, we identified different neuronal pathways that are activated or inhibited under each condition. Together, our results show that the development of sensitive and quantitative proteomic approaches (*e.g.*, involving biotin switch assay to study post translational modification) are relevant to understanding the mechanisms underlying the biological effects of ionizing radiation. Characterizing the S-nitrosocysteine proteomes of different organs in organisms exposed

to ionizing radiation, together with application of computational tools to understand functional pathways, will shed light on mechanisms contributed by nitric oxide biology.<sup>202</sup> It will uncover pathways that specifically underlay low and not high dose radiation, and those that are common to both levels of radiation. It will inform on crucial parameters that modulate tissue responses to diagnostic and therapeutic radiation,<sup>203,204</sup> including the cytoskeleton and the cellular microenvironment. They will enhance our understanding of the factors that determine radiation sensitivity and the propagation of radiation-induced damaging effects.<sup>202</sup>

As discussed in our paper<sup>10</sup>, “the availability of specific antibodies to SNO proteins found to be altered by low and high dose  $\gamma$  rays, coupled with *in situ* immune-detection in tissue sections of control and irradiated brains of mice would be informative of the affected tissues and cells. Studies of nitric oxide synthase (neuronal or inducible) activity, and the studies of modulation of SNO proteins would enhance our understanding of signaling events in the brain under stress conditions. Notably, studies of the kinetics of biochemical and molecular changes coupled with physiological and behavioral studies, would be a major step toward understanding of mechanisms leading to neuronal degeneration. Such studies may contribute to formulation of strategies to attenuate harmful conditions. Notably, clinical trials involving treatments with down-regulators of nitric oxide-mediated signaling events were found to attenuate neurotoxicity.<sup>205</sup>”

The early radiation damage to DNA and proteins were recognized over seven decades ago.<sup>206</sup> As reviewed in a recent paper from our research group, such damage can be either direct or mediated by radiolysis of water. It may also result from activation of oxidases and nitric oxide synthases.<sup>2</sup> The generation of excess levels of ROS and RNS

damage macromolecules, including enzymes<sup>70,207</sup> and perturbs signal transduction processes.<sup>39</sup> Such effects occur shortly after exposure and may persist for days, months and years. Here we have examined nitrosylated proteins at 2 weeks after exposure to <sup>137</sup>Cs  $\gamma$  rays, a time at which the oxidative species produced during or shortly after irradiation would have decayed. Therefore, oxidative effects detected long after the radiation exposure is relevant to disease development.<sup>208</sup>

Our results, obtained by immunoblotting and mass spectrometry analyses, suggest that an increase in radiation dose does not essentially result in increased effects on S-nitrosylation. Though, the specific nitric oxide synthases that mediate the post-translational change, the interrelated protein clusters whose regulation is modulated by radiation-induced S-nitrosylation, and the link to neurodegeneration remains to be investigated. The dependence on the level, timing, duration, and/or cellular location of nitric oxide production/exchange needs to be examined.

In this project, mass spectrometry measured only the amounts of SNO proteins and did not examine global changes in levels of the native proteins. Therefore, it is not clear whether the changes that were observed are due to changes in S-nitrosylation activity or are a reflection of change in native protein levels. Examining both, the changes in general and S-nitroso proteomes as a function of time after irradiation, would enhance our understanding of the underlying mechanisms. Another pitfall in our analysis involved the spectral counts. Count data usually suffer from poor resolution in the low abundance range (*e.g.* proteins detected with a single peptide-spectrum match), and there are ambiguities in counting peptides which are shared among homologous proteins, requiring careful

handling of counts in complex organisms such as human. Finally, the development of new clustering packages would enhance analysis of large proteomic data (optcluster).<sup>130</sup>

## VII Appendix

The following section is transcribed from our paper <sup>10</sup>.

### 7.1 “Radiation Treatment and Mass Spectrometry Protocol

#### **Radiation Treatment:**

Whole-body  $\gamma$ -irradiation of young adult mice (17 week old) C57BL/6 was administered at low (0.1 Gy) and high (4 Gy) doses of  $^{137}\text{Cs}$  with an energy of 661 keV and an LD50/30 of ~8Gy). The doses were delivered in 1 min time periods to the whole body in a ventilated irradiator (J.L. Shepherd, Mark I, San Fernando, CA). Animals were sacrificed for analyses by CO<sub>2</sub> asphyxiation at 13 days after irradiation. The organs were rapidly harvested and submitted to protein nitrosylation by the biotin-switch assay.

The contrast agent iopamidol (Isovue Multipack-370) was from Bracco Diagnostics Inc., (Princeton, NJ). A 100  $\mu\text{L}$  volume of Isovue 370 containing 37 mg of organically bound iodine was injected retro-orbitally in the right eye of the mouse using a 27G needle. Anesthesia was not used, and a one minute interval separated the injection and the start of irradiation.

The experimental groups (5 mice/group) were as follows: 1) Sham-irradiated without contrast agent; 2) sham-irradiated with contrast agent; 3) 0.1 Gy-irradiated without contrast agent; 4) 0.1 Gy-irradiated with contrast agent; 5) 4 Gy-irradiated without contrast agent. The mice were placed in sterile cages immediately after irradiation to simulate reverse isolation. The food (sterile Purina rodent chow) and sterile drinking water were given *ad libitum*.

#### **Biotin Switch Analysis of Protein Nitrosylation**

Mouse organs (brain, lung, liver, plasma) were minced, homogenized, and lysed in lysis/blocking buffer (LB, 50 mM Tris, pH 7.5, 150 mM NaCl, 1% Triton-X100, 2.5% SDS, 1 mM EDTA, 0.1 mM neocuproine, and 50 mM methyl-methane thiosulfate (MMTS)). The lysis/blocking buffer was supplemented with a protease inhibitor cocktail, and the samples were frequently vortexed at 50 °C for 30 min. Excess MMTS was removed by cold acetone precipitation. The protein pellets were washed with 20% ice cold acetone and reconstituted in HENS buffer containing 1% (w/v) SDS and 0.2 mM *N*-(6-(Biotinamido)hexyl)-3'-(2'-pyridyldithio)-propionamide (biotin-HPDP) (Pierce, Rockford, IL, USA) with 10 mM ascorbate. The reaction mixture was incubated in the dark for 1 h at room temperature. Excess reagents were removed by cold acetone precipitation. The protein pellets were solubilized in non-reducing SDS-PAGE loading buffer (100 mM Tris, pH 6.8, 2% SDS, 15% glycerol, 0.01% bromophenol blue) for western blotting or in resuspension buffer (RB consists of 50 mM Tris, pH 7.5, 150 mM NaCl, 1% Triton-X100, and 0.5% SDS) for immunoprecipitation as described below. For western blotting, 15  $\mu\text{g}$  aliquots of protein were separated using non-reducing SDS-PAGE and transferred onto nitrocellulose membrane. The biotinylated proteins were reacted with an anti-biotin antibody (Vector Laboratories, Burlingame, CA, USA) and visualized with enhanced chemiluminescent substrate (PerkinElmer, Waltham, MA, USA).

### Detection of S-Nitrosylation

#### *Immuno-Precipitation and Detection of S-nitrosylated Proteins:*

Proteins modified by the biotin switch assay were precipitated in acetone and dissolved in RB. Protein concentrations were determined by the BCA method. Biotinylated proteins (500 µg) in 500 µl RB were diluted with 500 µl PBS and mixed with 50 µl of streptavidin –agarose beads (Pierce, Rockford, IL, USA). The mixture was incubated for 1 h at 23 °C with agitation. The beads were washed 5X with 1 mL of PBS, suspended in 2X SDS-PAGE loading buffer, and heated at 100 °C for 5 min. For detection of specific nitrosylated proteins, supernatant proteins were separated by SDS-PAGE and transferred onto nitrocellulose membrane. The membranes were blocked with 5% milk, and reacted with specific antibodies to confirm the mass spectrometry results. After incubation with a specific secondary antibody conjugated with horseradish peroxidase, protein bands were detected by enhanced chemiluminescence system from GE Healthcare (Amersham). Luminescence was determined by exposure to X-ray film, and densitometry analysis was performed with an EPSON scanner and National Institutes of Health Image J software (NIH Research Services Branch).

#### **Analysis of Nitrosylated Proteins and Peptides by Mass Spectrometry:**

Mass measurement of S-nitrosylated proteins and peptides in brain tissues from mice exposed to 0, 0.1 or 4 Gy was performed on LTQ Orbitrap Velos Pro mass spectrometer (Thermo Fisher Scientific) according to an optimized method developed in our laboratory.<sup>85</sup> The mass spectrometer is coupled with a Dionex Chromatography System equipped with an Ultimate™ 3000 autosampler through a Proxeon nano-electrospray ion source. Mass spectrometry (MS) analyses were performed via direct infusion unless stated otherwise. For identification of nitrosylated cysteines, biotinylated proteins were recovered with 8 M urea following acetone precipitation of the proteins from the biotin switch assay. The proteins were diluted 10-fold with 50 mM NH<sub>4</sub>HCO<sub>3</sub> and digested with trypsin (1:30 w/w enzyme: protein ratio) at 37 °C overnight. The resulting peptides were loaded onto an avidin cartridge (ICAT kit from ABI) for enrichment of the biotinylated peptides. After washing the cartridge to remove unmodified peptides with 2 mL of PBS (pH 7.2) and 1 mL of a solution containing 50 mM ammonium bicarbonate and 20% methanol (pH 8.3), the biotinylated peptides were eluted with 30% ACN and 0.4% trifluoroacetic acid (TFA), dried in a SpeedVac concentrator and resuspended in 2% ACN and 0.1% TFA. For LC/MS/MS analysis, the biotinylated peptides were first separated by Dionex UltiMate® 3000 reversed phase liquid chromatography (RPLC, capillary PepMap 100 column, 75 µm X 150 mm, 3 µm, 100 Å, C<sub>18</sub>, Dionex, Sunnyvale, CA, USA). The eluted peptides were analyzed and MS spectra ( $m/z$  400–1900) were acquired in the positive ion mode. Argon was used as the collision gas. The collision energy was set from 16 to 60 V, depending on the precursor ion charge state and mass. MS/MS spectra were acquired in the Data-Dependent Analysis mode, in which the three most abundant precursors with two to five charges from each MS survey scan were selected for fragmentation. The peak lists were generated by ProteinLynx (v2.1) into PKL files.

Database searches were performed with Mascot (2.4.1) as a search engine against all of the mouse protein sequences in the UniRef100 protein database (downloaded on Jan 24, 2014). The following search parameters were used: trypsin was selected as enzyme with 1 missed cleavage, mass tolerance of 100 ppm for MS and 0.6 Da for MS/MS, MMTS-modified and biotin-HPDP-modified cysteines and methionine oxidation were set as variable modifications. For MS/MS identification of the peptide's nitrosylation site, a Mascot score threshold of at least 34 was set which corresponded to a  $p$  value of 0.05 or better, the spectra were manually validated for post-translational modifications (PTMs). False discovery rate was calculated to be  $< 0.5\%$  according to Peng *et al.*<sup>209</sup>

### Iopamidol Results in Decrease in Nitrosylation in the Brain

Iopamidol, an iodinated contrast agent used in radiodiagnostic procedure was delivered intravenously immediately prior to irradiation. Control group (0cGy) and low dose group (0.1 Gy) received irradiation with and without the contrast agent. The western blot analyses results are shown in the figure below. Relative to control, exposure to 0.1 Gy resulted in prominent decrease in the level of SNO proteins in brain and liver relative to 4 Gy. In lungs there was a comparable increase at both levels (Panel D), while in plasma there was a similar decrease at both levels.

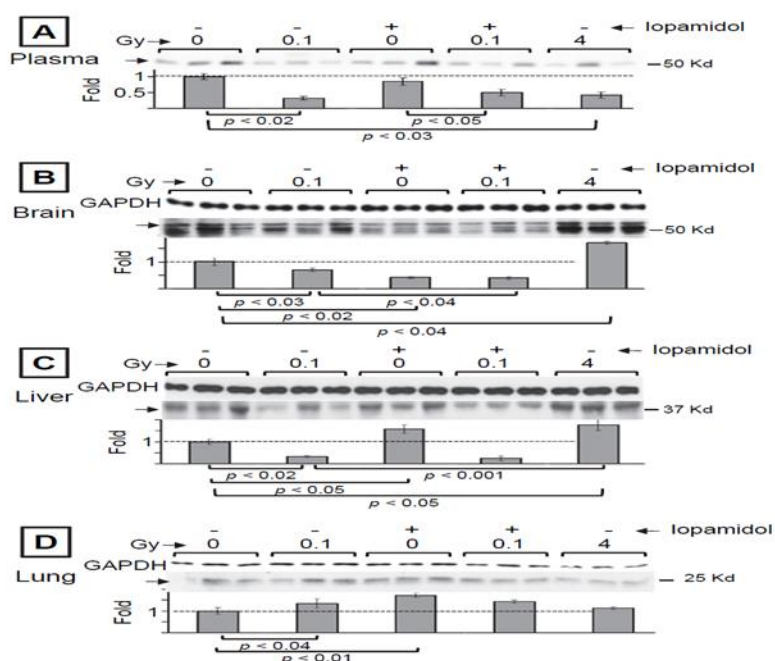


Figure 64. Modulation of S-nitrosylation by ionizing radiation and/or radiocontrast agent.

Western blot analyses, following biotin-switch assay, of nitrosylated proteins from organs of C57Bl/6J mice exposed 13 days earlier to  $^{137}\text{Cs}$   $\gamma$  rays in presence or absence of iopamidol. Proteins from mouse organs were freshly extracted and subjected to the biotin switch assay. The biotinylated proteins were detected with anti-biotin antibody. Protein aliquots (15  $\mu\text{g}$ ), before enrichment, were used as input standard and the expression level of GAPDH was used as loading control. In case of plasma, staining of the membrane with Ponceau S Red (not shown) indicated equal loading.

### **Iopamidol Dependent Nitrosylation**

Relative to control mice, administration of contrast agent alone or in combination with 0.1 Gy also resulted in modulation of S-nitrosylation in a few of the organs examined. The changes are highlighted in the autoradiograms for proteins of specific size. In plasma, for proteins of MW in the range of 45-50 KDa, treatment with iopamidol alone, or in combination with 0.1 Gy exposure, did not induce an apparent effect. In contrast, in brain, iopamidol alone resulted in greater decrease than induced by 0.1 Gy, but did not result in additional effect when combined with 0.1 Gy. In lung, iopamidol triggered a significant increase in S-nitrosylation of proteins in the 50-60 kDa MW range. This increase was not affected when iopamidol treatment was combined with 0.1 Gy exposure. In liver, iopamidol treatment enhanced S-nitrosylation of proteins in the 50 KDa range. However, when iopamidol treatment was combined with exposure to 0.1 Gy, a decrease similar to that observed following irradiation alone was observed.”

## **7.2 Copyright Permission**

### **7.2.1 Proteomes— Open Access Journal**

Creative Commons Attribution License CC BY license

### **7.2.2 IPA Copyright Permission**

QIAGEN Ingenuity product support  
To whom this may concern:

Dr. Nicolas has been granted permission by QIAGEN Silicon Valley to use copyrighted figures generated from Ingenuity Pathways Analysis in his/her publication. Figures produced from IPA are available under an open-access CC-BY license for purposes of publication.

If you have any further questions, please contact the QIAGEN Advanced Genomics Support team at [AdvancedGenomicsSupport@qiagen.com](mailto:AdvancedGenomicsSupport@qiagen.com).

Best regards,

Jasmin

Dr. Jasmin Droege  
Senior Scientist, Advanced Genomics Support  
[AdvancedGenomicsSupport@qiagen.com](mailto:AdvancedGenomicsSupport@qiagen.com)  
US Tel: +1 866 464 3684  
Danish Tel: +45 8082 0167  
[QiagenBioinformatics.com](http://QiagenBioinformatics.com)

## VIII References

1. NCRP. *Ionizing Radiation Exposure of the Population of the United States*. Bethesda: National Council on Radiation Protection and Measurements; 2009. Report No. 160.
2. Azzam EI, Jay-Gerin JP, Pain D. Ionizing radiation-induced metabolic oxidative stress and prolonged cell injury. *Cancer Lett*. 2012;327(1-2):48-60.
3. Tomonaga M. Leukaemia in Nagasaki atomic bomb survivors from 1945 through 1959. *Bulletin of the World Health Organization*. 1962;26:619-631.
4. Little JB. Failla Memorial Lecture. Changing views of cellular radiosensitivity. *Radiat Res*. 1994;140(3):299-311.
5. Ron E. Cancer risks from medical radiation. *Health Phys*. 2003;85(1):47-59.
6. Tubiana M, Feinendegen LE, Yang C, Kaminski JM. The linear no-threshold relationship is inconsistent with radiation biologic and experimental data. *Radiology*. 2009;251(1):13-22.
7. BEIR-VII. *Health Risks from Exposure to Low Levels of Ionizing Radiation*. Washington, D.C.: National Research Council of the National Academies;2005.
8. Averbeck D. Does scientific evidence support a change from the LNT model for low-dose radiation risk extrapolation? *Health Phys*. 2009;97(5):493-504.
9. Mullenders L, Atkinson M, Paretzke H, Sabatier L, Bouffler S. Assessing cancer risks of low-dose radiation. *Nature reviews Cancer*. 2009;9(8):596-604.
10. Nicolas F, Wu C, Bukhari S, et al. S-Nitrosylation in Organs of Mice Exposed to Low or High Doses of  $\gamma$ -Rays: The Modulating Effect of Iodine Contrast Agent at a Low Radiation Dose. *Proteomes*. 2015;3(2):56-73.
11. Amundson SA, Fornace AJ, Jr. Gene expression profiles for monitoring radiation exposure. *Radiat Prot Dosimetry*. 2001;97(1):11-16.
12. Azzam EI, de Toledo SM, Little JB. Expression of connexin43 is highly sensitive to ionizing radiation and environmental stresses. *Cancer Res*. 2003;63(21):7128-7135.
13. Coleman MA, Yin E, Peterson LE, et al. Low-dose irradiation alters the transcript profiles of human lymphoblastoid cells including genes associated with cytogenetic radioadaptive response. *Radiat Res*. 2005;164(4 Pt 1):369-382.

14. Paul S, Amundson SA. Development of gene expression signatures for practical radiation biodosimetry. *International journal of radiation oncology, biology, physics*. 2008;71(4):1236-1244.
15. Barjaktarovic Z, Anastasov N, Azimzadeh O, et al. Integrative proteomic and microRNA analysis of primary human coronary artery endothelial cells exposed to low-dose gamma radiation. *Radiation and environmental biophysics*. 2013;52(1):87-98.
16. Chaudhry MA, Omaruddin RA, Kreger B, de Toledo SM, Azzam EI. Micro RNA responses to chronic or acute exposures to low dose ionizing radiation. *Molecular biology reports*. 2012;39(7):7549-7558.
17. Zhang J, de Toledo SM, Pandey BN, et al. Role of the translationally controlled tumor protein in DNA damage sensing and repair. *Proc Natl Acad Sci U S A*. 2012;109(16):E926-933.
18. Bakshi MV, Azimzadeh O, Barjaktarovic Z, et al. Total Body Exposure to Low-Dose Ionizing Radiation Induces Long-Term Alterations to the Liver Proteome of Neonatally Exposed Mice. *Journal of proteome research*. 2014.
19. Zhang Q, Matzke M, Schepmoes AA, et al. High and low doses of ionizing radiation induce different secretome profiles in a human skin model. *PloS one*. 2014;9(3):e92332.
20. Chatgililoglu C, Ferreri C, Torreggiani A, Salzano AM, Renzone G, Scaloni A. Radiation-induced reductive modifications of sulfur-containing amino acids within peptides and proteins. *Journal of proteomics*. 2011;74(11):2264-2273.
21. Ozawa K, Whalen EJ, Nelson CD, et al. S-nitrosylation of beta-arrestin regulates beta-adrenergic receptor trafficking. *Mol Cell*. 2008;31(3):395-405.
22. Foster MW, McMahon TJ, Stamler JS. S-nitrosylation in health and disease. *Trends Mol Med*. 2003;9(4):160-168.
23. Switzer CH, Cheng RY, Ridnour LA, Glynn SA, Ambs S, Wink DA. Ets-1 is a transcriptional mediator of oncogenic nitric oxide signaling in estrogen receptor-negative breast cancer. *Breast cancer research : BCR*. 2012;14(5):R125.
24. Nakamura T, Tu S, Akhtar MW, Sunico CR, Okamoto S, Lipton SA. Aberrant protein s-nitrosylation in neurodegenerative diseases. *Neuron*. 2013;78(4):596-614.
25. Li F, Sonveaux P, Rabbani ZN, et al. Regulation of HIF-1alpha stability through S-nitrosylation. *Mol Cell*. 2007;26(1):63-74.
26. Matsumoto H, Hayashi S, Hatashita M, et al. Induction of radioresistance to accelerated carbon-ion beams in recipient cells by nitric oxide excreted from

- irradiated donor cells of human glioblastoma. *International journal of radiation biology*. 2000;76(12):1649-1657.
27. Leach JK, Van Tuyle G, Lin PS, Schmidt-Ullrich R, Mikkelsen RB. Ionizing radiation-induced, mitochondria-dependent generation of reactive oxygen/nitrogen. *Cancer Res*. 2001;61(10):3894-3901.
  28. Hall EJ, Giaccia AJ. *Radiobiology for the Radiologist*. 6<sup>th</sup> ed. Philadelphia, PA: Lippincott Williams & Wilkins; 2006.
  29. Durante M, Loeffler JS. Charged particles in radiation oncology. *Nature reviews*. 2010;7(1):37-43.
  30. Durante M. Eighth warren k. Sinclair keynote address: heavy ions in therapy and space: benefits and risks. *Health Phys*. 2012;103(5):532-539.
  31. Li M, Gonon G, Buonanno M, et al. Health Risks of Space Exploration: Targeted and Non-targeted Oxidative Injury by High Charge and High Energy Particles. *Antioxidants and Redox Signaling*. 2014;20(9):1501-1523.
  32. Spitz DR, Azzam EI, Li JJ, Gius D. Metabolic oxidation/reduction reactions and cellular responses to ionizing radiation: a unifying concept in stress response biology. *Cancer Metastasis Rev*. 2004;23(3-4):311-322.
  33. Mikkelsen RB, Wardman P. Biological chemistry of reactive oxygen and nitrogen and radiation-induced signal transduction mechanisms. *Oncogene*. 2003;22(37):5734-5754.
  34. Ferradini C, Jay-Gerin JP. Radiolysis of water and aqueous solutions: history and present state of the science. *Can J Chem*. 1999;77:1542-1575.
  35. Spinks JWT, Wodds RJ. *An Introduction to Radiation Chemistry*. 3<sup>rd</sup> ed. New York: Wiley; 1990.
  36. Finkel T. Redox-dependent signal transduction. *FEBS Lett*. 2000;476(1-2):52-54.
  37. Oberley LW, Oberley TD. Role of antioxidant enzymes in cell immortalization and transformation. *Mol Cell Biochem*. 1988;84(2):147-153.
  38. Weydert CJ, Waugh TA, Ritchie JM, et al. Overexpression of manganese or copper-zinc superoxide dismutase inhibits breast cancer growth. *Free Radic Biol Med*. 2006;41(2):226-237.
  39. O'Neill P, Wardman P. Radiation chemistry comes before radiation biology. *International journal of radiation biology*. 2009;85(1):9-25.
  40. Azzam EI, Little JB. The radiation-induced bystander effect: evidence and significance. *Hum Exp Toxicol*. 2004;23(2):61-65.

41. de Toledo SM, Azzam EI. Adaptive and bystander responses in human and rodent cell cultures exposed to low level ionizing radiation: the impact of linear energy transfer. *Dose Response*. 2006;4(4):291-301.
42. Brooks AL. Paradigm shifts in radiation biology: their impact on intervention for radiation-induced disease. *Radiat Res*. 2005;164(4 Pt 2):454-461.
43. Morgan WF. Non-targeted and delayed effects of exposure to ionizing radiation: II. Radiation-induced genomic instability and bystander effects *in vivo*, clastogenic factors and transgenerational effects. *Radiat Res*. 2003;159(5):581-596.
44. Lindahl T. DNA repair enzymes acting on spontaneous lesions in DNA. In: Nichols WW, Murphy DG, eds. *DNA Repair Processes*. Miami: Symposia Specialists; 1977:225-240.
45. Feinendegen LE. Reactive oxygen species in cell responses to toxic agents. *Hum Exp Toxicol*. 2002;21(2):85-90.
46. Schafer FQ, Buettner GR. Redox environment of the cell as viewed through the redox state of the glutathione disulfide/glutathione couple. *Free Radic Biol Med*. 2001;30(11):1191-1212.
47. Allen RG, Tresini M. Oxidative stress and gene regulation. *Free Radic Biol Med*. 2000;28(3):463-499.
48. Herrlich P, Bohmer FD. Redox regulation of signal transduction in mammalian cells. *Biochem Pharmacol*. 2000;59(1):35-41.
49. Meplan C, Richard MJ, Hainaut P. Redox signalling and transition metals in the control of the p53 pathway. *Biochem Pharmacol*. 2000;59(1):25-33.
50. Price BD, Calderwood SK. Gadd45 and Gadd153 messenger RNA levels are increased during hypoxia and after exposure of cells to agents which elevate the levels of the glucose-regulated proteins. *Cancer Res*. 1992;52(13):3814-3817.
51. Lopez-Barneo J, Lopez-Lopez JR, Urena J, Gonzalez C. Chemotransduction in the carotid body: K<sup>+</sup> current modulated by PO<sub>2</sub> in type I chemoreceptor cells. *Science*. 1988;241(4865):580-582.
52. Schulze-Osthoff K, Bauer M, Vogt M, Wesselborg S, Baeuerle PA. Reactive Oxygen Intermediates as Primary Signals and Second Messengers in the Activation of transcription Factors. In: Forman HJ, Cadenas E, eds. *Oxidative Stress and Signal Transduction*. New York: Chapman & Hall; 1997:239-259.
53. ICRU. ICRU Report No. 67. Absorbed-dose specification in nuclear medicine. *Journal of the ICRU*. 2002;2(1):3-110.

54. ICRU. *The Quality Factor in Radiation Protection*. International Commission on Radiation Units and Measurements, Bethesda, MD;1986. Report 40.
55. UNSCEAR. *Sources and effects of ionizing radiation: Sources*. New York: United Nations Scientific Committee on the Effects of Atomic Radiation 2000.
56. BEIR VII. *Health risks from exposure to low levels of ionizing radiation: BEIR VII Phase 2*. Washington, DC: Committee to assess health risks from exposure to low levels of ionizing radiation, Nuclear and radiation studies board, National research council of the national academies;2006.
57. Yin E, Nelson DO, Coleman MA, Peterson LE, Wyrobek AJ. Gene expression changes in mouse brain after exposure to low-dose ionizing radiation. *International journal of radiation biology*. 2003;79(10):759-775.
58. Ding L-H, Shingyoji M, Chen F, et al. Gene Expression Profiles of Normal Human Fibroblasts after Exposure to Ionizing Radiation: A Comparative Study of Low and High Doses. *Radiation Research*. 2005;164(1):17-26.
59. Brenner DJ, Doll R, Goodhead DT, et al. Cancer risks attributable to low doses of ionizing radiation: Assessing what we really know. *Proc Natl Acad Sci U S A*. 2003;100:13761-13766.
60. ICRP. *Recommendations of the International Commission on Radiological Protection*. Oxford: Pergamon Press;1990. Publication 60.
61. Tubiana M, Aurengo A. *La relation dose-effet et l'estimation des effets cancérogènes des faibles doses de rayonnements ionisants, Rapport commun de l'Académie Nationale de Médecine et de l'Académie des Sciences*. 2005.
62. Preston DL, Pierce DA, Shimizu Y, Ron E, Mabuchi K. Dose response and temporal patterns of radiation-associated solid cancer risks. *Health Phys*. 2003;85(1):43-46.
63. de Toledo SM, Asaad N, Venkatachalam P, et al. Adaptive responses to low-dose/low-dose-rate gamma rays in normal human fibroblasts: the role of growth architecture and oxidative metabolism. *Radiat Res*. 2006;166:849-857.
64. Azzam EI, de Toledo SM, Raaphorst GP, Mitchel RE. Réponse adaptative au rayonnement ionisant des fibroblastes de peau humaine. Augmentation de la vitesse de réparation de l'ADN et variation de l'expression des gènes. *J Chim Phys*. 1994;91(7/8):931-936.
65. Azzam EI, de Toledo SM, Raaphorst GP, Mitchel RE. Low-dose ionizing radiation decreases the frequency of neoplastic transformation to a level below the spontaneous rate in C3H 10T1/2 cells. *Radiat Res*. 1996;146(4):369-373.

66. Azzam EI, Raaphorst GP, Mitchel RE. Radiation-induced adaptive response for protection against micronucleus formation and neoplastic transformation in C3H 10T1/2 mouse embryo cells. *Radiat Res.* 1994;138(1 Suppl):S28-31.
67. Nagasawa H, Little JB. Induction of sister chromatid exchanges by extremely low doses of  $\alpha$ -particles. *Cancer Res.* 1992;52:6394-6396.
68. Redpath JL, Antoniono RJ. Induction of an adaptive response against spontaneous neoplastic transformation in vitro by low-dose gamma radiation. *Radiat Res.* 1998;149(5):517-520.
69. Little JB. Radiation carcinogenesis. *Carcinogenesis.* 2000;21(3):394-404.
70. Berovic N, Pratontep S, Bryant A, Montouris A, Green RG. The kinetics of radiation damage to the protein luciferase and recovery of enzyme activity after irradiation. *Radiat Res.* 2002;157(2):122-127.
71. NCRP. *Evaluation of the linear-nonthreshold dose-response model for ionizing radiation.* Bethesda, MD: National Council on Radiation Protection and Measurements;2001. Report No. 136.
72. Bonner WM. Low-dose radiation: thresholds, bystander effects, and adaptive responses. *Proc Natl Acad Sci U S A.* 2003;100(9):4973-4975.
73. Mitchel RE, Jackson JS, McCann RA, Boreham DR. The adaptive response modifies latency for radiation-induced myeloid leukemia in CBA/H mice. *Radiat Res.* 1999;152(3):273-279.
74. Redpath JL. Radiation-induced neoplastic transformation *in vitro*: Evidence for a protective effect at low doses of low LET radiation. *Cancer Metastasis Rev.* 2004;23(3-4):333-339.
75. Azzam EI, Colangelo N, Domogauer JD, Sharma N, de Toledo SM. Is Ionizing Radiation Harmful at any Exposure? An Echo that Continues to Vibrate. *Health physics.* 2016;110(3):249-251.
76. Hess DT, Stamler JS. Regulation by S-nitrosylation of protein post-translational modification. *The Journal of biological chemistry.* 2012;287(7):4411-4418.
77. Hess DT, Matsumoto A, Kim S-O, Marshall HE, Stamler JS. Protein S-nitrosylation: purview and parameters. *Nat Rev Mol Cell Biol.* 2005;6(2):150-166.
78. Brecht D, Snyder S. Nitric oxide: a physiologic messenger molecule. *Annual review of biochemistry.* 1994;63(1):175-195.
79. Lundberg JO, Weitzberg E, Gladwin MT. The nitrate–nitrite–nitric oxide pathway in physiology and therapeutics. *Nature reviews Drug discovery.* 2008;7(2):156-167.

80. Gaston BM, Carver J, Doctor A, Palmer LA. S-nitrosylation signaling in cell biology. *Molecular interventions*. 2003;3(5):253.
81. Wang Y, Liu T, Wu C, Li H. A strategy for direct identification of protein S-nitrosylation sites by quadrupole time-of-flight mass spectrometry. *J Am Soc Mass Spectrom*. 2008;19(9):1353-1360.
82. Qu Z, Greenlief CM, Gu Z. Quantitative proteomic approaches for analysis of protein S-nitrosylation. *Journal of proteome research*. 2015.
83. Gow AJD, C. W.; Munson, D.; Ischiropoulos, H. Immunohistochemical Detection of S-Nitrosylated Proteins. *Methods Mol. Biol.* 2004,, 279.
84. Meistrich ML, Samuels RC. Reduction in sperm levels after testicular irradiation of the mouse: A comparison with man. *Radiat Res*. 1985;102:138-147.
85. Wu C, Parrott AM, Liu T, Beuve A, Li H. Functional proteomics approaches for the identification of transnitrosylase and denitrosylase targets. *Methods*. 2013;62(2):151-160.
86. Zareba-Kozioł M, Sz wajda A, Dadlez M, Wyslouch-Cieszyńska A, Lalowski M. Global analysis of S-nitrosylation sites in the wild type (APP) transgenic mouse brain-clues for synaptic pathology. *Molecular & cellular proteomics : MCP*. 2014;13(9):2288-2305.
87. Kohr MJ, Aponte AM, Sun J, et al. Characterization of potential S-nitrosylation sites in the myocardium. *American journal of physiology Heart and circulatory physiology*. 2011;300(4):H1327-1335.
88. Nakamura T, Lipton SA. Protein S-nitrosylation as a therapeutic target for neurodegenerative diseases. *Trends in pharmacological sciences*. 2016;37(1):73-84.
89. Lipton SA, Choi YB, Pan ZH, et al. A redox-based mechanism for the neuroprotective and neurodestructive effects of nitric oxide and related nitroso-compounds. *Nature*. 1993;364(6438):626-632.
90. Choi MS, Nakamura T, Cho SJ, et al. Transnitrosylation from DJ-1 to PTEN attenuates neuronal cell death in parkinson's disease models. *The Journal of neuroscience : the official journal of the Society for Neuroscience*. 2014;34(45):15123-15131.
91. Choi YB, Tenneti L, Le DA, et al. Molecular basis of NMDA receptor-coupled ion channel modulation by S-nitrosylation. *Nature neuroscience*. 2000;3(1):15-21.
92. Kim WK, Choi YB, Rayudu PV, et al. Attenuation of NMDA receptor activity and neurotoxicity by nitroxyl anion, NO. *Neuron*. 1999;24(2):461-469.

93. Lei SZ, Pan ZH, Aggarwal SK, et al. Effect of nitric oxide production on the redox modulatory site of the NMDA receptor-channel complex. *Neuron*. 1992;8(6):1087-1099.
94. Takahashi H, Shin Y, Cho SJ, et al. Hypoxia enhances S-nitrosylation-mediated NMDA receptor inhibition via a thiol oxygen sensor motif. *Neuron*. 2007;53(1):53-64.
95. Gasperini L, Meneghetti E, Pastore B, Benetti F, Legname G. Prion protein and copper cooperatively protect neurons by modulating NMDA receptor through S-nitrosylation. *Antioxid Redox Signal*. 2015;22(9):772-784.
96. Cho DH, Nakamura T, Fang J, et al. S-nitrosylation of Drp1 mediates beta-amyloid-related mitochondrial fission and neuronal injury. *Science*. 2009;324(5923):102-105.
97. Ryan SD, Dolatabadi N, Chan SF, et al. Isogenic human iPSC Parkinson's model shows nitrosative stress-induced dysfunction in MEF2-PGC1alpha transcription. *Cell*. 2013;155(6):1351-1364.
98. Uehara T, Nakamura T, Yao D, et al. S-nitrosylated protein-disulphide isomerase links protein misfolding to neurodegeneration. *Nature*. 2006;441(7092):513-517.
99. Hara MR, Agrawal N, Kim SF, et al. S-nitrosylated GAPDH initiates apoptotic cell death by nuclear translocation following Siah1 binding. *Nat Cell Biol*. 2005;7(7):665-674.
100. Nakamura T, Wang L, Wong CC, et al. Transnitrosylation of XIAP regulates caspase-dependent neuronal cell death. *Mol Cell*. 2010;39(2):184-195.
101. Qu J, Nakamura T, Cao G, Holland EA, McKercher SR, Lipton SA. S-Nitrosylation activates Cdk5 and contributes to synaptic spine loss induced by beta-amyloid peptide. *Proc Natl Acad Sci U S A*. 2011;108(34):14330-14335.
102. Yao D, Gu Z, Nakamura T, et al. Nitrosative stress linked to sporadic Parkinson's disease: S-nitrosylation of parkin regulates its E3 ubiquitin ligase activity. *Proc Natl Acad Sci U S A*. 2004;101(29):10810-10814.
103. Sayed N, Baskaran P, Ma X, van den Akker F, Beuve A. Desensitization of soluble guanylyl cyclase, the NO receptor, by S-nitrosylation. *Proc Natl Acad Sci U S A*. 2007;104(30):12312-12317.
104. Bayir H, Kagan VE, Borisenko GG, et al. Enhanced oxidative stress in iNOS-deficient mice after traumatic brain injury: support for a neuroprotective role of iNOS. *Journal of cerebral blood flow and metabolism : official journal of the International Society of Cerebral Blood Flow and Metabolism*. 2005;25(6):673-684.

105. Wu C, Parrott AM, Liu T, et al. Distinction of thioredoxin transnitrosylation and denitrosylation target proteins by the ICAT quantitative approach. *Journal of proteomics*. 2011;74(11):2498-2509.
106. Feng X, Sun T, Bei Y, et al. S-nitrosylation of ERK inhibits ERK phosphorylation and induces apoptosis. *Scientific reports*. 2013;3:1814.
107. Wang Y, Wang J. The Role of Protein S-Nitrosylation in Alzheimer's Disease and its Treatment. *J Pharmaceu Pharmacol*. 2015;3(1):6.
108. Zahid S, Khan R, Oellerich M, Ahmed N, Asif AR. Differential S-nitrosylation of proteins in Alzheimer's disease. *Neuroscience*. 2014;256(0):126-136.
109. Seneviratne U, Nott A, Bhat VB, et al. S-nitrosation of proteins relevant to Alzheimer's disease during early stages of neurodegeneration. *Proceedings of the National Academy of Sciences of the United States of America*. 2016;113(15):4152-4157.
110. Hara MR, Thomas B, Cascio MB, et al. Neuroprotection by pharmacologic blockade of the GAPDH death cascade. *Proceedings of the National Academy of Sciences of the United States of America*. 2006;103(10):3887-3889.
111. Nagane M, Yasui H, Yamamori T, et al. Radiation-induced nitric oxide mitigates tumor hypoxia and radioresistance in a murine SCCVII tumor model. *Biochemical and biophysical research communications*. 2013;437(3):420-425.
112. Veeraraghavan J, Natarajan M, Herman TS, Aravindan N. Low-dose gamma-radiation-induced oxidative stress response in mouse brain and gut: regulation by NFkappaB-MnSOD cross-signaling. *Mutation research*. 2011;718(1-2):44-55.
113. Guan W, Sha J, Chen X, Xing Y, Yan J, Wang Z. S-Nitrosylation of mitogen activated protein kinase phosphatase-1 suppresses radiation-induced apoptosis. *Cancer Lett*. 2012;314(2):137-146.
114. Otani A, Kojima H, Guo C, Oishi A, Yoshimura N. Low-Dose-Rate, Low-Dose Irradiation Delays Neurodegeneration in a Model of Retinitis Pigmentosa. *The American Journal of Pathology*. 2012;180(1):328-336.
115. Fang J, Nakamura T, Cho D-H, Gu Z, Lipton SA. S-nitrosylation of peroxiredoxin 2 promotes oxidative stress-induced neuronal cell death in Parkinson's disease. *Proceedings of the National Academy of Sciences*. 2007;104(47):18742-18747.
116. Katsura M, Cyou-Nakamine H, Zen Q, et al. Effects of Chronic Low-Dose Radiation on Human Neural Progenitor Cells. *Scientific reports*. 2016;6:20027.
117. Liao EC, Hsu YT, Chuah QY, et al. Radiation induces senescence and a bystander effect through metabolic alterations. *Cell death & disease*. 2014;5:e1255.

118. Rabilloud T, Lescuyer P. The proteomic to biology inference, a frequently overlooked concern in the interpretation of proteomic data: A plea for functional validation. *PROTEOMICS*. 2014;14(2-3):157-161.
119. Wu X, Hasan MA, Chen JY. Pathway and network analysis in proteomics. *Journal of Theoretical Biology*. (0).
120. Gatto L, Christoforou A. Using R and Bioconductor for proteomics data analysis. *Biochimica et Biophysica Acta (BBA)-Proteins and Proteomics*. 2014;1844(1):42-51.
121. Guo S, Zhou Y, Xing C, et al. The Vasculome of the Mouse Brain. *PloS one*. 2012;7(12):e52665.
122. Di Foggia V, Zhang X, Licastro D, et al. Bmi1 enhances skeletal muscle regeneration through MT1-mediated oxidative stress protection in a mouse model of dystrophinopathy. *The Journal of Experimental Medicine*. 2014;211(13):2617-2633.
123. MacQueen J. Some methods for classification and analysis of multivariate observations. Paper presented at: Proceedings of the fifth Berkeley symposium on mathematical statistics and probability 1967.
124. Dunn† JC. Well-Separated Clusters and Optimal Fuzzy Partitions. *Journal of Cybernetics*. 1974;4(1):95-104.
125. Hastie T, Tibshirani R, Friedman J, Hastie T, Friedman J, Tibshirani R. *The elements of statistical learning*. Vol 2: Springer; 2009.
126. Higuera C, Gardiner KJ, Cios KJ. Self-organizing feature maps identify proteins critical to learning in a mouse model of down syndrome. *PloS one*. 2015;10(6):e0129126.
127. Oh DS, Cheang MCU, Fan C, Perou CM. Radiation-Induced Gene Signature Predicts Pathologic Complete Response to Neoadjuvant Chemotherapy in Breast Cancer Patients. *Radiation Research*. 2014;181(2):193-207.
128. Gould J. Gene Pattern: Agglomerative hierarchical clustering of genes/experiments. <http://software.broadinstitute.org/cancer/software/genepattern/modules/docs/HierarchicalClustering/6?cv=1>. Accessed 3/21, 2018.
129. Charrad M, Ghazzali N, Boiteau V, Niknafs A. NbClust: An R Package for Determining the Relevant Number of Clusters in a Data Set. *2014*. 2014;61(6):36.
130. Sekula MN. OptCluster: an R package for determining the optimal clustering algorithm and optimal number of clusters. 2015.

131. Brock G, Pihur V, Datta S, Datta S. clValid, an R package for cluster validation. *Journal of Statistical Software (Brock et al, March 2008)*. 2011.
132. Caliński T, Harabasz J. A dendrite method for cluster analysis. *Communications in Statistics-theory and Methods*. 1974;3(1):1-27.
133. Iyer NJ, Tang Y, Mahalingam R. Physiological, biochemical and molecular responses to a combination of drought and ozone in *Medicago truncatula*. *Plant Cell Environ*. 2013;36(3):706-720.
134. Delobel J, Prudent M, Tissot JD, Lion N. Proteomics of the red blood cell carbonylome during blood banking of erythrocyte concentrates. *Proteomics Clin Appl*. 2016;10(3):257-266.
135. Kono M, Tucker AE, Tran J, Bergner JB, Turner EM, Proia RL. Sphingosine-1-phosphate receptor 1 reporter mice reveal receptor activation sites in vivo. *J Clin Invest*. 2014;124(5):2076-2086.
136. Nguyen-Tran DH, Hait NC, Sperber H, et al. Molecular mechanism of sphingosine-1-phosphate action in Duchenne muscular dystrophy. *Disease models & mechanisms*. 2014;7(1):41-54.
137. Brenman JE, Chao DS, Xia H, Aldape K, Brecht DS. Nitric oxide synthase complexed with dystrophin and absent from skeletal muscle sarcolemma in Duchenne muscular dystrophy. *Cell*. 1995;82(5):743-752.
138. The Gene Ontology C, Ashburner M, Ball CA, et al. Gene Ontology: tool for the unification of biology. *Nature genetics*. 2000;25(1):25-29.
139. Jia P, Kao CF, Kuo PH, Zhao Z. A comprehensive network and pathway analysis of candidate genes in major depressive disorder. *BMC systems biology*. 2011;5 Suppl 3:S12.
140. Chen L, Shi Q, Zhang B, et al. Proteomic Analyses for the Global S-Nitrosylated Proteins in the Brain Tissues of Different Human Prion Diseases. *Molecular neurobiology*. 2015.
141. Thomas PD, Campbell MJ, Kejariwal A, et al. PANTHER: A Library of Protein Families and Subfamilies Indexed by Function. *Genome Research*. 2003;13(9):2129-2141.
142. Azimzadeh O, Sievert W, Sarioglu H, et al. PPAR alpha: a novel radiation target in locally exposed *Mus musculus* heart revealed by quantitative proteomics. *Journal of proteome research*. 2013;12(6):2700-2714.
143. Sun L, Li J, Zhou K, et al. Metabolomic analysis reveals metabolic disturbance in the cortex and hippocampus of subchronic MK-801 treated rats. *PloS one*. 2013;8(4):e60598.

144. Sinnamon JR, Waddell CB, Nik S, Chen EI, Czaplinski K. Hnrapab regulates neural development and neuron cell survival after glutamate stimulation. *RNA*. 2012;18(4):704-719.
145. Banerjee S, Liao L, Russo R, et al. Isobaric tagging-based quantification by mass spectrometry of differentially regulated proteins in synaptosomes of HIV/gp120 transgenic mice: implications for HIV-associated neurodegeneration. *Experimental neurology*. 2012;236(2):298-306.
146. Li L, Wang W, Welford S, Zhang T, Wang X, Zhu X. Ionizing radiation causes increased tau phosphorylation in primary neurons. *Journal of Neurochemistry*. 2014;131(1):86-93.
147. Qiagen I. IPA MP. <https://www.qiagenbioinformatics.com/products/ingenuity-pathway-analysis/>. Accessed 3/21, 2018.
148. dbSNO: Database of Cystein S-nitrosylation. <http://dbSNO.mbc.nctu.edu.tw>. Accessed 3/21, 2018.
149. Seco-Cervera M, Spis M, Garcia-Gimenez JL, et al. Oxidative stress and antioxidant response in fibroblasts from Werner and atypical Werner syndromes. *Aging (Albany NY)*. 2014;6(3):231-245.
150. Tian J, Kim SF, Hester L, Snyder SH. S-nitrosylation/activation of COX-2 mediates NMDA neurotoxicity. *Proceedings of the National Academy of Sciences*. 2008;105(30):10537-10540.
151. Mustafa AK, Kumar M, Selvakumar B, et al. Nitric oxide S-nitrosylates serine racemase, mediating feedback inhibition of d-serine formation. *Proceedings of the National Academy of Sciences*. 2007;104(8):2950-2955.
152. Raaijmakers LM, Giansanti P, Possik PA, et al. PhosphoPath: Visualization of Phosphosite-centric Dynamics in Temporal Molecular Networks. *Journal of proteome research*. 2015;14(10):4332-4341.
153. Pernot E, Hall J, Baatout S, et al. Ionizing radiation biomarkers for potential use in epidemiological studies. *Mutation Research/Reviews in Mutation Research*. 2012;751(2):258-286.
154. Hall J, Jeggo PA, West C, et al. Ionizing radiation biomarkers in epidemiological studies – An update. *Mutation Research/Reviews in Mutation Research*. 2017;771:59-84.
155. Karapiperis C, Kempf SJ, Quintens R, et al. Brain Radiation Information Data Exchange (BRIDE): integration of experimental data from low-dose ionising radiation research for pathway discovery. *BMC Bioinformatics*. 2016;17:212.

156. Thomas P. The PANTHER (Protein ANalysis THrough Evolutionary Relationships) Classification System <http://www.pantherdb.org/>. Accessed 3/21, 2018.
157. Qiagen I. IPA Main Page. <https://www.qiagenbioinformatics.com/products/ingenuity-pathway-analysis/>. Accessed 3/21, 2018.
158. Qiagen I. Neuropathic Pain-Signaling in Dorsal Horn Neurons. <https://www.qiagen.com/de/shop/genes-and-pathways/pathway-details/?pwid=311>. Accessed 3/21, 2018.
159. Qiagen I. Synaptic Long Term Potentiation. <https://targetexplorer.ingenuity.com/pathway/ING/ING:1deyl#!api/rest/v1/client/searchPathwayNodes?pathwayId=ING:1deyl&rows=0&facetLimit=5000&responseType=default>. Accessed 3/21, 2018.
160. Qiagen I. CERB Pathway. <https://www.qiagen.com/us/shop/genes-and-pathways/pathway-details/?cv=1&pwid=123>. Accessed 3/21, 2018.
161. FAQs about Using IPA. [http://lsl.sinica.edu.tw/en/Question/files/ipa\\_e.pdf](http://lsl.sinica.edu.tw/en/Question/files/ipa_e.pdf). Accessed 3/21, 2018.
162. Gene N. EEF2 eukaryotic translation elongation factor 2 [ Homo sapiens (human) ]. <https://www.ncbi.nlm.nih.gov/gene/1938>. Accessed 3/21, 2018.
163. Huttlin EL, Jedrychowski MP, Elias JE, et al. A tissue-specific atlas of mouse protein phosphorylation and expression. *Cell*. 2010;143(7):1174-1189.
164. Yang XJ, Seto E. Lysine acetylation: codified crosstalk with other posttranslational modifications. *Mol Cell*. 2008;31(4):449-461.
165. Numajiri N, Takasawa K, Nishiya T, et al. On-off system for PI3-kinase-Akt signaling through S-nitrosylation of phosphatase with sequence homology to tensin (PTEN). *Proc Natl Acad Sci U S A*. 2011;108(25):10349-10354.
166. Lee C, Kim JS, Waldman T. PTEN gene targeting reveals a radiation-induced size checkpoint in human cancer cells. *Cancer Res*. 2004;64(19):6906-6914.
167. Toulany M, Lee KJ, Fattah KR, et al. Akt promotes post-irradiation survival of human tumor cells through initiation, progression, and termination of DNA-PKcs-dependent DNA double-strand break repair. *Mol Cancer Res*. 2012;10(7):945-957.
168. Downward J. PI 3-kinase, Akt and cell survival. *Seminars in cell & developmental biology*. 2004;15(2):177-182.

169. Miller AC, Voelker LH, Shah AN, Moens CB. Neurobeachin is required postsynaptically for electrical and chemical synapse formation. *Current biology : CB*. 2015;25(1):16-28.
170. Duan J, Kodali VK, Gaffrey MJ, et al. Quantitative Profiling of Protein S-Glutathionylation Reveals Redox-Dependent Regulation of Macrophage Function during Nanoparticle-Induced Oxidative Stress. *ACS nano*. 2016;10(1):524-538.
171. Wu C, Parrott AM, Fu C, et al. Thioredoxin 1-mediated post-translational modifications: reduction, transnitrosylation, denitrosylation, and related proteomics methodologies. *Antioxidants & redox signaling*. 2011;15(9):2565-2604.
172. Rousseau M, Gaugler MH, Rodallec A, Bonnaud S, Paris F, Corre I. RhoA GTPase regulates radiation-induced alterations in endothelial cell adhesion and migration. *Biochemical and biophysical research communications*. 2011;414(4):750-755.
173. Jaffrey SR, Erdjument-Bromage H, Ferris CD, Tempst P, Snyder SH. Protein S-nitrosylation: a physiological signal for neuronal nitric oxide. *Nat Cell Biol*. 2001;3(2):193-197.
174. Hao G, Derakhshan B, Shi L, Campagne F, Gross SS. SNOSID, a proteomic method for identification of cysteine S-nitrosylation sites in complex protein mixtures. *Proc Natl Acad Sci U S A*. 2006;103(4):1012-1017.
175. Landino LM, Koumas MT, Mason CE, Alston JA. Modification of tubulin cysteines by nitric oxide and nitroxyl donors alters tubulin polymerization activity. *Chemical research in toxicology*. 2007;20(11):1693-1700.
176. McMurray CT. Neurodegeneration: diseases of the cytoskeleton? *Cell death and differentiation*. 2000;7(10):861-865.
177. D'Souza-Schorey C, Chavrier P. ARF proteins: roles in membrane traffic and beyond. *Nat Rev Mol Cell Biol*. 2006;7(5):347-358.
178. Myers KR, Casanova JE. Regulation of actin cytoskeleton dynamics by Arf-family GTPases. *Trends in cell biology*. 2008;18(4):184-192.
179. Takatsu H, Yoshino K, Toda K, Nakayama K. GGA proteins associate with Golgi membranes through interaction between their GGAH domains and ADP-ribosylation factors. *The Biochemical journal*. 2002;365(Pt 2):369-378.
180. Orlando G, Khoronenkova SV, Dianova, II, Parsons JL, Dianov GL. ARF induction in response to DNA strand breaks is regulated by PARP1. *Nucleic Acids Res*. 2014;42(4):2320-2329.

181. Jorgensen PL. Mechanism of the Na<sup>+</sup>, K<sup>+</sup> pump. Protein structure and conformations of the pure (Na<sup>+</sup> +K<sup>+</sup>)-ATPase. *Biochimica et biophysica acta*. 1982;694(1):27-68.
182. Clausen MJ, Poulsen H. Sodium/Potassium homeostasis in the cell. *Metal ions in life sciences*. 2013;12:41-67.
183. Norby JG, Jensen J. Functional significance of the oligomeric structure of the Na,K-pump from radiation inactivation and ligand binding. *Soc Gen Physiol Ser*. 1991;46:173-188.
184. Gisone P, Boveris AD, Dubner D, Perez MR, Robello E, Puntarulo S. Early neuroprotective effect of nitric oxide in developing rat brain irradiated in utero. *Neurotoxicology*. 2003;24(2):245-253.
185. Russel MC, Delman KA. Comparative Effectiveness in Melanoma. *Cancer treatment and research*. 2015;164:31-49.
186. Hallahan DE, Bleakman D, Virudachalam S, et al. The role of intracellular calcium in the cellular response to ionizing radiation. *Radiat Res*. 1994;138(3):392-400.
187. Dent P, Yacoub A, Fisher PB, Hagan MP, Grant S. MAPK pathways in radiation responses. *Oncogene*. 2003;22(37):5885-5896.
188. Kim YT, Jo SS, Park YJ, Lee MZ, Suh CK. Distinct Cellular Calcium Metabolism in Radiation-sensitive RKO Human Colorectal Cancer Cells. *Korean J Physiol Pharmacol*. 2014;18(6):509-516.
189. Haimovitz-Friedman A. Radiation-induced signal transduction and stress response. *Radiat Res*. 1998;150(5 Suppl):S102-108.
190. InterPro. Zinc finger, DPH-type (IPR007872). <https://www.ebi.ac.uk/interpro/entry/IPR007872>. Accessed 3/21, 2018.
191. Greganova E, Altmann M, Bütikofer P. Unique modifications of translation elongation factors. *FEBS Journal*. 2011;278(15):2613-2624.
192. Okamoto S, Lipton SA. S-Nitrosylation in neurogenesis and neuronal development. *Biochimica et biophysica acta*. 2015;1850(8):1588-1593.
193. Tischfield MA, Cederquist GY, Gupta ML, Jr., Engle EC. Phenotypic spectrum of the tubulin-related disorders and functional implications of disease-causing mutations. *Current opinion in genetics & development*. 2011;21(3):286-294.
194. Lundin VF, Leroux MR, Stirling PC. Quality control of cytoskeletal proteins and human disease. *Trends Biochem Sci*. 2010;35(5):288-297.

195. Vemu A, Atherton J, Spector JO, Moores CA, Roll-Mecak A. Tubulin isoform composition tunes microtubule dynamics. *Mol Biol Cell*. 2017;28(25):3564-3572.
196. Halpain S, Dehmelt L. The MAP1 family of microtubule-associated proteins. *Genome Biol*. 2006;7(6):224.
197. Gordon-Weeks PR, Fischer I. MAP1B expression and microtubule stability in growing and regenerating axons. *Microscopy research and technique*. 2000;48(2):63-74.
198. Togel M, Wiche G, Propst F. Novel features of the light chain of microtubule-associated protein MAP1B: microtubule stabilization, self interaction, actin filament binding, and regulation by the heavy chain. *The Journal of cell biology*. 1998;143(3):695-707.
199. Stroissnigg H, Trancikova A, Descovich L, et al. S-nitrosylation of microtubule-associated protein 1B mediates nitric-oxide-induced axon retraction. *Nat Cell Biol*. 2007;9(9):1035-1045.
200. Yan Y, Hein AL, Eteko A, et al. Inhibition of RAC1 GTPase sensitizes pancreatic cancer cells to gamma-irradiation. *Oncotarget*. 2014;5(21):10251-10270.
201. Preston RJ. Can radiation research impact the estimation of risk? *International journal of radiation biology*. 2017;93(10):1009-1014.
202. Matsumoto H, Tomita M, Otsuka K, Hatashita M, Hamada N. Nitric oxide is a key molecule serving as a bridge between radiation-induced bystander and adaptive responses. *Curr Mol Pharmacol*. 2011;4:126-134.
203. Heo J, Campbell SL. Mechanism of p21Ras S-nitrosylation and kinetics of nitric oxide-mediated guanine nucleotide exchange. *Biochemistry*. 2004;43(8):2314-2322.
204. Carrier S, Hricak H, Lee SS, et al. Radiation-induced decrease in nitric oxide synthase--containing nerves in the rat penis. *Radiology*. 1995;195(1):95-99.
205. Ginsberg MD. Neuroprotection for ischemic stroke: past, present and future. *Neuropharmacology*. 2008;55(3):363-389.
206. Lea DE. The inactivation of viruses by radiations. *The British journal of radiology*. 1946;19:205-212.
207. Barker S, Weinfeld M, Zheng J, Li L, Murray D. Identification of mammalian proteins cross-linked to DNA by ionizing radiation. *The Journal of biological chemistry*. 2005;280(40):33826-33838.

208. Tsang AH, Lee YI, Ko HS, et al. S-nitrosylation of XIAP compromises neuronal survival in Parkinson's disease. *Proc Natl Acad Sci U S A*. 2009;106(12):4900-4905.
209. Peng J, Elias JE, Thoreen CC, Licklider LJ, Gygi SP. Evaluation of multidimensional chromatography coupled with tandem mass spectrometry (LC/LC-MS/MS) for large-scale protein analysis: the yeast proteome. *Journal of proteome research*. 2003;2(1):43-50.